Evolutionary games between epithelial cells: the impact of population structure and tissue dynamics on the success of cooperation

Jessie Renton

A dissertation submitted in partial fulfillment

of the requirements for the degree of

Doctor of Philosophy

of

University College London.

Department of Mathematics

University College London

Supervised by Prof. Karen M. Page

September 3, 2021

I, Jessie Renton, confirm that the work presented in this thesis is my own. Where information has been derived from other sources, I confirm that this has been indicated in the work.

Abstract

Cooperation is usually understood as a social phenomenon. However, it also occurs on the cellular level. A number of key mutations associated with malignancy can be considered cooperative, as they rely on the production of diffusible growth factors to confer a fitness benefit. Evolutionary game theory provides a framework for modelling the evolutionary dynamics of these cooperative mutations.

This thesis uses evolutionary game theory to examine the evolutionary dynamics of cooperation within epithelial cells, which are the origin point of most cancers. In particular, we consider how the structure and dynamics of an epithelium affect cooperative success. We use the Voronoi tessellation model to represent an epithelium. This allows us much greater flexibility, compared to evolutionary graph theory models, to explore realistic dynamics for population updating.

Initially, we consider a model where death and division are spatially decoupled. We analyse pairwise social dilemma games, focussing on the additive prisoner's dilemma, and multiplayer public goods games. We calculate fixation probabilities, and conditions for cooperative success, by simulation, as well as deriving quasi-analytic results. Comparing with results for graph structured populations with spatially coupled birth and death, or well-mixed populations, we find that in general cooperation is promoted by local game play, but global competition for offspring.

We then introduce a more realistic model of population updating, whereby death and division are spatially coupled as a consequence of contact inhibition. The strength of this coupling is positively correlated with the strength of contact inhibition. However, the extent to which strong spatial coupling inhibits cooperation depends on mechanical properties of the tissue.

Impact Statement

Results from this thesis contribute to the understanding of basic evolutionary processes relevant to cancer, and could benefit modelling efforts for the development of cancer therapeutics. They are also highly relevant within the mathematical field of evolutionary game theory.

Evolutionary models of cancer are becoming increasingly used, not only to improve our understanding of cancer, but also as a tool for improving treatment. An example is the use of evolutionary modelling to predict optimal drug scheduling and dosage, in order to prevent drug-resistant clones becoming dominant within a tumour.

Existing models tend to focus on well-mixed or graph-structured populations. Our results suggest it may be important to take into account not only spatial structure, but factors such as the strength of contact inhibition and possibly even the tissue tension, in these models. This is especially true if the mutations under consideration are frequency-dependent.

Our results also have potential impact at the theoretical level, within the field of evolutionary game theory. In particular, we have derived analytical results to determine the conditions for cooperation to be beneficial or favoured for pairwise and multiplayer games (in Chapters 4 and 5, respectively), when birth and death are decoupled. We have used these results to analyse the Voronoi tessellation model, however they could also be applied more generally to other population models, so long as decoupling birth and death is possible.

Work done as part of this thesis has so far resulted in two peer-reviewed publications:

1. Jessie Renton and Karen M. Page. Evolution of cooperation in an epithelium. *Journal of the Royal Society Interface*, 16:20180918, 2019;

2. Jessie Renton and Karen M. Page. Cooperative success in epithelial public goods games. *Journal of Theoretical Biology*, 528:110838, 2021.

A further publication based on Chapter 6 is planned. The Voronoi tessellation model code is available at https://github.com/jessierenton.

Acknowledgements

I am extremely grateful to my supervisor, Karen Page for all her guidance and inspiration during my PhD, and for getting me to this point. Also, to the various members of her group who have come and gone since I started, especially Pilar and Rubén, for taking me under their wing from the very beginning and making everything fun.

Thank you to Jean Lagacé for his insightful feedback on the final manuscript. And also to the staff in the UCL maths department for their help over the years. I am very grateful to the incredible friends I made at UCL, especially Sean, Niki and Giulia, who always took me for a pint when it was needed.

A big thank you to Richard Blythe, my masters supervisor, who first got me interested in evolution, and made me realise the broad possibilities of what I could do with a physics degree that aren't really physics.

There are so many people who have helped me along the way. My parents Adrian and Annie who are always generous with their love and support. My sister Hannah who has been with me through everything. My brother Ben who has (nearly) convinced me of his philosophy that most problems go away on their own. Milli and Jake, thank you for distracting me with board games and football.

Most of my PhD was done while I lived on Ranelagh Road, where I had the best housemates and neighbours. To Freya and Lucy thank you for keeping me going through Covid and for the living room dance parties. And Kamla, thank you for being the other half of my double act (as Jojo would say) and for answering my random questions about how cells work. Thank you to Josh and Ellen for always supporting me. To friends, near and far, thank you for making everything worthwhile. Lastly, to my girl Katy, love you always.

Contents

List of Figures

List of Tables

Chapter 1

Introduction

1.1 Cooperation on the cellular level

Cooperation is prevalent in nature. We usually think of cooperation as a social phenomenon, whereby individuals work together towards a mutual benefit. When animals hunt in groups, they can catch larger prey, leading to a greater share of food than if they had hunted alone. Cooperation is not, however, limited to interactions between animals, but can be observed on every scale of life, from complex human societies, right down to the cellular level [1].

Within multicellular organisms, cells perform specialised functions, sacrificing their own proliferative potential for the benefit of the whole. Just as cooperation between humans can lead to much richer and more complex forms of social organisation, so we see within our own bodies that the organisation of cells leads to high complexity life forms.

What happens, then, if cells cease to cooperate? The problem of free-riders is well known in a social context. When people work together for a common good there is an incentive to defect, to leave the work to others, and still take a share of the reward. When cells become malignant, they stop functioning in the best interests of the organism and prioritise their own proliferation. Thus, cancer is often considered to represent a breakdown of cellular cooperation [2].

This does not present the whole picture, however. As malignant cells grow and replicate, they form their own subpopulation within the host. Therefore, while

cancer cells defect from the organism as a whole, they can evolve cooperative traits which benefit the tumour.

This thesis is focused on the evolution of cooperation in epithelial cells, which are the origin point for most cancers. These cells are organised into tissues, known as epithelia, which form linings and surfaces in the body. We seek to understand how the population structure and dynamics of epithelia impact on the evolution of cooperation. Before considering specific models of cooperating epithelial cells, we address the important question of how cooperative behaviour is possible from an evolutionary perspective, and the important role of population structure and update dynamics.

1.2 Evolutionary game theory and cooperation

As we have discussed, cooperation occurs on all scales of life, but how it is able to evolve presents a conundrum, as it seems to defy Darwinian principles. Evolution by natural selection occurs on the level of the individual, favouring traits with higher reproductive value. We know that there are myriad circumstances where a better outcome will come from cooperation. However, if the fitness of an individual, be it cell, plant, or animal, is increased by defecting, we expect the selection pressure to push the population towards total defection. Why then, is cooperation so prevalent in the natural world?

Evolutionary game theory provides a framework for modelling evolutionary dynamics when selection is frequency-dependent. That is, the fitness of an individual depends not only on its own traits, but on the traits of others in the population. This is the case with cooperation, where, for example, a cooperator in a population of cooperators will have high fitness, while a cooperator in a population of defectors will not. Evolutionary game theory was in fact conceived to explain the existence of 'limited war' type fighting, a form of cooperative behaviour amongst animals [3, 4].

Games played between cooperators and defectors are commonly referred to as social dilemmas [5], and the evolutionary success of each strategy depends on the specific formulation of the game. The prisoner's dilemma is arguably the most

famous example. Within a group of interacting individuals playing the prisoner's dilemma, mutual cooperation would result in the best collective outcome. However, the best strategy for any individual is to defect. Correspondingly, if it is assumed interactions occur randomly, defection is the only evolutionarily successful strategy.

For cooperation to be successful, an additional mechanism is necessary. Kin selection, direct and indirect reciprocity, group selection, and network reciprocity can all fulfil this role [6]. Network reciprocity is particularly important for our purposes, because it refers to the introduction of population structure. In many cases, and certainly for cell populations, which are often organised into tissues, this is more realistic than assuming a well-mixed population. The introduction of population structure into evolutionary game theory models has, therefore, been the focus of extensive work over the past thirty years [7–15].

Introducing population structure can have a significant effect on evolutionary dynamics [11], in particular in promoting cooperation [6]. The established framework for modelling games on structured populations is evolutionary graph theory [14, 16–23]. Individuals occupy vertices on a fixed graph and interact with their neighbours. This means cooperators are able to form clusters and interact preferentially with other cooperators, thus providing one another reciprocal benefits.

Evolutionary graph theory imposes spatial constraints, not only on interactions, but also on birth and death. To maintain the fixed graph structure, it is necessary to define an update rule, which determines exactly how birth and death occur. Two commonly used are the birth-death and death-birth update rules, which essentially differ in the order in which birth and death events occur. These ensure that a death always occurs simultaneously with a neighbouring birth event, so there is an empty vertex on the graph for the offspring to occupy. Enforcing these spatial constraints means that competition occurs on a local, rather than global, level. The choice of update rule has a substantive effect on the success of cooperation.

The success of cooperation is also dependent on the game itself, and the prisoner's dilemma is by no means the only choice. The stag-hunt and snowdrift games present slightly weaker forms of social dilemma, for which cooperation can be suc-

cessful, even in a well-mixed population [24]. These social dilemma games involve pairwise interactions, however, there is a broader class of public goods games, which consider interactions between cooperators and defectors within larger groups [25].

Much of the literature is focused towards social behaviour, however, evolutionary game theory has also been used to model cellular evolution. Many examples, including signalling, cross-talk and host-cell/parasite interactions, have been explored over the last two decades (see [26] for a review). In the next section, we will consider how evolutionary games have been used to model cellular mutations relevant to cancer, and some of the shortcomings of using evolutionary graph theory to represent epithelial structure and dynamics.

1.3   Somatic evolution of cancer

Oncogenesis is a process of somatic evolution[1], whereby cells must undergo a number of genetic changes to become malignant. These mutations lead to acquired capabilities that confer some growth advantage, known as the hallmarks of cancer. Currently, eight hallmarks have been identified: self-sufficiency in growth signalling, evading growth suppressors, evading apoptosis, enabling replicative immortality, inducing angiogenesis, activating tissue invasion and metastasis, reprogramming energy metabolism, and avoiding immune destruction [27, 28].

As we discussed in Section 1.1, cancer can be considered as the breakdown of cellular cooperation, as malignant cells cease performing their role as part of the whole organism. However, these malignant cells can evolve new cooperative traits which benefit the tumour population.

Many of the hallmarks, such as self-sufficiency in growth signalling and inducing angiogenesis, rely on the production of diffusible growth factors[2] [29]. This means the resulting fitness benefit is not necessarily reserved for the cell that produces the growth factor, but may be shared. Furthermore, there is likely an en-

---

[1]Somatic evolution refers to the evolution of somatic cells. These are the cells comprising the body of an organism, as opposed to reproductive cells.

[2]Growth factors are proteins, or other molecules, used for cell signalling. They can stimulate various processes, such as growth, proliferation, wound healing and differentiation.

ergy cost associated with the production of the growth factor. Producer cells can, therefore, be considered cooperators, as they produce a shared benefit at a cost to themselves [30, 31].

Within the game-theoretical context, the evolution of growth factor production has been modelled as a two-player game between cooperators and defectors in a well-mixed population [32]. Cooperators produce a growth factor, at a cost, which benefits both themselves and the cells they interact with, while defectors produce no growth factor. The original model is a borderline case of the snowdrift game and has been extended to include additional strategies [33] and spatial structure by placing cells on a lattice [34]. This latter study considered both snowdrift and prisoner's dilemma games. More realistic models have been developed in recent years that consider the exchange of growth factors as a multiplayer public goods game with non-linear benefit function and variable diffusion range [35–39]. Furthermore, these games have been considered on fixed graph structures that reflect the heterogeneity of tissues [40].

Another hallmark which provides an example of cellular cooperation is the reprogramming of energy metabolism. Commonly known as the Warburg effect [41], this relates to the fact that cancer cells produce energy through glycolysis. Metabolism by glycolysis, which produces lactic acid as a biproduct, is less efficient than aerobic respiration and is usually only used by healthy cells when oxygen is scarce. Cancer cells, however, tend to use glycolysis even when oxygen is abundant. One proposed explanation for this is that although the individual suffers a cost, as glycolysis is less efficient, the resultant increase in acidity is beneficial to the tumour as a whole, due to its deleterious effect on healthy cells [42].

Models of the Warburg effect have been developed for pairwise games in well-mixed populations [43, 44] and extended to include strategies of invasion [43, 45]. Furthermore, recent work has been done to model the Warburg effect using multiplayer public goods games [46, 47]. These differ from growth factor models in that overproduction of the public good (lactic acid) can have a deleterious effect on the cancer cells, as well as the healthy cells. A combined model of glycolysis and

growth factor production has also been developed, which utilises a double public goods game [48]. Further examples of the application of game theory to cancer evolution include microenvironment dependency [49, 50], environmental poisoning [51] and invasion [52]. There are also a number of models for therapeutics, which attempt to find better strategies for deploying cancer drugs [53–55].

These models either consider a well-mixed population or use evolutionary graph theory to incorporate population structure, however, there are several short-comings of this approach when applied to somatic evolution. Tissue and tumour structures are not fixed but dynamic, due to processes such as cell division, apopto-sis (programmed cell death), differentiation (cell specialisation), and motility. Ad-ditionally, the constraints imposed by the update rule imply strong spatial coupling between birth and death, which is not necessarily realistic. The choice of update rule is one of the main determinants of evolutionary outcomes [56], so it is an essential consideration.

Dynamic graph models of evolutionary games do exist, however, they mostly focus on switching connections between vertices, either at random or to increase fitness [57–60]. These types of models are relevant in social networks, for exam-ple, where agents choose who they interact with, and can break social ties with individuals who do not cooperate [61]. They are not good models, however, for populations of cells which are spatially constrained in two- or three-dimensional structures. Furthermore, they still require birth and death to be coupled.

Recent work has introduced a new 'shift update' with the aim of addressing the unsuitability of the traditional update rules for somatic evolution. Within this up-date rule, birth and death occur in independent locations, and a process of shifting is used to fill the empty space left by the dead cell and make space for the offspring. It works extremely well in one-dimension [62], predicting enhanced cooperative suc-cess compared to other update rules. However, the extension into two dimensions [63] is not straightforward as the shifting of cells disrupts the cluster formation of cooperators. This can be resolved by introducing a repulsive force between cells of different types and choosing energy-minimising shift paths. If the force is strong

enough, the shift dynamics is again an effective promoter of cooperation. However, it relies on this somewhat artificial preferential sorting.

An alternative framework, developed in [64, 65], uses a topological tissue model [66] to generate a dynamic graph, which represents cellular interactions, and allows for spatially decoupled birth and death. Graph topologies, however, do not necessarily correspond to normal tissues. In particular, all defector populations have abnormal polygon distributions, and cooperators on the boundary of a defector cluster can end up with unrealistically high numbers of neighbours. The introduction of forces in a spatial tissue model could resolve these issues.

This thesis aims to consider the effect of population structure and tissue dynamics on the evolution of cooperation in an epithelium. To resolve some of the shortcomings of previous models, we represent epithelial dynamics explicitly using a mechanical model—the Voronoi tessellation (VT) model [67, 68]. This allows us to consider the effects of fully decoupled birth and death, while maintaining a realistic tissue structure. It also provides the flexibility to introduce more realistic forms of spatial coupling as a result of density-dependent proliferation.

1.4   Thesis outline

The remainder of this thesis is set out as follows. In Chapter 2 we give an outline of evolutionary game theory and how it is used to model cooperation. We begin by introducing pairwise games and then extend to multiplayer games. In both cases, we look at known results for well-mixed and structured populations, and consider the difference between local and global update rules.

In Chapter 3 we introduce epithelia in more detail, explaining their role within the body and their key characteristics. We give an overview of agent-based models which have been used to represent epithelial dynamics, and outline the VT model in detail, which we use extensively in the subsequent chapters.

We then begin our analysis of evolutionary games in epithelial cells by using the VT model and a spatially decoupled update rule to represent epithelial population structure and dynamics. In Chapter 4 the focus is on pairwise games, in

particular, a simple version of the prisoner's dilemma. We find that spatially decoupling cell division and death promotes cooperation. This holds for the prisoner's dilemma, but also more broadly for pairwise social dilemma games. We show that cooperation is always favoured in the snowdrift and stag hunt games for the VT model with decoupled update rule. Additionally, there is likely a small deleterious effect on cooperation due to cellular motion in the VT model.

We extend these results to multiplayer games in Chapter 5. These allow for cases where the benefit to a cell is a non-linear function of the number of cooperators, which provides a more realistic model for the effect of a diffusible growth factor. We derive conditions under which cooperation is favoured and/or beneficial for populations where birth and death are spatially decoupled, and apply these to the VT model. We find, once again, that the VT model with decoupled updating promotes cooperation. We also consider how the gradient of selection can provide insights into the evolutionary dynamics.

In Chapter 6 we begin to consider the spectrum of spatial dependence of birth and death between the decoupled and death-birth update rules. This is done by introducing contact inhibition, the phenomenon whereby cells stop proliferating at high density, into the VT model. The strength of contact inhibition determines the strength of spatial coupling, which in turn affects the success of cooperation. We also find an effect on cooperative success which relates to the tissue tension, and explore this using a one-dimensional version of the VT model.

Finally we discuss our key results in chapter 7, namely that cooperative success is maximised by local game interactions and global competition, and consider the implications for models of cancer evolution. We also discuss possible extensions and future avenues of research.

Chapter 2

Evolutionary game theory

2.1 Introduction

The focus of this thesis is to explore how the structure and dynamics of epithelia affect the evolutionary success of cooperation. To do this, we utilise evolutionary game theory, which provides a robust framework for modelling the evolution of cooperation. In this chapter, we outline this modelling framework, introducing key concepts and results that will be used extensively throughout this thesis.

Games between cooperators and defectors can take many forms, with the commonality that cooperation benefits the collective, but there is always an individual incentive to defect. These games can broadly be divided into two categories: pairwise social dilemma games and multiplayer public goods games. The former, describing the case where individuals interact one-on-one with other players, is introduced in Section 2.2. The latter case of multiplayer games, which allows for group interactions, is outlined in Section 2.3.

2.2 Pairwise games

Evolutionary game theory was originally formulated for pairwise games [3, 4] in which individual players interact one-on-one to derive a payoff. These games can be represented as an $n \times n$ matrix, where n is the number of possible strategies or types. The focus here is on 2×2 social dilemma games [5, 69], which describe interactions between players of two types: cooperators (C) and defectors (D).

Payoffs are determined by the types of the interacting players. Mutual co-

operation results in a 'reward' *R*, while mutual defection leads to a 'punishment' *P*. Interactions between defectors and cooperators result in a 'temptation' *T* and a 'sucker's payoff' *S* awarded, respectively. These are summarised by the payoff matrix

$$
\begin{array}{c}
\quad\, C \quad D \\
\begin{array}{c} C \\ D \end{array}
\begin{pmatrix} R & S \\ T & P \end{pmatrix}.
\end{array}
\tag{2.1}
$$

In order that a game is considered a social dilemma [69–71] the following conditions must be satisfied:

1. $R > P$: mutual cooperation is preferred over mutual defection,

2. $R > S$: mutual cooperation is preferred over unilateral cooperation,

3. $2R > T + S$: mutual cooperation is preferred over an equal probability of unilateral cooperation and defection.

One (or both) of the following is also required for the game to be a social dilemma, either

4a. $T > R$: unilateral defection is preferred over mutual cooperation, or

4b. $P > S$: mutual defection is preferred over unilateral cooperation.

These conditions create tension between the interests of the collective and the individual [70]. The best mutual strategy is for both players to cooperate, however, this is put at risk by either the temptation to defect due to greed (4a), or the fear that one's opponent will defect (4b).

There are thus three distinct social dilemmas with different incentives to defect [70]: the snowdrift game ($T > R > S > P$) for which the incentive is greed, the stag-hunt game ($R > T > P > S$) where the incentive is fear, and the prisoner's dilemma ($T > R > P > S$) for which both fear and greed are involved, and there is a double inducement to defect.

Figure 2.1 shows these parameter regions schematically, additionally including the harmony game, which is not a social dilemma, as there is no temptation to defect. We have used the standard parameterisation, which is to set $R = 1$ and $P = 0$. This is done without loss of generality for the replicator equation, described in Section 2.2.1, which is invariant under translation, while positive rescalings can be absorbed by the selection strength parameter. Additionally, there is no loss of generality under this parameterisation for the Moran process, described in Section 2.2.2, so long as the weak selection limit is employed. Here, translation refers to the addition of a constant to each element of the payoff matrix, while rescaling refers to multiplication by a constant. For a full classification of two-strategy pairwise games, see [26, 72].

In the remainder of this section we outline the framework for modelling the evolutionary dynamics of these pairwise social dilemma games. First, we consider introducing the replicator equation for infinite well-mixed populations, as well as the stochastic dynamics in finite populations. We then move on to spatial extensions, focusing on evolutionary graph theory. We consider the special case of the additive prisoner's dilemma (APD) game and outline how the structure coefficients can be used to generalise APD results to any 2×2 matrix game.

2.2.1 The replicator equation

If we assume an infinite well-mixed population, the standard model of evolutionary game dynamics is the replicator equation [73–77], which describes the deterministic selection process. Let $x_C = x \in [0,1]$ and $x_D = 1 - x$, be the cooperator and defector frequencies, respectively. The respective payoffs are then given by

$$\pi_C(x) = xR + (1-x)S \tag{2.2}$$

$$\pi_D(x) = xT + (1-x)P. \tag{2.3}$$
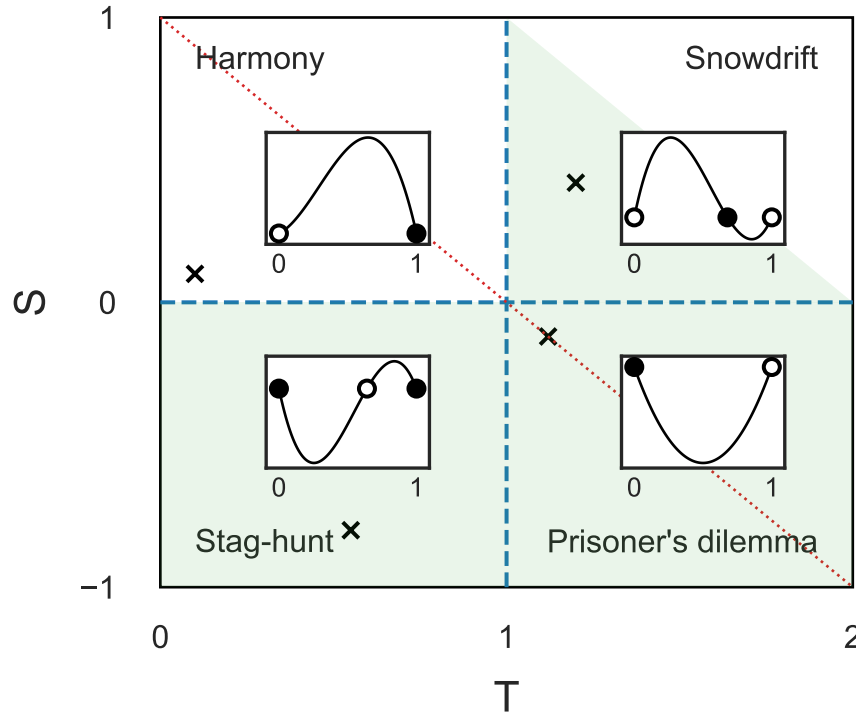
Figure 2.1: Social dilemma games in the *T*-*S* plane, as defined by Equation (2.1), with $R = 1$ and $P = 0$. Green shading indicates the regions where the game is a social dilemma. The inset graphs plot $\dot{x}$ vs. *x*, as defined by the Equation (2.7). Stable and unstable fixed points are indicated by filled and open circles, respectively. Crosses in the *T*-*S* plane show parameter values used for each inset plot. An example is given for each game showing the qualitatively different behaviour: cooperator domination for the harmony game, defector domination for the prisoner's dilemma, bistability for the stag-hunt, and stability of coexistence for the snowdrift game. The red dotted line, $S = 1 - T$ is the additive prisoner's dilemma (or harmony) game.

It is reasonable to assume that there will be other contributions to fitness besides payoffs, thus we define fitness to be

$$F_X = 1 + \delta \pi_X, \tag{2.4}$$

where the *selection strength parameter* δ determines the relative importance of the payoff compared to other factors. The subscript *X* refers to the player type, *C* or *D*.

The replicator equation, which assumes reproduction is proportional to fitness,

is given by

$$\dot{x} = x(F_C - F) = \delta x(\pi_C - \pi) \tag{2.5}$$

where $F = xF_C + (1-x)F_D$ and $\pi = x\pi_C + (1-x)\pi_D$ are the average fitness and payoff respectively. Here we assume faithful reproduction, i.e. offspring inherit the parent type with no mutation. Equivalently, we can write the replicator equation as

$$\dot{x} = x(1-x)(F_C - F_D) = \delta x(1-x)(\pi_C - \pi_D). \tag{2.6}$$

Substituting in Equations (2.2) and (2.3) we obtain

$$\dot{x} = \delta x(1-x)[S - P + x(R - S - T + P)] \tag{2.7}$$

for the rate of change of cooperator frequency in terms of the game parameters.

Equation (2.7) always has two fixed points at $x = 0$ and $x = 1$, regardless of the parameter values. A third fixed point is also present at

$$x^* = \frac{P - S}{R - S - T + P} \tag{2.8}$$

if $R > T$ and $P > S$ (stag-hunt) or $R < T$ and $P < S$ (snowdrift). Thus there are four qualitatively different regimes corresponding to the different games (see Figure 2.1):

- **Prisoner's dilemma:** there is a stable fixed point at $x = 0$ and an unstable fixed point at $x = 1$, so defection dominates.

- **Snowdrift:** there are two unstable fixed points at $x = 0$ and $x = 1$ as well as an internal stable fixed point, so cooperation and defection are able to coexist.

- **Stag-hunt:** there are two stable fixed points at $x = 0$ and $x = 1$ (bistability) and an internal fixed point which is unstable. This is also known as a coordination game, as the best strategy is that of your opponent.

- **Harmony game:** the fixed points at $x = 0$ and $x = 1$ are unstable and stable,

respectively, so cooperation dominates. This is not a social dilemma, as there is no incentive to defect.

Of course, for many real-world applications, the assumption of an infinite population size will not be appropriate. For smaller population sizes, stochastic effects will be important. For a finite population, there are only two absorbing states, at $x = 1$ and $x = 0$. Thus, we can consider the probability of ending up in each of these states, for different initial conditions in each region of the parameter space.

2.2.2 Stochastic dynamics in finite populations

For a finite population, we consider a Moran process [76, 78] with frequency-dependent fitness. At discrete time intervals, an individual is selected uniformly at random to die. Simultaneously, an individual is chosen to reproduce, with probability proportional to its fitness. The offspring inherits the parent type and replaces the dead cell. Thus, the population size Z remains constant in time.

The number of cooperators is denoted n and the number of defectors $Z - n$. Thus, the payoffs are

$$\pi_C = \frac{(n-1)R + (Z-n)S}{Z-1} \tag{2.9}$$

$$\pi_D = \frac{nT + (Z-n-1)P}{Z-1}, \tag{2.10}$$

respectively for a cooperator and defector. The probabilities of changing the number of cooperators from n to $n \pm 1$ in a single timestep are given by the transition probabilities $T_n^{\pm}$. These define a Markovian birth-death process with two absorbing states at $n = 0$ and $n = Z$. We can write down the transition probabilities explicitly in terms of fitnesses:

$$T_n^+ = \left(1 - \frac{n}{Z}\right)\frac{nF_C}{ZF} \qquad T_n^- = \frac{n}{Z}\left(1 - \frac{nF_C}{ZF}\right), \tag{2.11}$$

or in terms of payoffs by substituting in Equations (2.4), (2.9) and (2.10).

In the weak selection limit $\delta \ll 1$, assuming that the payoffs are a small con-

tribution to the overall fitness, the transition probabilities become

$$T_n^+ = \frac{n}{Z}\frac{Z-n}{Z}[1+\delta(\pi_C-\pi)]+\mathcal{O}(\delta^2) \tag{2.12}$$

$$T_n^- = \frac{n}{Z}\frac{Z-n}{Z}\left[1-\delta\frac{n}{Z-n}(\pi_C-\pi)\right]+\mathcal{O}(\delta^2). \tag{2.13}$$

We can then calculate the cooperator fixation probability ϕ_l, defined as the probability of reaching the absorbing state $n=Z$, given the initial state has l cooperators. The fixation probability for a single initial cooperator, denoted as ρ_C, is of particular interest, and unless otherwise stated, we refer to this as the fixation probability.

The fixation probabilities are found by solving the recursion relation [76, 77]

$$\phi_n = T_n^-\phi_{n-1}+(1-T_n^--T_n^+)\phi_n+T_n^+\phi_{n+1}, \tag{2.14}$$

with the boundary cases

$$\phi_0 = 0 \text{ and } \phi_Z = 1. \tag{2.15}$$

Letting $\gamma_n = \dfrac{T_n^-}{T_n^+}$, this gives

$$\rho_C = \phi_1 = \left[1+\sum_{m=1}^{Z-1}\prod_{n=1}^{m}\gamma_n\right]^{-1} \tag{2.16}$$

for the fixation probability of a single cooperator and

$$\phi_l = \phi_1\left(1+\sum_{m=1}^{l-1}\prod_{n=1}^{m}\gamma_n\right). \tag{2.17}$$

for an arbitrary initial state l.

From Equations (2.12) and (2.13) we obtain, in the weak selection limit,

$$\gamma_n = 1-\delta(\pi_C-\pi_D)+\mathcal{O}(\delta^2) \tag{2.18}$$

$$= 1-\frac{\delta}{Z-1}[n(R-S-T+P)+Z(S-P)-R+P]+\mathcal{O}(\delta^2), \tag{2.19}$$

where in the second equality we have substituted in the payoffs from Equations (2.9)

and (2.10). Thus from Equation (2.16) we obtain an expression for the fixation probabilities in the weak selection limit:

$$\rho_C \approx \frac{1}{Z} + \frac{\delta}{4Z}\left[(R-S-T+P)\frac{2Z-1}{3} - R-S-T+3P+2(S-P)Z\right]. \quad (2.20)$$

Figure 2.2 plots Equation (2.20) in the T-S plane, where we have set $R = 1$ and $S = 0$.
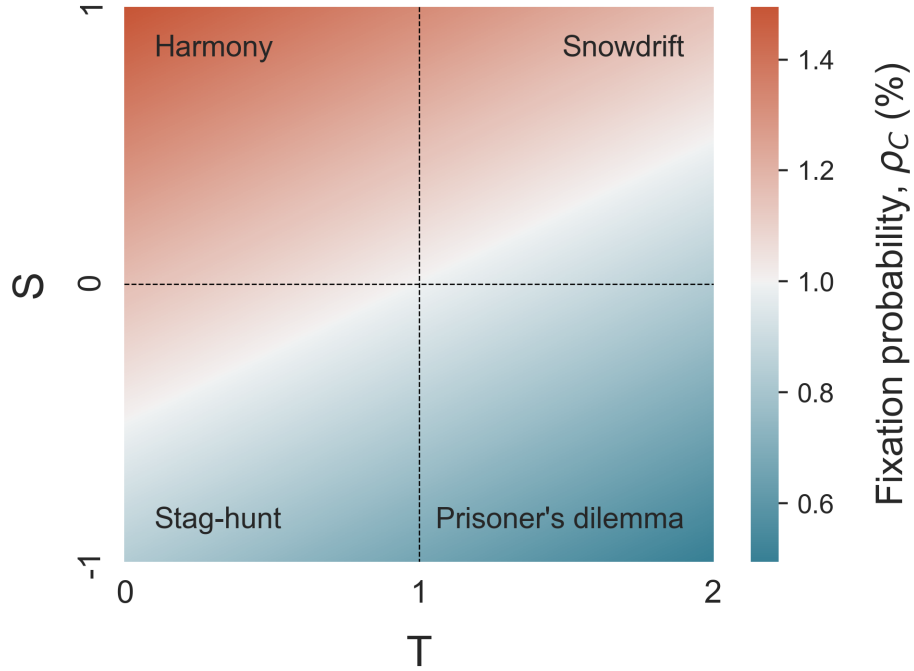
Figure 2.2: Fixation probabilities for a single initial cooperator in a population of $Z = 100$ individuals. The parameter space is divided into four regions corresponding to different social dilemma games. We have set $R = 1$, $P = 0$. Cooperation is a beneficial mutation when $\rho_C > 1/Z$, shown by red. Note that for the prisoner's dilemma cooperation is never beneficial.

In addition to the cooperator fixation probability, we can define the defector fixation probability, ρ_D, and the neutral fixation probability, ρ_0. The latter gives the probability of fixation for a randomly chosen cell in a population of identical cells and is obtained by setting $\delta = 0$. Thus, it is clear from Equation (2.20) that $\rho_0 = 1/Z$. Based on these three fixation probabilities, we can define two measures of success for a cooperative mutant [56, 79]:

- cooperation is a *beneficial* mutation when $\rho_C > \rho_0$,

- cooperation is *favoured* by selection, or has an evolutionary advantage, when $\rho_C > \rho_D$[1].

Similarly, defection is beneficial if $\rho_D > \rho_0$ and favoured if $\rho_D > \rho_C$.

The conditions for a mutant to be beneficial and favoured are not necessarily equivalent. For example, if $\rho_C > \rho_0$ and $\rho_D > \rho_0$, it is possible that $\rho_C < \rho_D$ and thus cooperation is beneficial but not favoured. It is also possible that cooperation is favoured but not beneficial. For payoff matrices which satisfy equal-gains-from-switching, i.e. $R + P = S + T$, $\rho_C > \rho_0$ implies $\rho_C > \rho_0 > \rho_D$ [79]. Thus the fact that a cooperator is favoured guarantees that it is also beneficial if there is equal-gains-from-switching. This holds for the APD game, which we will introduce in Section 2.2.3, for which $S = 1 - T$.

From Equation (2.20) we obtain the condition for cooperation to be a beneficial mutation, given by

$$(Z-2)R + (2Z-1)S > (Z+1)T + (2Z-4)P, \qquad (2.21)$$

which becomes

$$R + 2S > T + 2P \qquad (2.22)$$

in the large population limit, $Z \to \infty$. To find the condition for cooperation to be favoured, we examine the ratio of fixation probabilities

$$\frac{\rho_C}{\rho_D} = \prod_{j=1}^{Z-1} \gamma_j \qquad (2.23)$$

$$\approx 1 - \frac{\delta}{2}[(R-S-T-P)(Z-1) - R - S - T + 3P + 2(S-P)Z] \qquad (2.24)$$

where the approximation is once again taken in the weak selection limit. Thus,

---

[1]This is equivalent to the condition that the equilibrium frequency of cooperators is greater than a half when mutation is allowed [10].

$\rho_C > \rho_D$ is satisfied when

$$(Z-2)R + ZS > ZT + (Z-2)P, \tag{2.25}$$

which in the large population limit $Z \to \infty$, becomes

$$R + S > T + P. \tag{2.26}$$

These conditions are plotted in Figure 2.3
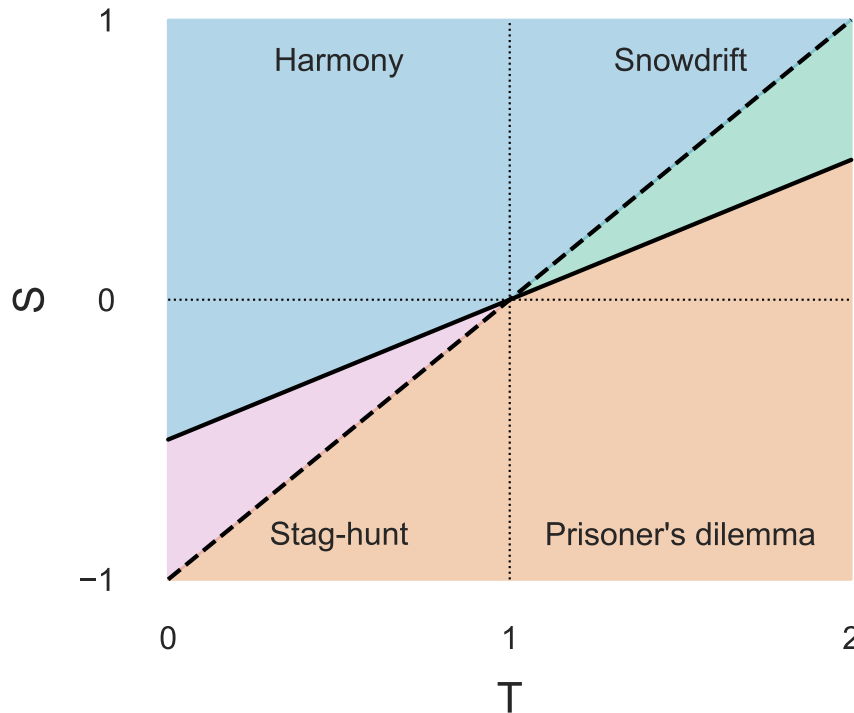
Figure 2.3: Conditions for cooperation to be favoured and beneficial for a pairwise social dilemma game in a large well-mixed population. The dashed line corresponds to $\rho_C = \rho_D$ and the solid line to $\rho_C = \rho_0$. These are $S = 1 - T$ and $S = (1-T)/2$ respectively, by Equations (2.22) and (2.26), where we have set $R = 1$ and $P = 0$.

Blue region (top): C is beneficial and favoured ($\rho_C > \rho_0 > \rho_D$).
Pink region (left): C is favoured but not beneficial ($\rho_0 > \rho_C > \rho_D$).
Green region (right): C is beneficial but not favoured ($\rho_D > \rho_C > \rho_0$).
Orange region (bottom): C is neither beneficial nor favoured ($\rho_C < \rho_0$ and $\rho_C < \rho_D$).

It is clear from Figures 2.2 and 2.3 that cooperation can be beneficial and/or favoured for the stag-hunt and snowdrift games. However, this is never the case for the prisoner's dilemma. As discussed previously, the prisoner's dilemma presents the strongest form of social dilemma, as there is a double incentive to defect (the temptation to increase ones own payoff and the fear that others will defect). This is also consistent with the deterministic result for the prisoner's dilemma, that defection always dominates.

The introduction of spatial structure can promote cooperation, even under the prisoner's dilemma [7, 10, 11]. As the assumption of a well-mixed population will not in many cases be biologically realistic, introducing population structure is a natural extension to the theory. Spatial models have been introduced based on sets [80, 81], phenotype space [82] and graphs [16–18, 21]. In the next section, we introduce evolutionary graph theory, which is most relevant for representing epithelial structure.

2.2.3 Evolutionary graph theory

Evolutionary graph theory provides a framework for incorporating structure into evolutionary models, by representing the population as a fixed graph [16]. This can have a profound effect on evolutionary outcomes, with certain structures amplifying or suppressing selection [83, 84] These effects depend on both the graph topology and the particular update rule, which is used to mediate birth and death and maintain fixed graph structure. Evolutionary games, and cooperation in particular, have been modelled extensively using evolutionary graph theory [14, 17, 18, 21]. Here we introduce the standard evolutionary graph theory framework and explain some key results from the past two decades.

Consider a population of individuals, labelled $i \in \{1, \dots Z\}$, as the vertices of a graph with adjacency matrix

$$A_{ij} = \begin{cases} 1, & \text{if } i \text{ and } j \text{ are neighbours,} \\ 0, & \text{otherwise.} \end{cases} \tag{2.27}$$

The type of individual i is given by $s_i \in \{0, 1\}$, with $s_i = 0$ denoting a defector and $s_i = 1$ a cooperator. The state of the population is then given by the Z-dimensional vector $\mathbf{s}$.

For a population in state $\mathbf{s}$, individual i obtains a payoff $\pi_i(\mathbf{s})$ from its neighbours, which is calculated according to a payoff matrix. For a general 2×2 game, as described by the matrix (2.1), this is given by

$$\pi_i(\mathbf{s}) = s_i s_i^{(1)} R + s_i(1 - s_i^{(1)})S + (1 - s_i)s_i^{(1)}T + (1 - s_i)(1 - s_i^{(1)})P, \qquad (2.28)$$

where

$$s_i^{(1)} = \sum_{j \in G} \frac{A_{ij} s_j}{k_i}, \qquad (2.29)$$

and $k_i = \sum_{j \in G} A_{ij}$ is the degree of vertex i (i.e. number of neighbours). Fitness is then defined to be

$$F_i(\mathbf{s}) = 1 + \delta \pi_i(\mathbf{s}), \qquad (2.30)$$

where $\delta > 0$ is once again the selection strength parameter.

2.2.3.1 The additive prisoner's dilemma

As we saw in Sections 2.2.1 and 2.2.2, the prisoner's dilemma is the strongest form of social dilemma and, for the well-mixed population, always promotes defection. Much of the work done on evolutionary graph theory, therefore, focuses on the APD, which we recall is the additive prisoner's dilemma. In this simplified version of the prisoner's dilemma, cooperators provide a benefit b to their neighbours at a cost c. This is summarised by the payoff matrix

$$\begin{array}{cc} & \begin{array}{cc} C & D \end{array} \\ \begin{array}{c} C \\ D \end{array} & \begin{pmatrix} b-c & -c \\ b & 0 \end{pmatrix} \end{array}, \qquad (2.31)$$

where $b > c$. The payoff to an individual i is, therefore,

$$\pi_i(\mathbf{s}) = -cs_i + b \sum_{j \in G} \frac{A_{ij}s_j}{k_i}. \tag{2.32}$$

Rescalings of the payoff matrix can be absorbed by δ. Therefore, without loss of generality, the game can be defined by a single parameter. This is chosen to be the benefit-to-cost ratio b/c.

As noted in Section 2.2.2, these payoffs have equal-gains-from-switching. Thus, the conditions for cooperation to be beneficial and favoured are equivalent. In the remainder of this section we will introduce some results derived for the APD, before considering how they can be generalised to an arbitrary two-strategy game, as described by Equation (2.1).

One important note is that throughout this thesis we use an average payoff, i.e. the contribution from each neighbour is normalised by the total number of neighbours. An alternative would be to use an accumulative payoff, in which contributions are simply added together. For a regular graph (including a complete graph representing the well-mixed population) this choice does not affect the dynamics other than to alter the selection strength, however for heterogeneous graphs it can impact the dynamics. For example, on scale-free networks, which exhibit high degree heterogeneity, this choice affects whether cooperation is sustainable [9, 79]. For the most part, we are focused on regular graphs, or graphs with small degree heterogeneity.

2.2.3.2 Update rules

Evolution proceeds via a spatial extension of the Moran process [16, 78], whereby at each time step an individual dies and another reproduces. The exact mechanism for this process is decided by the *update rule*, and can have a substantive effect on the evolutionary outcomes. Evolutionary graph theory usually requires a *local* update rule to maintain the fixed graph structure.

Local updating involves a spatial relationship between birth and death events. Two commonly used local update rules are defined as follows:

- *birth-death:* an individual is selected to reproduce with probability proportional to fitness; one of its neighbours is chosen to die uniformly at random;

- *death-birth:* an individual is chosen to die uniformly at random, one of its neighbours is selected to reproduce with probability proportional to fitness.

In both cases, the offspring is able to occupy the empty vertex left after the death has occurred, thus keeping the graph structure fixed [56]. These update rules are sometimes referred to as BD-B (birth-death with selection on birth) and DB-B (death-birth with selection on birth) to emphasise that selection is acting on birth. Alternative update rules, for which selection acts on death, can then be referred to as BD-D and DB-D [85]. In this paper, we limit ourselves to the case where selection acts on birth, thus we do not use this notation to differentiate the two cases.

Under a global update rule, there is no spatial dependence between birth and death events [81]. Thus, the probability of an individual reproducing is dependent only on its own fitness and the population fitness. This contrasts with local update rules, in which local competition plays a role.

Within evolutionary graph theory, the *shift* update rule is an example of global updating. In this case, an individual is chosen to reproduce with probability proportional to fitness, and another is chosen uniformly at random to die. A path is then selected on the graph which connects the two events. Individuals are shifted along this path until there is an empty vertex next to the parent for its offspring to occupy. This kind of update works well on a one-dimensional lattice [62], however it becomes more complex in two dimensions [63]. This is because shifting causes significant rearrangement of individuals and breaks up clusters. Global updating is implemented much more naturally within set or phenotype structured populations [81].

2.2.3.3   Critical benefit-to-cost ratios

The APD is fully described by the benefit-to-cost ratio, b/c. Therefore, we can consider how this parameter affects the success of cooperation. As discussed in Section 2.2.2, we consider that cooperation is beneficial when $\rho_C > \rho_0$ and favoured

when $\rho_C > \rho_D$. However, as the APD has equal-gains-from-switching, these conditions are equivalent. Thus, we can define a single critical benefit-to-cost ratio $(b/c)^*$ at which $\rho_C = \rho_0 = \rho_D$. Cooperation is both beneficial and favoured when $b/c > (b/c)^*$.

The value of $(b/c)^*$ can be considered a measure of the success of cooperation in a particular population, which is defined by its structure and update rule. Low $(b/c)^*$ implies that only a small incentive is needed for cooperation, and thus cooperation is more successful than in the case of high $(b/c)^*$, when a larger incentive is needed.

We saw in Section 2.2.2 that cooperation is never favoured or beneficial for the APD in a well-mixed population. In such a case $(b/c)^*$ is infinite. Similar results are obtained for graph-structured populations with the birth-death update rule. Homogeneous graphs, for example, cannot support cooperation with the birth-death update rule for finite $(b/c)^*$ [17, 20, 56].

On the other hand, the death-birth update rule has been found to support cooperation, and the critical benefit-to-cost ratios have been calculated for various graphs. A simple rule for large k-regular graphs is that $(b/c)^* = k$ in the weak selection limit, $\delta \ll 1$ [17]. Simulation results indicate that this condition also provides a good approximation for random graphs and scale-free networks, where k is taken to be the average number of neighbours. For finite bi-transitive graphs, which include regular graphs, the critical benefit-to-cost ratio

$$(b/c)^* = \frac{Z-2}{Z/k-2},\qquad(2.33)$$

is derived in [20].

More recently, the fixation probabilities and corresponding critical benefit-to-cost ratios have been derived for any graph G in the weak selection limit [14]. This was done by expressing ancestral lineages in terms of random walks and applying coalescence theory. The coalescence time τ_{ij} is the expected meeting time of two independent random walks starting from vertices i and j. These can be found

computationally by solving a Z^2-dimensional system of linear equations

$$\tau_{ij} = \begin{cases} 1 + \frac{1}{2}\sum_k (p_{ik}\tau_{jk} + p_{jk}\tau_{ik}) & i \neq j \\ 0 & i = j, \end{cases} \tag{2.34}$$

where $p_{ij} = A_{ij}/k_i$ is the probability of moving from vertex i to j in a one-step random walk.

Furthermore, we can define t_n, the expected coalescence time from the two ends of an n-step random walk, where the initial vertex for the random walk is chosen with probability proportional to its degree k_i. Letting $p_{ij}^{(n)}$ be the probability of moving from vertex i to j in an n-step random walk, values of t_n can be found by solving the recurrence relation

$$t_{n+1} = t_n + \frac{1}{K}\sum_{i \in G} k_i p_{ii}^{(n)} \tau_i - 1, \tag{2.35}$$

with $t_0 = 0$. Here, $K = \sum_{i \in G} k_i$ and

$$\tau_i = 1 + \sum_{j \in G} p_{ij}\tau_{ij} \tag{2.36}$$

is the expected remeeting time of two random walks starting at i.

For a death-birth update rule and APD game, the cooperator fixation probability is then given by

$$\rho_C = \frac{1}{Z} + \frac{\delta}{2Z}(-ct_2 + b(t_3 - t_1)) + \mathcal{O}(\delta^2) \tag{2.37}$$

and the critical benefit-to-cost ratio is

$$\left(\frac{b}{c}\right)^* = \frac{t_2}{t_3 - t_1}. \tag{2.38}$$

Therefore, by solving computationally for the coalescence times, it is possible to calculate the critical benefit-to-cost ratio for any graph with death-birth updating in the weak selection limit. Results are also derived for the birth-death update rule in

[14].

Thus far, we have considered results for the APD, while neglecting the full spectrum of social dilemma games defined by Equation (2.1). However, it is possible to use the critical benefit-to-cost ratios derived for the APD, to determine the success of mutants under any two-strategy pairwise game by calculating the structure coefficients.

2.2.3.4   Structure coefficients

Recall that a two-strategy game between two players can be defined by a 2×2 payoff matrix, such as Equation (2.1). Individual payoffs are defined on the graph by Equation (2.28). A simple rule for strategy C to be favoured over D is derived in [10] for the weak selection limit. It tells us that $\rho_C > \rho_D$ if

$$\sigma R + S > T + \sigma P, \tag{2.39}$$

where σ is the structure coefficient. This structure coefficient depends on the population structure and update rule, as well as the mutation rate if mutation is allowed. However, it is independent of the game. Note that the condition for C to be favoured is not equivalent to the condition for C to be beneficial ($\rho_C > \rho_0$), unless equal-gains-from-switching is satisfied.

In the case of the APD, the structure coefficient can be written in terms of the critical benefit-to-cost ratio,

$$\sigma = \frac{(b/c)^* + 1}{(b/c)^* - 1}. \tag{2.40}$$

Therefore, the critical benefit-to-cost ratios derived for the APD can be used to find the condition for a mutant to be favoured under any two-strategy pairwise game. However, this does not encompass all classes of games. We now move on to consider what happens when individuals interact within groups.

2.3   Multiplayer games

There are many cases where pairwise games are not the most natural description for interacting individuals. Within the context of animal behaviour, for example,

individuals may cooperate in a group to hunt. Cellular cooperation through the production of diffusible growth factors can also be considered a group interaction, as the benefit is shared between a number of cells within the diffusion range.

In the following, we extend the theory of evolutionary games, introduced in Section 2.2, to incorporate multiplayer games [86] for well-mixed [87, 88] and graph-structured populations [15, 89]. We begin by introducing a general formulation for two-strategy multiplayer games, before focusing on public goods games (PGGs) between cooperators and defectors [25], which provide an analogue for pairwise social dilemma games. We look at how the concept of structure coefficients is generalised to multiplayer games, reporting some known results and deriving structure coefficients for the cycle graph with birth-death and shift update rules.

We consider an arbitrary multiplayer game with two strategies, *A* and *B*. Players interact in groups of size $N = k + 1$, where k is the number of co-players for the focal player. For a well-mixed population co-players are randomly selected from the population, whereas for a graph-structured population they correspond to the nearest neighbours. As a result of these interactions, an *A*-type player receives payoff $a_{j,k}$, while a *B*-type player receives payoff $b_{j,k}$. Here, j is the number of *A* co-players. The fitness of each individual is then defined as $1 + \delta a_{j,k}$ or $1 + \delta b_{j,k}$, where δ is the selection strength parameter. The population evolves according to a Moran process, as described in Sections 2.2.2 and 2.2.3.

2.3.1 Public goods games

Many of the results in the following sections are for general games, however we are focused on PGGs played between cooperators and defectors. These games are defined by a benefit function $b \cdot \beta(x)$ and a cost function which we take to be constant c, with $b > c$. The function $\beta(x)$ is constrained to take values in $[0, 1]$. Here, x is the proportion of cooperators within the interacting group. Thus, the cooperator and

defector payoffs are defined, respectively, as

$$a_{j,k} = b \cdot \beta \left(\frac{j+1}{k+1} \right) - c, \qquad b_{j,k} = b \cdot \beta \left(\frac{j}{k+1} \right). \qquad (2.41)$$

To ensure that the payoff is higher when all players cooperate than when no players cooperate, we enforce the condition $b \cdot \beta(1) - c \geq b \cdot \beta(0)$. Often this is done by setting $c = 1$, $b > 1$, $\beta(1) = 1$ and $\beta(0) = 0$.

The most common PGG, known as the *N*-player prisoner's dilemma (NPD), uses a linear benefit function [72, 90, 91]. However, non-linear benefit functions may be more realistic and can lead to much richer dynamics, even for well-mixed populations [92]. An example is the volunteer's dilemma (VD), which defines the benefit as a Heaviside step function [33, 91, 93–95]. The NPD and VD can be defined by specifying their benefit functions:

$$\beta(x) = x, \qquad\qquad \text{(NPD)} \qquad (2.42)$$

$$\beta(x) = \Theta(x - \tilde{x}), \qquad\qquad \text{(VD)} \qquad (2.43)$$

where $\tilde{x}$ is the critical proportion of cooperators required to receive the benefit and $\Theta(x)$ is the Heaviside step function.

Both the NPD and VD can be represented as limiting cases of a more general sigmoid benefit function. This is defined by

$$\beta(x) = \frac{\alpha(x) - \alpha(0)}{\alpha(1) - \alpha(0)}, \qquad (2.44)$$

where

$$\alpha(x) = \frac{1}{1 + e^{s(h-x)}} \qquad (2.45)$$

is the logistic function, s is the steepness and h is the inflection point. The sigmoid benefit function allows for a wide spectrum of behaviour from purely diminishing returns ($h = 0$) to purely increasing returns ($h = 1$). The NPD and VD are obtained in the limits $s \to 0$ and $s \to \infty$, respectively. This can be seen in Figure 2.4.

To assess the impact of population structure and the choice of update rule on
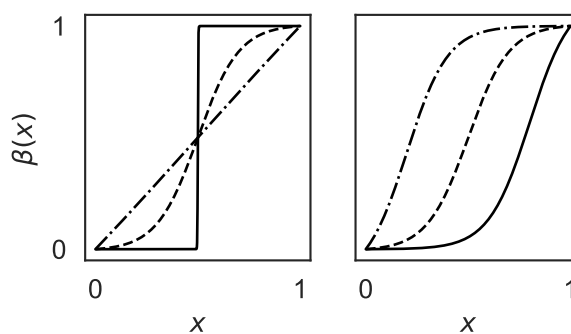
Figure 2.4: Sigmoid benefit function, defined by Equation (2.44). *Left panel: h = 0.5; s = 1* (dash-dot), *s = 10* (dash) and *s = 1000* (solid). We regain the limiting cases by letting *s → 0* (NPD) or *s → ∞* (VD). *Right panel: s = 10; h = 0.2* (dash-dot), *h = 0.5* (dash), *h = 0.8* (solid).

cooperation under these various regimes, we introduce the σ-rule. This is an extension of Equation (2.39), which gave the condition for cooperation to be favoured for a pairwise game. *N*-player games require *N* structure coefficients, which are uniquely defined up to a constant factor [15]. We can, therefore, choose to set one of them equal to one, which is why only a single structure coefficient was required for pairwise games ($N = 2$).

2.3.2 Structure coefficients

Recall from Section 2.2.2, that a strategy *A* is favoured over *B*, when $\rho_A > \rho_B$. The σ-rule, derived in [88], states that

$$\rho_A > \rho_B \iff \sum_{j=0}^{k} \sigma_j (a_j - b_{k-j}) > 0, \qquad (2.46)$$

where σ_j are the structure coefficients. It is assumed here that the group size $N = k+1$ is fixed. Therefore, we have dropped the explicit dependence of the payoffs on k, letting $a_{j,k} = a_j$ and $b_{j,k} = b_j$. Structure coefficients depend on the population structure and update rule, but are independent of the game. If we calculate σ_j for a given population structure and update rule, we can, therefore, determine the favoured strategy for any game by Equation (2.46).

For certain population structures, such as the well-mixed population and the cycle graph, the state is fully described by the number of *A*-players *n*. Thus, we can

define the ratio of fixation probabilities as

$$\frac{\rho_A}{\rho_B} = \prod_{n=1}^{Z-1} \frac{T_n^+}{T_n^-}, \tag{2.47}$$

where $T_n^\pm$ are the transition probabilities to go from $n \to n \pm 1$ A-type individuals [77]. This does not hold in general, as the transition probabilities in more complex population structures will depend on the spatial configurations of different player types, and thus are not uniquely defined by n.

In the remainder of this section, we consider various cases where the structure coefficients can be calculated from transition probabilities in the weak selection limit. For PGGs, we can use Equation (2.46) to obtain the critical benefit-to-cost ratios $(b/c)_1^*$, above which cooperation is favoured. We use the subscript 1 to make clear that, unlike for the APD, the value of b/c above which cooperation is favoured, is not necessarily equivalent to the value above which cooperation is beneficial. For the latter case, we define $(b/c)_0^*$, such that $\rho_C > \rho_0$ when $b/c > (b/c)_0^*$.

2.3.3 Well-mixed population

The structure coefficients for a well-mixed population [87] are given by

$$\sigma_j = \begin{cases} 1, & \text{if } 0 \leq j \leq N-2 \\ \frac{Z-N}{Z}, & \text{if } j = N-1. \end{cases} \tag{2.48}$$

Thus, we can obtain the condition under which $\rho_A > \rho_B$, for any game, by plugging these into Equation (2.46). For a PGG defined by Equation (2.41) the condition that cooperators are favoured is

$$\frac{Z-N}{Z} b \left[\beta(1) - \beta(0) \right] > \sum_{j=0}^{N-1} \sigma_j c. \tag{2.49}$$

Clearly, the shape of the benefit function does not impact whether cooperation is favoured, as this condition depends only on the end points of the benefit function.

The critical benefit-to-cost ratio is given by

$$\left(\frac{b}{c}\right)^*_1 = \frac{N(Z-1)}{Z-N}, \tag{2.50}$$

where we have set $\beta(1) = 1$ and $\beta(0) = 0$. For a large population, this becomes $(b/c)^*_1 = N$.

2.3.4 Cycle graph

Exact expressions for the structure coefficients of the cycle graph can be obtained in the weak selection limit. The cycle is a one-dimensional lattice with periodic boundary conditions. Individuals interact with their two nearest neighbours, thus the group size is $N = 3$.

2.3.4.1 Death-birth update

The structure coefficients for the death-birth update rule are derived in [15]. They are given by

$$\sigma_0 = 1, \qquad \sigma_1 = Z - 2, \qquad \sigma_2 = Z - 3. \tag{2.51}$$

From Equation (2.46) we obtain the conditions for cooperation to be favoured under an NPD, as defined by Equation (2.42). This gives the critical benefit-to-cost ratio

$$\left(\frac{b}{c}\right)^*_1 = \frac{3(Z-2)}{2(Z-3)}, \tag{2.52}$$

which for $Z \to \infty$ becomes $(b/c)^*_1 = 3/2$. Therefore, the conditions for cooperation to be favoured are less stringent than those obtained for a well-mixed population. For a general PGG defined by Equation (2.41) the critical benefit-to-cost ratio is

$$\left(\frac{b}{c}\right)^*_1 = \frac{2(Z-2)}{(Z-3)[\beta(1)+\beta(2/3)-\beta(1/3)-\beta(0)]}. \tag{2.53}$$

2.3.4.2 Birth-death update

We derive the structure coefficients for the birth-death update rule, following a similar method used in [15] for the death-birth updating. For the cycle, the transition

probabilities are uniquely defined by the number of A-players in the population n. Thus, we can write down the ratio of transition probabilities, which for a birth-death update are

$$\frac{T_n^+}{T_n^-} = \begin{cases} (1 + \delta a_0)/(1 + \delta b_1), & \text{if } n = 1 \\ (1 + \delta a_1)/(1 + \delta b_1), & \text{if } 1 < n < Z - 1 \\ (1 + \delta a_1)/(1 + \delta b_2), & \text{if } n = Z - 1. \end{cases} \tag{2.54}$$

Substituting these into Equation (2.47), and taking the limit, $\delta \ll 1$, we obtain

$$\frac{\rho_A}{\rho_B} \approx 1 + \delta[a_0 - b_2 + (Z - 2)(a_1 - b_1)]. \tag{2.55}$$

In order that $\rho_A > \rho_B$, the second term must be positive. Thus, comparing this condition with Equation (2.46), we find the structure coefficients

$$\sigma_0 = 1, \qquad \sigma_1 = Z - 2, \qquad \sigma_2 = 0. \tag{2.56}$$

For the NPD, cooperation is favoured when b/c is greater than

$$\left(\frac{b}{c}\right)_1^* = \frac{3(Z - 1)}{Z - 3}, \tag{2.57}$$

which becomes $b/c > 3$ in the limit, $Z \to \infty$. These conditions are equivalent to those obtained for the well-mixed population. For a general PGG defined by Equation (2.41) the critical benefit-to-cost ratio is

$$\left(\frac{b}{c}\right)_1^* = \frac{Z - 1}{(Z - 3)[\beta(2/3) - \beta(1/3)]}. \tag{2.58}$$

Interestingly, this depends only on the internal points of the benefit function. This differs from the result for the well-mixed population, which depends only on the end points, $\beta(0)$ and $\beta(1)$.

2.3.4.3 Shift update

We follow the same procedure to derive the structure coefficients for the shift update rule. This time the ratio of transition probabilities is given by

$$\frac{T_n^+}{T_n^-} = \begin{cases} \frac{(Z-1)(1+\delta a_0)}{2(1+\delta b_1)+(Z-3)(1+\delta b_0)}, & \text{if } n = 1 \\[2ex] \frac{(Z-n)(2(1+\delta a_1)+(n-2)(1+\delta a_2))}{n(2(1+\delta b_1)+(Z-n-2)(1+\delta b_0))}, & \text{if } 1 < n < Z-1 \\[2ex] \frac{2(1+\delta a_1)+(Z-3)(1+\delta a_2)}{(Z-1)(1+\delta b_2)}, & \text{if } n = Z-1. \end{cases} \qquad (2.59)$$

Letting $\delta \ll 1$, Equation (2.47) becomes

$$\frac{\rho_A}{\rho_B} \approx 1 + \delta \left[(a_0 - b_2) + 2(H_{Z-1} - 1)(a_1 - b_1) + (Z - 2H_{Z-1})(a_2 - b_0) \right], \quad (2.60)$$

where H_m is the m-th harmonic number:

$$H_m = \sum_{n=1}^{m} \frac{1}{n}. \qquad (2.61)$$

Thus, the structure coefficients are given by

$$\sigma_0 = 1, \qquad \sigma_1 = 2(H_{Z-1} - 1), \qquad \sigma_2 = (Z - 2H_{Z-1}). \qquad (2.62)$$

The critical benefit-to-cost ratio for the NPD is

$$\left(\frac{b}{c}\right)_1^* = \frac{3(Z-1)}{3(Z-1) - 4H_{Z-1}}. \qquad (2.63)$$

In the large population limit, this becomes $(b/c)_1^* = 1$. As the NPD requires that $b > c$, cooperation is always favoured in the large population limit for a shift update under weak selection.

In fact, if we consider a general cooperation game as defined by Equation (2.41) we obtain

$$\left(\frac{b}{c}\right)_1^* = \frac{1}{\beta(1) - \beta(0)} \qquad (2.64)$$

in the large population limit, $Z \to \infty$. Letting $\beta(1) = 1$ and $\beta(0) = 0$, we again

obtain $(b/c)_1^* = 1$. Thus, for the shift update on the cycle, as with the well-mixed population, the condition for cooperation to be favoured is not dependent on the shape of the benefit function (although in this case we required the large population limit). Furthermore, cooperation is favoured for the cycle with shift update for all PGGs, as defined by Equation (2.41), given that the population is sufficiently large.

2.3.5 Regular graphs

In higher dimensions, the transition probabilities are no longer uniquely defined by the number of A-players in the population, but depend also on their configuration. Expressions for the structure coefficients of k-regular graphs, with $k \geq 3$ and death-birth updating, have been derived [15] using pair approximation and diffusion approximation [17]. It was found, for a VD game, that the predicted results fit well with simulation data for random regular graphs, but they underestimate the critical benefit-to-cost ratio for lattices [15].

We do not state the full expressions here, which are non-trivial functions of k. However, they yield a simple condition for cooperation to be favoured with the NPD in the large population limit, $Z \gg k$. The critical benefit-to-cost ratio in this case is given by

$$\frac{b}{c} > \frac{k+1}{2}.$$
(2.65)

2.4 Other population types and extensions

In the preceding sections, we have given an overview of the aspects of evolutionary game theory most relevant to this thesis. However, this is by no means a comprehensive overview of this vast topic. Before concluding, therefore, we will briefly mention several extensions which, while not explored fully in this thesis, are relevant for future research.

We have focused exclusively on symmetric two-strategy games. Of course, games can be asymmetric [96] and have many strategies [97]. Indeed interactions between tumour cells have been modelled as games with three [43] or more strategies [45, 47]. Furthermore, strategies need not even be discrete. The evolution of continuous traits is modelled using adaptive dynamics [39, 98], which have also

been applied to cancer [99].

Evolutionary graph theory, as we have seen, allows for the introduction of structure, whereby a population is represented as a static graph. This is not the only possible representation of population structure, however. Other studies have considered set-structured populations [80], as well as those organised in phenotype space [82], both of which are able to promote cooperation. Unlike fixed graphs, populations structured by sets or phenotypic similarity use global updating (see Section 2.2.3.2), so the probability of reproduction depends on the individual fitness and total population fitness, rather than local effects.

For fixed graph-structured populations, it is possible to incorporate motion, by allowing individuals to swap vertices [22]. Dynamic graphs have also been studied, whereby individuals are able to alter their edge connections based on their interactions [58–60].

Thus far, we have considered PGGs where the benefit is shared equally within a group. A further extension is to consider the public good explicitly diffusing through the population. One example is a model in which a public good diffuses through a graph-structured population and the benefit to cells is proportional to the local concentration of public good [15]. More recently a model has been developed which explicitly represents the production, diffusion and decay of a public good in continuous space [100].

2.5 Discussion

Evolutionary game theory provides a comprehensive framework for modelling the evolution of cooperation within a population. We have provided an overview of the theory for both pairwise and multiplayer games in well-mixed and structured populations. It is clear that there are three key determinants for the evolutionary success of cooperation: the game, the population structure, and the update rule. The choice of game is clearly important. For pairwise games, we have seen that cooperation can succeed for the snowdrift and stag-hunt games in well-mixed populations, but not for the prisoner's dilemma. In general, whether cooperation is favoured is

summarised by the σ-rule, given by Equations (2.39) and (2.46) for pairwise and multiplayer games, respectively. These depend on the specific game parameters.

The role of population structure and update rule in Equations (2.39) and (2.46), is summarised by structure coefficient σ_i. The effects of each are difficult to disentangle from one another, and while it is commonly accepted that population structure promotes cooperation, this is clearly not always the case. We have seen a number of examples where a birth-death update rule leads to outcomes indistinguishable from the well-mixed population. Thus, the cooperation-promoting effects of the population structure appear to be suppressed by this choice of update rule. By contrast, population structure with death-birth updating does promote cooperation. Results for the cycle graph suggest that global update rules, such as the shift update, can promote cooperation in structured populations, more so even than the death-birth update.

The central question of this thesis is to consider how population structure and tissue dynamics affect the ability of cooperative mutants to succeed in epithelia. It is clearly possible to incorporate realistic epithelial structure into the evolutionary graph theory framework. However, the impact of tissue dynamics is less clear. An epithelium is a dynamic structure, with new cells arising after division, and cells leaving the tissue due to apoptosis, extrusion, or differentiation. How these processes are connected will clearly impact the update dynamics and therefore should determine our choice of update rule. However, it is not clear that any choice of update rule available within evolutionary graph theory is appropriate. To consider these questions, we go beyond evolutionary graph theory and incorporate evolutionary games into an explicit tissue model, which is able to more realistically represent epithelial dynamics.

Chapter 3

Modelling epithelia

3.1 Introduction

Multicellular organisms are built of cells, which are tightly regulated to maintain the life of the whole. Cells are organised into tissues, which in turn form organs. Epithelia are the tissues which form surfaces, such as skin and the linings of organs. They consist of sheets of tightly packed cells, which can be single-layered (simple) or multilayered (stratified). We focus on simple epithelia.

Epithelial cells are approximately polygonal on their apical surfaces. These polygons have characteristic side number distributions, which are remarkably conserved across a range of animal and plant species [101, 102]. Without exception, the most common cell shape in an epithelium is the hexagon, and the distributions are uni-modal with a low probability of having more than seven or less than five sides.

This characteristic epithelial structure must be taken into account when considering evolutionary dynamics. An epithelium could be represented as a planar graph, for example, a hexagonal lattice would be a reasonable first approximation. More realistic representations, which incorporate variation in neighbour number, can be obtained using a Voronoi tessellation (VT) which has been shown to replicate the topological properties of epithelia [103, 104].

A VT is a partitioning of the plane, or some domain, into regions based on the placement of seeds [105, 106]. Each Voronoi region is defined to contain every
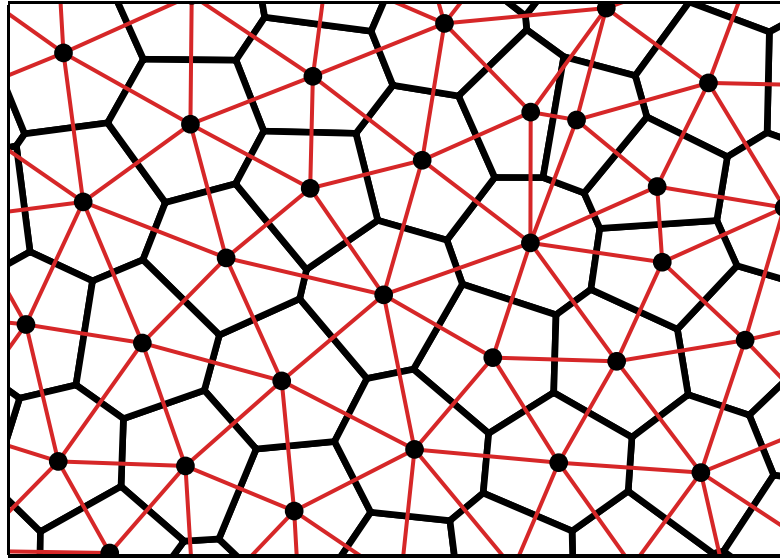
Figure 3.1: Voronoi tessellation (VT, black) and Delaunay triangulation (DT, red) of a set
of seeds. The VT divides the plane into polygons such that every point in a
polygon is closer to its corresponding seed than any other. The DT partitions
the plane into triangles, with the seeds as vertices, and is the dual graph to the
VT. In the VT model, the seeds correspond to cell centres, and spring forces
act along the lines of the DT.

point in the domain closer to the given seed than any other. Cell shapes correspond
to these Voronoi regions, which are polygons. The dual graph of the VT, known as
the Delaunay triangulation (DT), corresponds to the neighbour structure. The VT
and DT for a given set of seeds are shown in Figure 3.1.

Epithelia have conserved topological properties, however they are not static
structures. Constituent cells within an epithelium are undergoing a number of dy-
namic processes. Cells grow and proliferate by cell division. They are able to move,
thus leading to rearrangements of cell neighbours. Cells may also leave the tissue
for various reasons, such as differentiation (cell specialisation), live-cell extrusion,
or apoptosis (programmed cell death).

For adult homeostatic tissues, it is vital that these processes are well-regulated.
If the cell population is depleted, the epithelium will no longer perform its barrier
function [107]. Over-proliferation on the other hand, can lead to tumour forma-
tion. Thus, to maintain homeostatic population size, the number of cell divisions
must match the number of cell deaths [108–111]. We use the term death here, and
throughout this thesis, to refer to any event causing a cell to leave the tissue, includ-

ing differentiation, whereby cells become specialised.

In Chapter 2 we saw that evolutionary dynamics are impacted, not only by the structure of a population, but also by the update rule, which defines how birth and death occur. In order to maintain the static graph structure required in evolutionary graph theory, these update rules tend to make the restriction that birth and death occur simultaneously at neighbouring sites (the exception is the shift update rule, see Section 2.2.3.2).

To relax this restriction, we seek to utilise an explicit tissue model, rather than relying on static graph representations. In the remainder of this section, we give an overview of the literature on agent-based tissue modelling, before outlining the VT model in detail, which is used throughout this thesis. Finally, we consider two alternative ways in which the population can be updated, while maintaining homeostasis. The first way is by spatially decoupling birth and death, while still maintaining temporal coupling, so the population size remains constant. The second is by introducing contact inhibition into the model, which enables the epithelium to maintain homeostatic population size. This leads to some level of spatial coupling between division and death, which depends on the strength of contact inhibition.

3.2 Agent-based tissue modelling

Agent-based tissue models represent cells as discrete units, with tissue level behaviour emerging as a result of cellular interactions. Models of this type, in contrast to continuum tissue models, are ideal for our purpose, as evolutionary processes are also based on cellular behaviour. There is an extensive literature on agent-based tissue models, which can be separated into two categories: lattice-based and lattice-free models. These can be in two- or three- dimensions, however we are focused on the former, as they are able to provide good representations of epithelial sheets and are computationally much faster. For a comprehensive review, the reader is referred to [112]. Here we will outline the main types of model, before describing the VT model in detail, which is used throughout this thesis.

3.2.1 Lattice-based models

The defining characteristic of lattice-based models is that the spatial arrangement of cells is restricted by some sort of lattice. This could be a regular grid, such as a square or hexagonal lattice, or a more realistic non-symmetric structure. Whichever lattice is chosen, it remains fixed throughout the simulation.

The simplest examples are cellular automata, whereby each lattice site can be occupied by a single cell [113–116]. These cellular automata models incorporate cell death, division, and movement, but are not able to represent mechanical processes. Death is simple to implement by removing the cell and leaving an empty lattice site. Division can be realised by placing one progeny cell at the lattice site of the parent, and a second in a neighbouring empty site. If no such site is available, the parent cell may be able to shift cells along to make space for its progeny. Movement can be incorporated by a simple swapping procedure. Additionally, cells may attempt to move to empty lattice sites or push cells out the way.

The cellular Potts model is a more complex lattice-based model, whereby each cell consists of multiple lattice sites [117]. Variation in cell area and shape is therefore possible, and some mechanical processes can be incorporated. Furthermore, cell divisions can be implemented without the shoving process needed for the cellular automaton, simply by assigning half the lattice sites of a parent cell to each progeny cell. The cellular Potts model has been used to model a range of processes such as morphogenesis [118, 119], angiogenesis [120] and tumour growth [121, 122].

3.2.2 Lattice-free models

Lattice-free models are not restricted by a discrete lattice structure, but rather represent cells in continuous space. Here we outline the two main classes of lattice-free models: cell-centre and vertex models.

As the name suggests, cell-centre models represent the tissue as a set of points corresponding to cell centres, which move freely in space and exert forces on one another. Different cell-centre models are characterised by the choice of force law and the definition of cell size/shape and neighbourhood.

Force laws range from spring-like forces governed by Hooke's law [67], to more complex nonlinear laws, which incorporate repulsion and adhesion forces [123, 124]. There are two main methods for determining cell neighbourhood. Models of overlapping spheres define an interaction radius, such that all cell centres inside the radius belong to that cell's neighbourhood [125]. Alternatively, in the VT model, the neighbourhood is defined by performing a VT on the set of cell centres. Recall from Section 3.1, that a VT is a partitioning of the plane into polygons. Thus, the VT not only defines the neighbourhood structure, but also the shape of each cell. The VT model has been used extensively to represent intestinal crypt dynamics [67, 68], as well as to study tissue mechanics [124] and cell fate selection [126]. Further details of the VT model are provided in Section 3.3.

An alternative class of lattice-free models are vertex models. These represent the tissue by the positions of cell vertices, which form polygonal cells. Vertices are subject to forces and move in space [127]. These forces consist area elasticity, line tension, and contractility contributions [128]. Additional rules must be implemented to mediate cell neighbour rearrangements. Vertex models have been used extensively in studies of packing geometry and epithelial morphogenesis (see [129, 130]).

In selecting a model for the purposes of this thesis, we had several competing priorities. Evolutionary processes occur over large timescales and it is necessary to run a large number of simulations to determine quantities such as fixation probabilities (see Chapter 2). Therefore, computational speed is desirable. However, the cellular automata, which is by far the fastest and simplest agent-based tissue model, is not ideal for our purposes. In particular, cell division relies on moving cells along a path to make space for the new cell. This process is reminiscent of the shift update rule implemented in evolutionary graph theory (see Section 2.2.3), and can lead to instantaneous topological effects at a considerable distance from the division event, which has evolutionary consequences.

We, therefore, prefer to choose a model that is able to incorporate division and death with only local topological effects. While the cellular Potts, overlapping

spheres, and vertex models all satisfy this requirement, we choose to use the VT model. This is because, as a cell-centre model, it very naturally provides the graph structure needed for evolutionary modelling. Furthermore, it uses a very simple force law, and, compared to overlapping spheres, has a more realistic and well-defined concept of area and cell shape. However, we note that other choices of model would also be acceptable, in particular the vertex model could provide a good alternative.

3.3 Voronoi tessellation model

In this section, we outline the VT model [67, 68, 131] used throughout this thesis. Parameter values used in Chapters 4 and 5 can be found in Table 4.1 and those used in Chapter 6 in Table 6.1.

The VT model is a cell-centre model. Cells exert spring-like forces on one another, with spring constant μ, such that

$$\mathbf{F}_{ij}^S(t) = -\mu\hat{\mathbf{r}}_{ij}(t)(|\mathbf{r}_{ij}(t)| - s_{ij}(t)) \tag{3.1}$$

is the force exerted on cell i due to j. Here $\mathbf{r}_{ij} = \mathbf{r}_i - \mathbf{r}_j$, is the displacement vector pointing from j to i and $\hat{\mathbf{r}}_{ij}$ is the corresponding unit vector, with $\mathbf{r}_i$ indicating the position of i. The natural separation between cells, $s_{ij}(t) = s_M$, is constant and the same for all neighbour pairs. The exception to this is for newborn sibling cells for whom s_{ij} grows linearly, from ε to s_M, over time period t_M. This period corresponds to the mitosis part of the cell cycle, i.e. the time it takes for a cell to divide. In some cases, it will be set to zero.

Defining $\mathcal{N}_i(t)$ to be the set of cells neighbouring i, the total force acting on cell i is given by

$$\mathbf{F}_i^S(t) = \sum_{j \in \mathcal{N}_i(t)} \mathbf{F}_{ij}^S. \tag{3.2}$$

The cellular environment is highly viscous, with drag forces dominating over inertia (low Reynolds number) [132–134]. It is therefore usual to ignore inertial forces,

resulting in a first-order equation of motion for each cell i, given by

$$\eta \frac{d\mathbf{r}_i}{dt} = \mathbf{F}_i^S(t)\,, \tag{3.3}$$

where η is the drag coefficient. This is solved numerically using a forward Euler method:

$$\mathbf{r}_i(t + \Delta t) = \mathbf{r}_i(t) + \frac{\Delta t}{\eta} \mathbf{F}_i^S\,, \tag{3.4}$$

where Δt is a sufficiently small time step for numerical stability.

The cell shapes correspond to Voronoi regions, which are obtained by performing a VT using the cell centres as seeds. Each cell, therefore, has a well-defined shape and area within the VT model. The dual graph of the VT is known as the Delaunay triangulation. This comprises vertices corresponding to each cell, and edges, which connect neighbouring cells. Thus, performing the VT also defines the neighbour connections which are used to determine the forces. Neighbours will also be important for determining cell fitnesses, when we introduce evolutionary game theory into the model in Chapter 4. To account for topological changes which may occur, it is necessary to recompute the VT after every timestep during which cells may have moved, divided or died.

It is simple to implement division and death events within the VT model. When death occurs, the cell centre is removed from the tissue and a VT is performed. For a division, the cell centre is removed and two new centres are placed, separated by a small distance ε, across a uniformly random axis. These events result in local topological changes, rather than long range effects.

3.4   Division and death in homeostatic epithelia

There is significant freedom in choosing how and when divisions and deaths occur within the VT model. Our main constraint is that homeostasis must be maintained, else there is a risk the population will die out or grow excessively. Within evolutionary graph theory, as outlined in Chapter 2, it is guaranteed that the population size is constant, as birth and death events occur simultaneously via the Moran process.

However, it also requires that the population structure is static, and birth and death are spatially coupled by a local update rule.

We take advantage of the greater flexibility within the VT model to define a decoupled update rule, whereby birth and death occur simultaneously, but are spatially independent. This is an example of a global update rule (see Section 2.2.3.2). The population size therefore remains constant, however the population structure is dynamic. In contrast to the discrete time Moran process commonly used in evolutionary graph theory, a continuous time process fits more naturally with the VT model. As our focus is on fixation probabilities, rather than fixation times, we can compare results between the two models.

The decoupled update rule models epithelial dynamics under the assumption that birth and death are spatially independent of one another. This allows us, in Chapters 4 and 5, to examine the opposite extreme to the local update rules used in evolutionary graph theory, where birth and death are tightly coupled, and compare the two.

In a real epithelium, the spatial coupling of birth and death will be connected to its mechanisms for maintaining homeostasis. These mechanisms are still being understood experimentally; however, there is a growing body of evidence that both density-dependent proliferation [108, 135] and density-dependent cell extrusion could play an important role [136, 137].

Density-dependent control of division or death is likely to result in some level of spatial coupling between the two processes, therefore the specifics of these mechanisms could play an important role in the evolutionary dynamics of the tissue. We, therefore, also consider a model where homeostasis is maintained by density-dependent proliferation, i.e. contact inhibition. We choose to focus on density-dependence of proliferation, because there is evidence that it plays the more important role in homeostatic tissues [110], while density-dependence of death is more important in developing tissues [111, 136]. The VT model with contact inhibition, which we introduce in Chapter 6, allows for fluctuations of population size around an equilibrium. It provides an intermediate and more realistic model of spatial cou-

pling in between the local and decoupled update rules.

3.5 Discussion

In this chapter, we have outlined some of the key properties of epithelia that are likely to affect their evolutionary dynamics, in particular their structure and update dynamics. We have considered how an epithelium may be modelled within evolutionary graph theory, by representing the population as a hexagonal lattice or VT, as well as the limitations of this approach. Namely, that it is necessary to enforce a local update rule to maintain the fixed graph structure.

To remove this limitation, we have considered how epithelial dynamics can be represented explicitly with agent-based tissue models. We have outlined a number of lattice-based and lattice-free models commonly used in the literature, and chosen to focus on the VT model. This cell-centred model is simple to integrate with evolutionary models, and crucially, allows divisions and deaths to occur with only local rearrangements of the population structure.

Using the VT model, we have substantial flexibility to explore how the update dynamics affect evolutionary outcomes. Initially, we will focus on the case where division and death are spatially decoupled, considering how this affects the evolutionary dynamics of pairwise social dilemma games and multiplayer public goods games in Chapters 4 and 5, respectively. We will then consider how density-dependent proliferation, which maintains homeostatic population size, causes spatial coupling of division and death that is intermediate between the decoupled update rule and death-birth update rule. We will explore in Chapter 6 how this affects evolutionary outcomes for pairwise games.

Chapter 4

Pairwise games between epithelial cells

This chapter is based on the paper: Jessie Renton and Karen M. Page. Evolution of cooperation in an epithelium. *Journal of the Royal Society Interface*, 16:20180918, 2019 [138].

4.1 Introduction

In this chapter, we begin our analysis of the impact of population structure and dynamics on cooperative success in an epithelium. We consider the case where birth and death are spatially decoupled by incorporating evolutionary dynamics into the VT model. We consider pairwise social dilemma games, which we introduced in Section 2.2, primarily focusing on the additive prisoner's dilemma (APD). We choose this game as a starting point, as it can be described by a single parameter, and is a particularly strong form of social dilemma. In Chapter 5 we extend the analysis to multiplayer public goods games.

This chapter is set out as follows. In Section 4.2, we outline the model, which integrates evolutionary game theory with the VT model, before deriving approximate analytic results for the cooperator fixation probabilities. These are verified by simulation results. Section 4.3 then considers results from evolutionary graph theory and how these compare with the VT model. We find that cooperation is significantly promoted under the VT model and postulate that this is due to the de-

coupling of birth and death. To verify this we implement a death-birth update rule in the VT model. We also introduce a migration analogue into evolutionary graph theory simulations to consider whether there could be an effect due to cell rearrangement in the VT model. Our results confirm that the decoupling of birth and death promotes cooperation in the VT model, and migration may be having a minor deleterious effect. In Section 4.4 we extend our results to general pairwise social dilemma games.

4.2 Evolutionary games in the Voronoi tessellation model

4.2.1 The model

The framework used here integrates evolutionary game theory with the VT model. These are described extensively in Chapters 2 and 3 respectively. Here we outline the integrated model for pairwise games.

Recall that the VT model represents a two-dimensional tissue, such as an epithelium, as a set of points corresponding to the cell centres. This model is described in Section 3.3 and we use the parameters summarised in Table 4.1 throughout this chapter.

Table 4.1: Parameters for the Voronoi tessellation model used in Chapters 4 and 5. Space is measured in units of cell diameter (CD). Explicit units are not given for μ and η, as the cell dynamics depend only on their ratio μ/η, which has units h^{-1}. Note that μ has dimensions [mass]/[time]^2 and η has dimensions [mass]/[time].

Symbol	Description	Value
Z	Population size	100
μ	Spring constant	50.0
η	Drag coefficient	1.0
t_M	Growth time for new cells	1.0 hours
s_M	Natural separation of mature cells	1.0 CD
ε	Initial separation of sibling cells	0.1 CD
Δt	Time step	0.005 h
λ	Division & death rate	12.0^{-1} h^{-1}

The cells are labelled $i \in \{1, \ldots Z\}$, for a population size Z. Cell shapes are

defined by performing a VT on these points. Recall that the dual graph to the VT is the DT, which defines the connectivity graph, G. This graph has adjacency matrix

$$A_{ij}(t) = \begin{cases} 1, & \text{if } i \text{ and } j \text{ are neighbours at time } t, \\ 0, & \text{otherwise.} \end{cases} \qquad (4.1)$$

Cell fitnesses can therefore be determined from this adjacency matrix, in the same way as they are in evolutionary graph theory (see Section 2.2.3). The main difference is that the graph is no longer static, thus the adjacency matrix is time dependent. For the APD, cooperators provide a benefit $b > c$ to their neighbours at a cost $c > 0$. Thus, the payoff to cell i is

$$\pi_i(\mathbf{s}) = -cs_i + b \sum_{j \in G} \frac{A_{ij}s_j}{k_i} , \qquad (4.2)$$

where $k_i = \sum_{j \in G} A_{ij}$ is the degree of vertex i (i.e. number of neighbours). Fitness is then

$$F_i(\mathbf{s}) = 1 + \delta \pi_i(\mathbf{s}) , \qquad (4.3)$$

where $\delta \geq 0$ is the selection strength parameter and the constant 1 takes into account other contributions to fitness. As rescalings of the payoffs can be absorbed by δ, the APD can be defined by the single parameter, b/c.

The population evolves according to a Moran process, whereby division and death events occur simultaneously. However, in contrast to evolutionary graph theory, we implement the process in continuous rather than discrete time. We note that a translation to continuous time in evolutionary graph theory models does not affect fixation probabilities [14], and therefore the results are directly comparable between discrete and continuous time.

In the continuous time Moran process update events occur at exponentially distributed times with per-cell rate λ. When an update event occurs a parent cell is chosen at random from the population with probability proportional to fitness. This cell divides creating two offspring cells, which are exact clones of the parent.
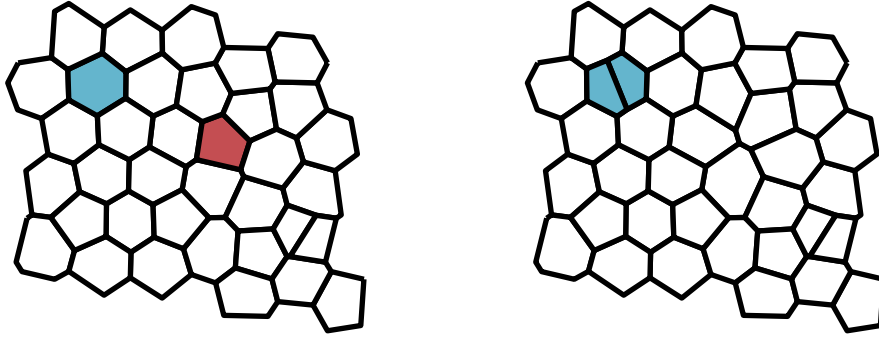
Figure 4.1: Spatially decoupled update rule in the Voronoi tessellation model. When an update event occurs a parent cell is chosen to reproduce with probability proportional to fitness (blue). A second cell is chosen to die uniformly at random (red). The parent cell divides across a random axis, and the dead cell is removed from the tissue.

Simultaneously, a cell is chosen to die and removed from the population. If the same cell is chosen to divide and to die, it produces a single offspring cell. We call this a *decoupled* update rule, as there is no spatial dependence between birth and death events (see Figure 4.1). It is an example of a global update rule, as described in Section 2.2.3.2.

To calculate fixation probabilities for a single mutant cooperator invading a defector population in the VT model, we run simulations as follows. We begin with defector cells placed on a regular hexagonal lattice with periodic boundary conditions and the simulation algorithm proceeds until the system has relaxed into a dynamic equilibrium. We then choose a random cell to become a cooperator and continue the simulation until only cooperators or defectors remain. The simulation algorithm consists of the following steps:

  (i) DT is performed to determine the cell neighbours,

 (ii) forces are calculated and the cells moved accordingly,

(iii) an update event occurs with probability $Z\lambda\Delta t$.

Time snapshots for an example simulation are shown in Figure 4.2. In this example, the simulation was initiated with a single neutral mutant (i.e. $\delta = 0$) and run to fixation.
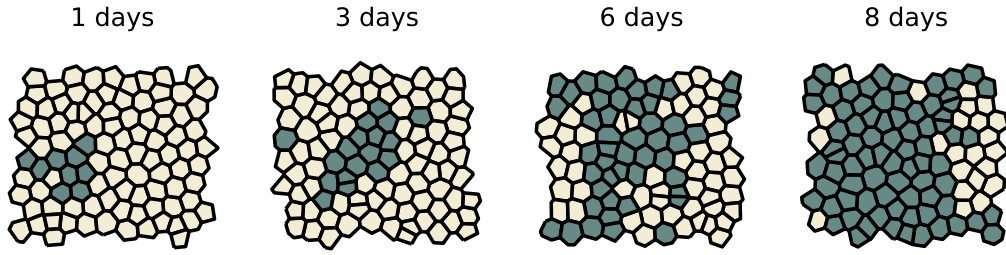
Figure 4.2: Time snapshots for a simulation of mutant invasion in the Voronoi tessellation model with decoupled update rule. The simulation is initialised with a single neutral mutant (grey) in a population of $Z = 100$ cells and run until fixation. Selection is neutral ($\delta = 0$), so all cells have equal fitness. Parameters for the Voronoi tessellation model are given in Table 4.1.

4.2.2 Approximating the fixation probabilities

Due to the complexities of the VT model it is not possible to derive exact analytical expressions for the fixation probabilities. Instead we look for approximate solutions by considering the expected fitness for different cell types in populations with a given number of cooperators [139]. Although the graph is dynamic and dependent on the spatial distribution of points, it is also planar and mechanically constrained by the intercellular forces. Furthermore, if we begin with a single mutated cell, its progeny are likely to remain in a cluster as the clone grows. Thus, we assume that variation in fitnesses for cells of each type will be small, for a given number of cooperators in the population, and that the average over a large number of states is a reasonable approximation.

Let $S_n = (\mathbf{s}_n, G)$ denote a state with n cooperators, where $\mathbf{s}_n$ is the vector of cell types and G is the graph. Then $T^{+/-}(S_n)$ is the probability that, when an event occurs, the number of cooperators is increased/decreased by one, i.e

$$T^+(S_n) = \left(1 - \frac{n}{Z}\right) \frac{\sum_{i \in G} s_i F_i}{\sum_{i \in G} F_i} \qquad (4.4)$$

$$T^-(S_n) = \frac{n}{Z} \left(1 - \frac{\sum_{i \in G} s_i F_i}{\sum_{i \in G} F_i}\right). \qquad (4.5)$$

We can then define the average transition probabilities for a state with n cooperators to be $T_n^{\pm} = \langle T^{\pm}(S_n) \rangle$ where the average is taken over a large ensemble of possible

states. Substituting in for the fitnesses (4.3) and taking the weak selection limit $\delta \ll 1$ we obtain

$$T_n^+ = \frac{n}{Z}\left(\frac{Z-n}{Z}\right)(1 + \delta\langle\pi_C - \pi\rangle_0) + \mathcal{O}(\delta^2) \tag{4.6}$$

$$T_n^- = \frac{n}{Z}\left(\frac{Z-n}{Z}\right)\left(1 - \frac{n}{Z-n}\delta\langle\pi_C - \pi\rangle_0\right) + \mathcal{O}(\delta^2)\,, \tag{4.7}$$

where $\langle.\rangle_0$ denotes an average over a large ensemble of possible states for the neutral process $\delta = 0$, and

$$\pi_C = \frac{1}{n}\sum_{i \in G} s_i \pi_i \qquad\qquad \pi = \frac{1}{Z}\sum_{i \in G} \pi_i\,. \tag{4.8}$$

These are the population mean cooperator fitness and population mean fitness, respectively. From (4.2) and (4.8) we obtain

$$\langle\pi_C - \pi\rangle_0 = -c\left(1 - \frac{n}{Z}\right) + b\left(\Lambda_n^{CC} - \frac{n}{Z}\right)\,, \tag{4.9}$$

where

$$\Lambda_n^{CC} = \frac{1}{n}\left\langle\sum_{i,j \in G} \frac{s_i s_j A_{ij}}{k_i}\right\rangle_0 \tag{4.10}$$

is the expected proportion of cooperator neighbours for a cooperator in a population with n cooperators. This can be calculated computationally by running simulations for a neutral process ($\delta = 0$) and tracking clones (groups of cells with common ancestry). At each time interval, we calculate the contribution to Λ_n^{CC} for all clones in the system, treating each lineage as a group of n cooperators in a population of defectors. Figure 4.3 plots Λ_n^{CC} for $Z = 100$.

We use the equation for cooperator fixation probability derived in [76] (see Section 2.2.2) for a well-mixed population:

$$\rho_C = \left[1 + \sum_{m=1}^{Z-1}\prod_{n=1}^{m} \gamma_n\right]^{-1}\,, \tag{4.11}$$

where $\gamma_n = T_n^-/T_n^+$. For the well-mixed population, the transition probabilities, and
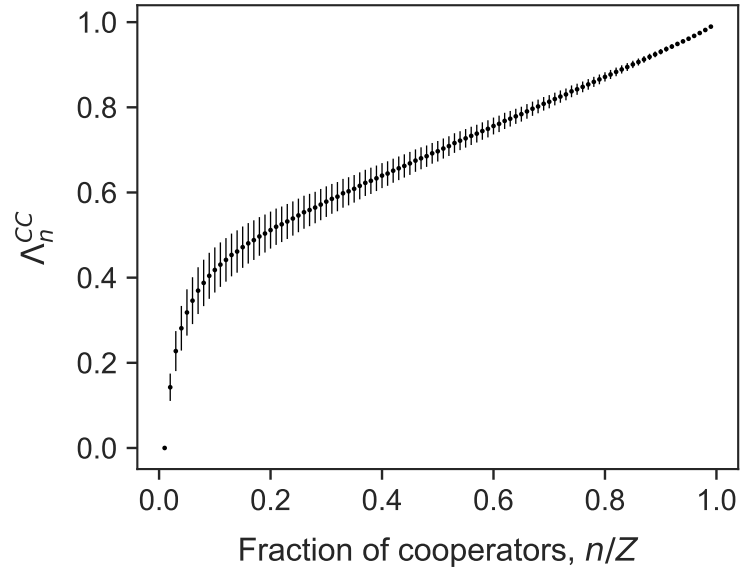
Figure 4.3: Expected proportion of cooperator neighbours for a cooperator Λ_n^{CC}. This is calculated using Equation (4.10) by running simulations of the Voronoi tessellation model with $Z = 100$ and neutral selection $\delta = 0$. In each simulation we track clones, which have a common ancestor, and look at snapshots of the simulated tissue in time. Each snapshot gives us a potential 'state' from which to find the population mean proportion of cooperator neighbours for a cooperator, for different clone sizes. Λ_n^{CC} is then calculated by taking the mean over at least 5000 values. Error bars show standard deviation.

thus γ_n, are uniquely defined for each value of n. For the VT model, we substitute in the mean transition probabilities given by Equations (4.6) and (4.7), to obtain

$$\rho_C \approx \frac{1}{Z} + \frac{\delta}{Z} \left\{ \frac{-c(Z-1)}{2} + b \sum_{m=1}^{Z-1} \sum_{n=1}^{m} \left(\frac{\Lambda_n^{CC} - n/Z}{Z-n} \right) \right\} + \mathcal{O}(\delta^2) \qquad (4.12)$$

for the cooperator fixation probability in the weak selection limit. The critical benefit-to-cost ratio is then obtained by setting $\rho_C = 1/Z$, giving

$$\left(\frac{b}{c} \right)^* \approx \frac{Z-1}{2} \left[\sum_{m=1}^{Z-1} \sum_{n=1}^{m} \left(\frac{\Lambda_n^{CC} - n/Z}{Z-n} \right) \right]^{-1}. \qquad (4.13)$$

Figure 4.4 compares Equation (4.12) with simulation results for the VT model, where we have set $Z = 100$, $\delta = 0.025$ and $c = 1$. The fixation probability for each value of b/c is obtained by running 10^4 simulations to fixation, starting with

a single mutant cooperator. Figure 4.4 shows there is a reasonable fit between our approximation of the fixation probabilities with the simulation data in the region $2.0 < b/c < 3.5$. These values are close to the critical benefit-to-cost ratio and therefore represent the region in which we would expect the weak selection limit to hold, thus this equation for the fixation probabilities is a reasonable approximation.
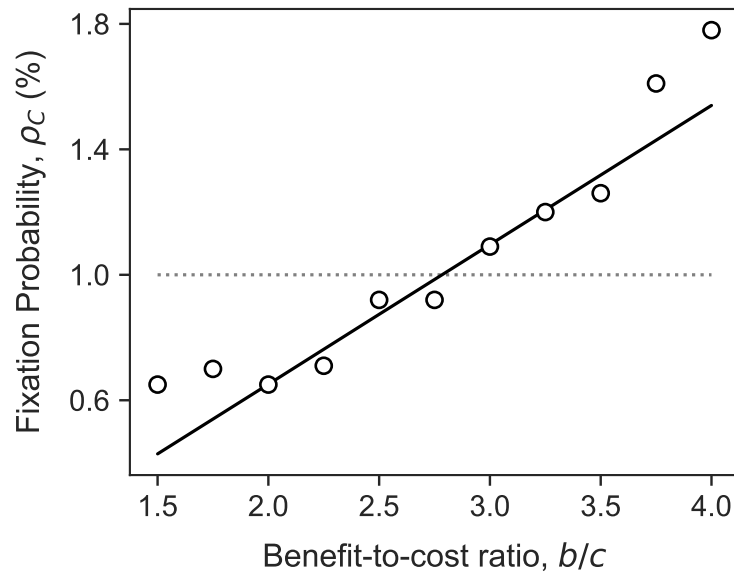
Figure 4.4: Fixation probabilities for the additive prisoner's dilemma in the Voronoi tessellation model with decoupled updating are approximated by Equation (4.12) and plotted here (solid line) for $\delta = 0.025$, $c = 1$ and $Z = 100$. Comparison with simulation results (points) shows that the approximation is good near the critical benefit-to-cost ratio (i.e. where $\rho_C = \rho_0 = 1/Z$, dotted line), but breaks down outside the region $2 < b < 3.5$. This is consistent with the fact that the equation is derived in the weak selection limit, and suggests that it can be used to calculate the critical ratio. Individual data points are calculated from 10^4 simulations, each of which starts with a single cooperator and is run to fixation.

The critical benefit-to-cost ratios, calculated from simulations and Equation (4.13), are given in Table 4.2. For both we get a value of $(b/c)^* = 2.8$, correct to one decimal place. In the next section we will compare this with results from evolutionary graph theory.

	Theory	Simulation
DT (death-birth)	6.69	6.74
HL (death-birth)	6.68	6.67
VT model (decoupled update)	2.78	2.83
VT model (death-birth)	-	7.26

Table 4.2: Summary of critical benefit-to-cost ratios $(b/c)^*$ for the additive prisoner's dilemma: death-birth update on a fixed Delaunay triangulation graph (DT) and a hexagonal lattice (HL); Voronoi tessellation (VT) model with decoupled and death-birth update rules. Simulation results are given in all cases, and theoretical results are given where available.

4.3   Comparing with evolutionary graph theory

Within the framework of evolutionary graph theory, population structure is represented by a static graph. Using the theory outlined in Section 2.2.3 it is possible to calculate fixation probabilities for any graph using Equation (2.37) [14]. The coalescence times are found computationally, by solving Equations (2.34) and (2.35).

We represent epithelial structures using two graph types. Epithelial cells have on average six neighbours, therefore the hexagonal lattice (HL) is a natural choice. Of course, epithelia exhibit some variation in neighbour number, thus we also consider a more realistic graph structure derived from a VT [104]. This is done by taking snapshots of the population structure from the VT model. We label these DT as they correspond to the Delaunay triangulation (see Section 3.3).

For the birth-death update rule, cooperation is never favoured by selection for the APD game [17, 20, 56]. The critical benefit-to-cost ratio is given by $(b/c)^* = \infty$. This is equivalent to the well-mixed population result. Thus, it is clear that cooperation does much worse on a fixed graph with birth-death updating, than it does in the VT model, as the latter has a finite critical benefit-to-cost ratio.

Figure 4.5 plots fixation probabilities for the death-birth update rule on both HL and DT graphs, with a population size of $Z = 100$ and periodic boundary conditions. Simulation results are determined by running 10^5 simulations to fixation, starting with a single mutant cooperator, and calculating the fixation probability for each benefit-to-cost ratio. Again we set $\delta = 0.025$ and $c = 1$. Theoretical results are calculated using Equation (2.37). Figure 4.5 shows a good fit between simulation

and theory in the range $4 < b/c < 12$.

It is clear from Figure 4.5 that there is negligible difference between the HL and DT graph results. We show results for a single instance of a DT graph, however we have calculated fixation probabilities for an additional five DT graphs using Equation (2.37), and find the results are indistinguishable. Critical benefit-to-cost ratios from both theory and simulation are given in Table 4.2 for the HL and DT graphs. In both cases we obtain $(b/c)^* = 6.7$, correct to one decimal place.

The HL therefore seems to be a reasonable approximation to the structure. Using the more realistic DT, with neighbour number heterogeneity, does not significantly alter fixation probabilities or the critical benefit-to-cost ratio, at least in the weak selection limit we are using. We note, however, that these results are for an average payoff. Using an accumulative payoff, for which payoffs are summed over interactions, can amplify the differences due to heterogeneity [79].

Figure 4.6 plots fixation probabilities for the HL with death-birth updating alongside the VT model results for decoupled birth and death. It is clear that fixation probabilities are significantly higher in the latter case. Furthermore, the critical benefit-to-cost ratio for the VT model is less than half that for the HL with death-birth update (see Table 4.2). Therefore, cooperation is more successful in the VT model.

Thus far, we have considered only results for weak selection, i.e. $\delta \to 0$. However, in Appendix C we calculate fixation probabilities for non-small values of δ, by simulation. We show that the weak selection result, that cooperation is more successful for the VT model with decoupled update rule, compared to the HL with death-birth update rule, also holds for intermediate δ. However, for sufficiently large δ this breaks down, as neither population is able to support the invasion of cooperation, at least for the values of b/c we consider.

The question then arises as to what mechanism is causing this amplifying effect in the VT model. There are two key differences between the evolutionary graph theory models and the VT model. Firstly, the VT model uses a spatially decoupled update rule, and secondly, it allows for some level of cell motion. Cells are able to
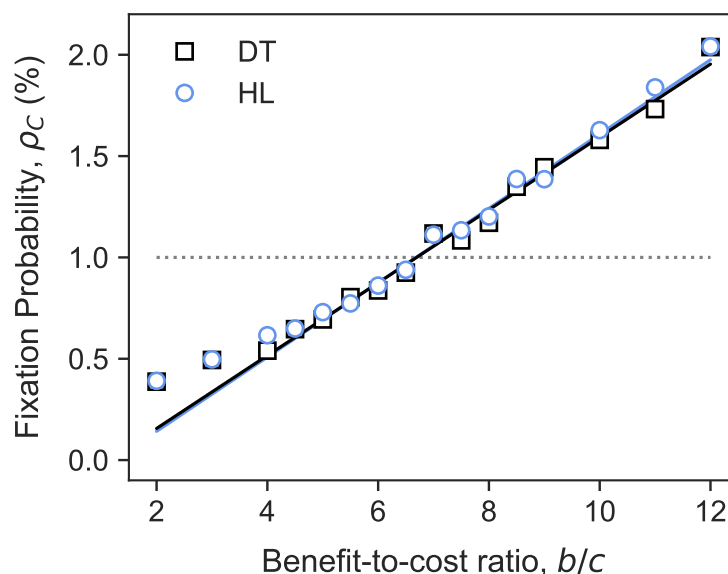
Figure 4.5: Fixation probabilities for the additive prisoner's dilemma game on fixed graphs, with death-birth updating. We have set $Z = 100$, $c = 1$ and $\delta = 0.025$. Solid lines plot evolutionary graph theory results for the fixation probabilities on a hexagonal lattice (HL; blue circles) and a Delaunay triangulation (DT; black squares), obtained from Equation (2.37). The critical benefit-to cost ratio, which occurs where fixation probability is equal to $\rho_0 = 1/Z$ (dotted line), is $(b/c)^* \approx 6.7$ for the HL and DT.

Simulation points are also shown for both cases and fit well with the theory when $(b/c) > 4$. As Equation (2.37) was derived in the weak selection limit we only expect it to be accurate near the critical benefit-to-cost ratio. Individual data points are calculated from 10^5 simulations, each of which starts with a single cooperator and is run to fixation.

move past one another, and thus there is some local rearrangement of neighbours.

We consider the effect of motion on the evolutionary success of cooperation by introducing an analogue into the evolutionary graph theory model, whereby we allow cells to swap sites with their neighbours [22]. At each time step, a swap occurs with probability m and a cell is chosen uniformly at random to switch places with one of its neighbours. This process is independent of cell fitness. The parameter m quantifies the amount of motion. By setting $m = 0$, we regain the original model without motion.

Figure 4.7 plots the fixation probability against benefit-to-cost ratio for a range of m values, demonstrating that increased motion within this framework leads to a
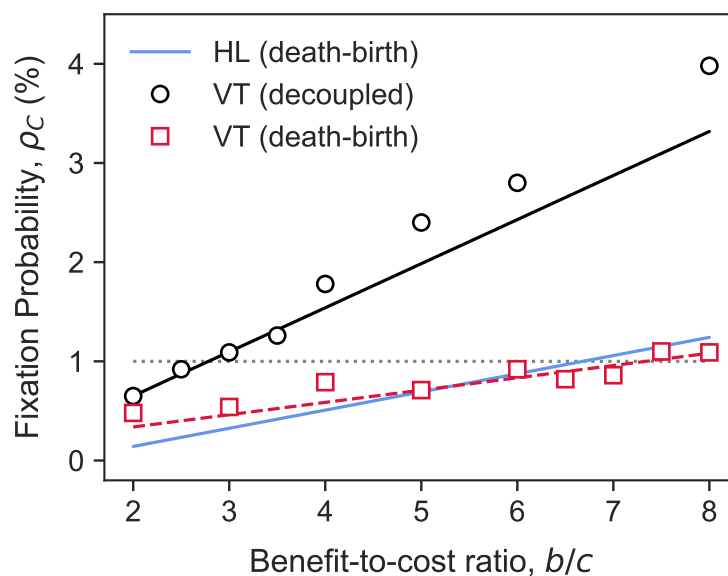
Figure 4.6: Fixation probabilities for the additive prisoner's dilemma game in the Voronoi tessellation (VT) model with $Z = 100$, $c = 1$ and $\delta = 0.025$. Points show simulation results for a decoupled update rule (black, circles) and a death-birth update rule (red, squares). Each data point is obtained from 10^4 simulations. For the decoupled update rule the approximate fixation probabilities given by Equation (4.12) are plotted (black, solid line) and for the death-birth update we plot a best fit line (red, dashed line). Fixation probabilities, given by Equation (2.37), for a fixed hexagonal lattice (HL) with death-birth update (blue, solid line) are also shown for comparison.

The dotted line shows the fixation probability for a neutral mutant. It is clear that cooperation is significantly favoured in the VT model with decoupled update rule when compared to the fixed HL with death-birth update rule, as the critical benefit-to-cost ratio is more than halved for the former. However when a death-birth update is introduced on the VT model this effect is suppressed and the critical benefit-to-cost ratio is very close to the fixed HL case.

decrease in the evolutionary success of cooperation. An intuitive explanation for this result is that motion can break up clusters and lead to more mixing of defectors and cooperators. Cooperators are most successful when they are able to cluster, whereas defectors benefit from mixing, therefore motion is detrimental to cooperative success. It therefore seems unlikely that the ability of cells to move past each other in the VT model is the reason for increased cooperative success.

Alternatively, we postulate that the spatial decoupling of birth and death promotes cooperation. To verify this, we consider the VT model with a death-birth
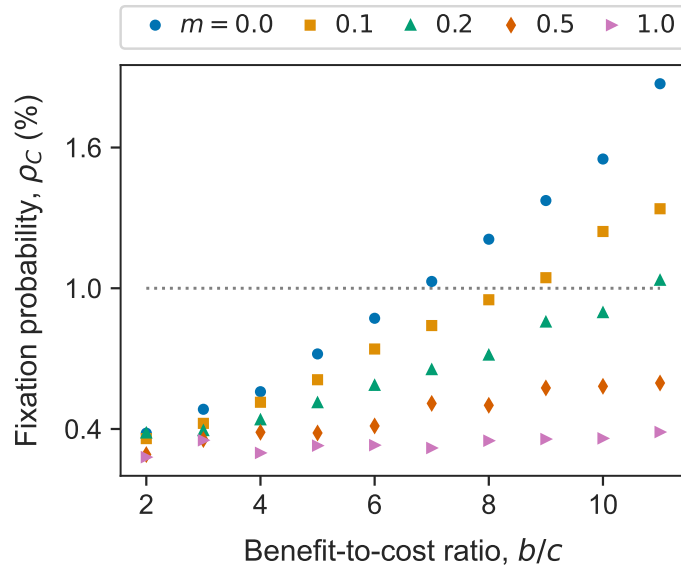
Figure 4.7: Fixation probabilities for the additive prisoner's dilemma with migration on a hexagonal lattice with death-birth update rule. These are obtained through simulation with $Z = 100$, $c = 1$ and $\delta = 0.025$. The parameter m is the probability that a migration event will occur in each timestep. If such an event occurs two neighbouring cells are randomly selected to swap places. Increasing m leads to decreased cooperative success. The case where $m = 0$ corresponds to the original evolutionary graph theory model we have used, with no migration.

update rule. This is implemented by following the simulation algorithm defined in Section 4.2.1, however birth and death are no longer spatially independent. When an update event occurs, a cell is chosen for death uniformly at random. Fitnesses are then calculated for the neighbouring cells, and one of these is chosen to divide, with probability proportional to fitness. This process is shown schematically in Figure 4.8.

Fixation probabilities for the VT model with death-birth update rule are shown in Figure 4.6. These are calculated for each value of b/c from 10^4 simulations. The figure shows that cooperation is less successful for the death-birth update rule, compared to the decoupled update rule, when using the VT model. In fact, cooperation is less successful in the VT model than for the static HL graph, when both use a death-birth update rule. This is evidenced by the higher critical benefit-to-cost ratio for the former, as can be seen in Table 4.2.

We therefore conclude that the spatial decoupling of birth and death leads to
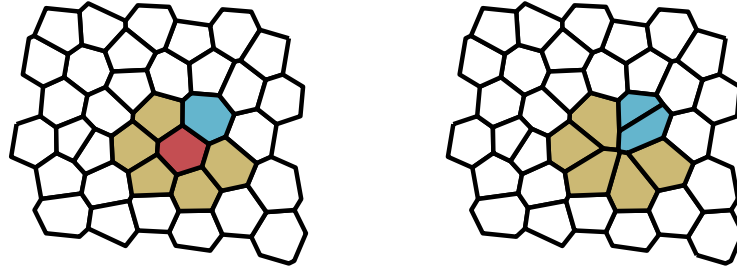
Figure 4.8: Death-birth update rule in the Voronoi tessellation model. When an update event occurs a cell is chosen to die uniformly at random from the population (red). From the neighbourhood of the dead cell (yellow) a parent cell (blue) is then chosen with probability proportional to fitness. The parent cell divides and the dead cell is removed from the tissue.

the promotion of cooperation in the VT model. This is consistent with results for other global update rules, such as shift updating [62, 63]. The fact that migration appears to suppress the success of cooperation could also provide an explanation as to why, if a death-birth update rule is used in both cases, cooperation is more successful for the static HL graph than the VT model.

We can understand intuitively why decoupling birth and death promotes cooperation by considering which cells compete for proliferation. In structured populations, the individual cell types tend to remain clustered. In general, cooperator cells have the highest fitness when they are surrounded by other cooperators, i.e. they are in the bulk of the cooperator cluster. By contrast, defectors have highest fitness when they are near cooperators, i.e. on the boundary of the defector and cooperator clusters.

When birth and death are spatially decoupled, all cells compete to reproduce, and any update event can lead to a change in the number of cooperators. Therefore, the cooperator population is able to benefit from the high fitness contribution from bulk cooperators. By contrast, for the death-birth update, the cooperator population only changes when a boundary cell dies. The only cells which can replace it are nearest neighbours, therefore it is boundary cooperators competing with boundary defectors, which is not optimal for cooperators.

We can verify that invading cooperators in the VT model are clustered visually, e.g. by considering Figure 4.2. However, we can also verify clustering more

formally by plotting the join count statistics [140]. The join counts for cooperator-cooperator (CC) or cooperator-defector (CD) pairs are given by

$$\text{CC} = \frac{1}{2} \sum_{i,j \in G} s_i s_j A_{ij} \qquad \text{and} \qquad \text{CD} = \frac{1}{2} \sum i, j \in G(s_i - s_j)^2 A_{ij}, \qquad (4.14)$$

respectively, for a population represented by graph G. Essentially these count the number of neighbouring cooperator-cooperator and cooperator-defector pairs. The former (CC) is a measure of positive spatial autocorrelation, while the latter (CD), is a measure of negative spatial autocorrelation.

In Figure 4.9 we plot the observed join counts for invading cooperators, averaged over 50 simulations. We also plot join counts calculated for the same simulations, where we have randomised the positions of cooperators and defectors. It
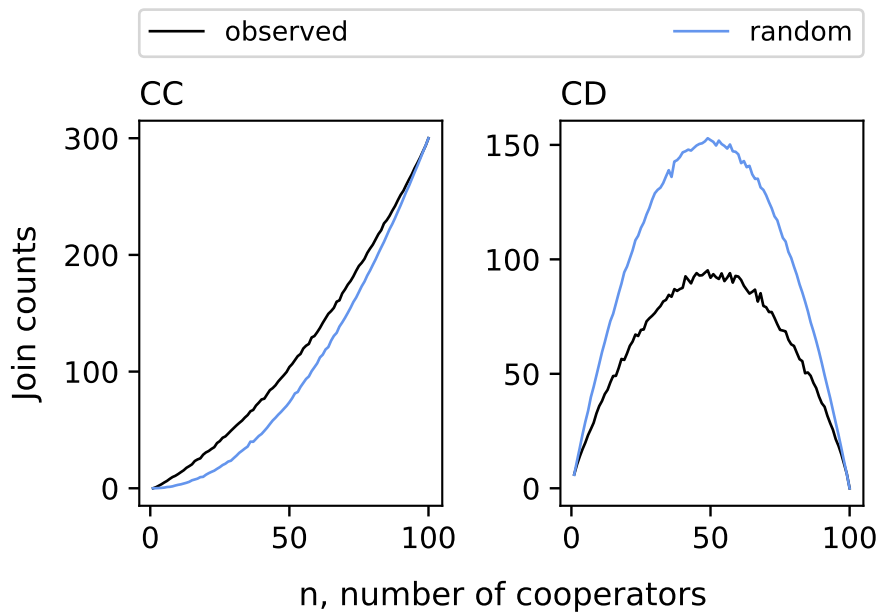
Figure 4.9: Join count statistics for the Voronoi tessellation model plotted against the number of cooperators n. The join count gives the number of cooperator-cooperator (CC) or cooperator-defector (CD) pairs. We compare the observed join count for invading cooperators (black) with random permutations of cooperators (red). It is clear that the join count for CC pairs is higher, and the join count for CD pairs is lower, for invading cooperators, than we would expect if cooperators were randomly distributed. This is true for all values of n. Thus, we can conclude that there is positive spatial autocorrelation, i.e. invading cooperators in the VT model are clustered.

is clear from Figure 4.9 that the join count for CC pairs is higher for the observed data, than the randomised data, while CD is lower for the observed data compared to the randomised data. As expected, this implies positive spatial autocorrelation, i.e. that cooperators are clustered.

4.4 Social dilemma games

Thus far, this chapter has focused on the APD as a model of cooperation, calculating the critical benefit-to-cost ratios above which cooperation is favoured. The APD is a natural choice for initial investigation, as it presents the strongest form of social dilemma, and can be defined by a single parameter. However, we saw in Section 2.2 that there is a spectrum of social dilemma games. Furthermore, it is trivial to calculate the structure coefficients for a given population structure and update rule, from the critical benefit-to-cost ratios, using Equation (2.40) [10]. These can be used to determine conditions for cooperation to be favoured using the σ-rule, defined by Equation (2.39).

These conditions are plotted in Figure 4.10 for a general pairwise social dilemma game defined by Equation (2.1). For each population type and update rule σ is calculated according to Equation (2.40) using the values of $(b/c)^*$ defined in Table 4.2. The well-mixed population has $\sigma = 1$. We then plot the critical line, $\sigma R + S = T + \sigma P$, for each case. This divides the parameter space into one region where cooperation is favoured, and one where defection is favoured.

Introducing population structure shifts the critical line so that cooperation is favoured for a greater region of parameter space compared to the well-mixed population. This is true for the death-birth update, both when used with the static HL and with the VT model. The largest effect is observed when the VT model is used with decoupled updating. In this case, cooperation is favoured for all snowdrift, stag-hunt and harmony games, and the majority of prisoner's dilemma games. The birth-death update on a static HL has structure coefficient $\sigma = 1$ [10, 17], therefore the critical line is equivalent to that of the well-mixed population.
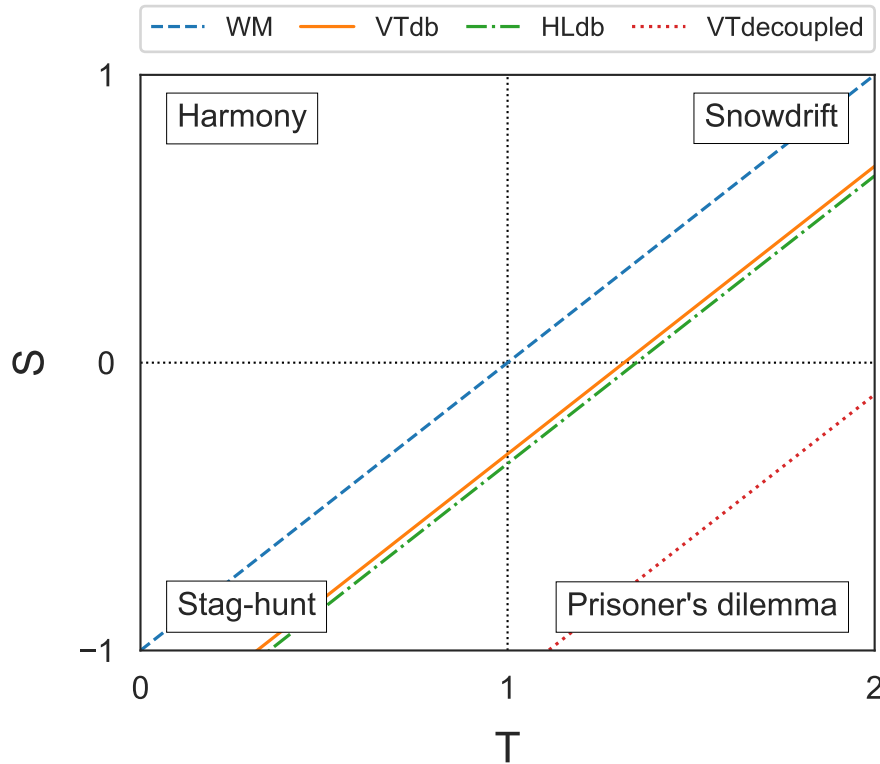
Figure 4.10: Conditions for cooperation to be favoured for pairwise social dilemma games defined by Equation (2.1) with $R = 1$ and $P = 0$. Each line divides the T-S plane into regions where cooperation is favoured ($\sigma R + S > T + \sigma P$) and defection is favoured ($\sigma R + S < T + \sigma P$). The structure coefficient σ depends on the population structure and the update rule.

Results are shown for a well-mixed population (WM), VT model with death-birth update (VTdb), hexagonal lattice with death-birth update (HLdb) and VT model with decoupled update (VTdecoupled). The latter case gives the largest region of parameter space for which cooperation is favoured, including the entirety of the harmony, snowdrift and stag-hunt games, and majority of the prisoner's dilemma.

4.5 Discussion

It is well-established that population structure, such as that exhibited by epithelia, can lead to better evolutionary outcomes for cooperators [6, 10, 17]. This can be understood intuitively, as population structure allows cooperators to cluster together. The cooperator population therefore retains a greater proportion of the benefit it produces, while defectors, which are less likely to neighbour cooperators, lose out.

The link between population structure and the evolutionary success of cooper-

ation, however, depends on the update dynamics. This is because the exact mechanism for population updating affects which cells compete. Within evolutionary graph theory, it is usually necessary to use a local update rule, which spatially couples birth and death. In this chapter we have compared graph theory results to evolutionary dynamics in the VT model, which provides a more realistic representation of an epithelium and has allowed us to introduce a global update rule which decouples birth and death.

Within evolutionary graph theory we considered two update rules: the birth-death and death-birth. For the former, cooperation is never beneficial for the APD and the critical benefit-to-cost ratio is infinite. This result is equivalent to the well-mixed population. For the death-birth update rule, cooperation is beneficial when b/c exceeds the critical benefit-to-cost ratio. This was calculated to be $(b/c)^* = 6.7$ for both HL and DT graphs using known results [14].

The fact that the results are so similar for the HL and DT suggests that there is a negligible affect on cooperative success due to the heterogeneity of neighbour number, which is exhibited by DT. However, the choice of an averaged payoff could be suppressing the effect of heterogeneity compared to an accumulated payoff, as it does for scale-free networks [9, 79]. It would be advisable, therefore, to compare fixation probabilities of the two structures for an accumulated payoff. We do not expect a substantial difference, however. Vertex degrees in scale-free networks follow a polynomial distribution and therefore exhibit large variance, whereas degree variance in DTs is comparatively small.

For the VT model with decoupled update rule, we derived an approximate equation for the cooperator fixation probability in the weak selection limit, which is verified by simulation. From this we calculated the critical benefit-to-cost ratio, above which cooperation is beneficial, which is given by $(b/c)^* \approx 2.8$. This is significantly lower than the evolutionary graph theory results for both death-birth and birth-death updating.

Furthermore, when the VT model was run with a death-birth update, cooperation did worse than in the evolutionary graph theory model of a static HL. This

led us to conclude that the decoupling of birth and death is the main mechanism for increased success of cooperation in the VT model. This is consistent with previous work looking at a shift update rule within evolutionary graph theory, which found that decoupling birth and death led to increased cooperative success in one-dimension [62], and in two dimensions if a repulsive force was introduced between cells of different types [63].

The fact that the critical benefit-to-cost ratio is slightly higher in the VT model with death-birth update, compared to evolutionary graph theory results, could be due to the fact that cells can move and change neighbours in the former. Indeed we found that introducing migration into an evolutionary graph theory model suppressed cooperation, and it is therefore possible that the motion of cells is acting to reduce cooperative success in the VT model.

The majority of this chapter focused on the APD game; however, we also extended our results to consider general pairwise social dilemma games. Using the σ-rule [10] we calculated conditions for cooperation to be favoured ($\rho_C > \rho_D$) for pairwise social dilemma games. We found that for the VT model with decoupled update, cooperation is favoured for all stag-hunt and snowdrift games, and for a majority region of the prisoner's dilemma parameter space. For the death-birth update (within the VT model or a static HL) smaller regions of parameter space lead to cooperation being favoured for the stag-hunt, snowdrift and prisoner's dilemma games. These get even smaller for the birth-death update, which is equivalent to the well-mixed population.

Thus far, we have limited the analysis to pairwise games. However, it has been argued that multiplayer public goods games are more realistic for cancer modelling, and can lead to substantively different results. In the next chapter we extend our modelling framework to incorporate multiplayer games, again comparing results for well-mixed populations and evolutionary graph theory, with the VT model.

Chapter 5

Cooperative success in epithelial public goods games

This chapter is based on the paper: Cooperative success in epithelial public goods games. *Journal of Theoretical Biology*, 528:110838, 2021 [141].

5.1 Introduction

Applications of evolutionary game theory to cancer evolution have mainly focused on pairwise games [26, 51, 142]. It is arguable, however, that multiplayer public goods games (PGGs) better represent cellular interactions which occur within groups [25]. For example, a cell producing a growth factor will provide a benefit to other cells within its diffusion range.

The focus of this chapter, therefore, is to consider how epithelial structure and dynamics affect cooperation when it is modelled by a PGG. We extend the analysis of Chapter 4, which incorporated evolutionary dynamics into the VT model for pairwise games. Once again, we spatially decouple birth and death, comparing with the local update rules primarily used in evolutionary graph theory models.

Multiplayer PGGs were introduced in Chapter 2. The most common PGG, the NPD, uses a linear benefit function [72, 90]. However, nonlinear benefit functions may be more realistic [92], and can lead to much richer dynamics, even for well-mixed populations. An example is the volunteer's dilemma (VD), which defines the benefit as a Heaviside step function [33, 93–95].

A sigmoid benefit function has been proposed as an appropriate model for growth factor production. Experiments on neuroendocrine pancreatic cancer cells *in vitro* have found sigmoid dependence of proliferation rates on the concentration of growth factor IGF-II [38]. Furthermore such a function is relatively general, with both the NPD and VD arising as limiting cases [143].

Throughout this chapter we focus on a sigmoid benefit function, however the results are applicable to any two-strategy multiplayer game, as described in Section 2.3. Details of the evolutionary game theory framework for multiplayer games can be found in that section.

The remainder of this chapter is set out as follows. In Section 5.2 we consider conditions under which cooperation is favoured or beneficial for multiplayer PGGs. In both cases, we derive approximate results for a global update rule with an arbitrary population structure. Then in Section 5.3 we apply this theory to consider conditions for cooperator success in an epithelium, using spatial statistics calculated through simulation of the VT model. Finally, in Section 5.4, we discuss the implications of our work for the evolution of cooperative public goods in epithelia and make some remarks on the different significance of beneficial and favourable mutants.

5.2 Multiplayer games with global updating

In this section we derive results for the evolutionary dynamics of arbitrary multiplayer games with global updating. First we consider conditions under which cooperation is favoured, and then conditions for cooperation to be beneficial. The decoupled update we introduced for the VT model in Chapter 4 is an example of a global update rule (see Section 2.2.3.2). Thus, we will be able, in Section 5.3, to use these results to consider cooperative success for multiplayer PGGs in the VT model.

We consider an arbitrary multiplayer game with two strategies, *A* and *B*, as introduced in Section 2.3. Individuals interact in groups of size $N = k + 1$, which consist of the focal player and its k co-players. The focal player obtains a payoff

$a_{j,k}$ or $b_{j,k}$, depending on whether it is of type *A* or *B*. Here *j* is the number of *A* co-players in the group. For a graph-structured population, the co-players are the direct neighbours of an individual. The fitness of each individual is defined as $1 + \delta a_{j,k}$ or $1 + \delta b_{j,k}$, where δ is the selection strength parameter.

The population evolves according to a Moran process [78]. We have outlined a number of results from evolutionary graph theory in Section 2.3. Here we derive results for global update rules, for which the probability of an individual reproducing is dependent only on its own fitness and total population fitness, but not on any local effects.

5.2.1 Conditions for cooperation to be favoured

Recall from Section 2.3 that the σ-rule, defined by Equation (2.46), can be used to determine when a strategy is favoured for any game, if the structure coefficients for the population are known. These structure coefficients depend on the population structure and update rule, but not the game.

In the following we derive a general expression for the structure coefficients under a global update rule. This could apply to the well-mixed population, the cycle graph with shift update rule or the VT model with decoupled update rule. Results outlined in Section 2.3 assumed that games were played on a fixed graph or well-mixed population, within groups of constant size, *N*. For well-mixed populations we were free to choose *N* (although some results required $N \ll Z$, where *Z* is the population size), while for regular graphs we set $N = k + 1$, where *k* is the degree of the graph. Here we relax this condition and allow for variable population structure and group size.

We make the assumption that there is a fixed distribution, $f_j^{A/B}(n,k)$, defining the probability that an A/B-player interacts with *j* co-players of type *A*, given it has *k* co-players in total and there are *n* players of type *A* in the population. If the population were defined on a graph, this would be the probability of an A/B-player having *j* *A*-type neighbours, given *k* total neighbours. This assumption is true for a well-mixed population or cycle graph, but not necessarily for other population structures where $f_j^{A/B}(n,k)$ depends on the specific configuration of players.

The frequency of individuals with k neighbours is given by g_k. We make the further assumptions that this distribution is fixed, and does not depend on type. See Appendix E for a discussion of the validity of this assumption for the VT model.

In general, for a global update rule, we can define the transition probabilities

$$T_n^+ = \frac{Z-n}{Z} \frac{nF_A}{nF_A + (Z-n)F_B} \qquad T_n^- = \frac{n}{Z} \frac{(Z-n)F_B}{nF_A + (Z-n)F_B}, \qquad (5.1)$$

where

$$F_A = 1 + \delta \sum_{k=1}^{Z-1} \sum_{j=0}^{k} f_j^A(n,k) g_k a_{j,k} \qquad (5.2)$$

$$F_B = 1 + \delta \sum_{k=1}^{Z-1} \sum_{j=0}^{k} f_j^B(n,k) g_k b_{j,k} \qquad (5.3)$$

are the population averaged fitnesses. The payoffs $a_{j,k}$ and $b_{j,k}$ depend explicitly on the number of neighbours k.

Substituting Equations (5.1) to (5.3) into Equation (2.47), and taking the weak selection limit we obtain

$$\frac{\rho_A}{\rho_B} \approx 1 + \delta \underbrace{\sum_{n=1}^{Z-1} \sum_{k=1}^{Z-1} \sum_{j=0}^{k} g_k [f_j^A(n,k)a_{j,k} - f_j^B(n,k)b_{j,k}]}_{\Gamma}. \qquad (5.4)$$

Thus $\rho_A > \rho_B$ when $\Gamma > 0$. In the weak selection limit,

$$f_j^A(n,k) = f_{k-j}^B(Z-n,k) \qquad (5.5)$$

must hold by symmetry, and thus

$$\sum_{n=1}^{Z-1} f_j^A(n,k) = \sum_{n=1}^{Z-1} f_{k-j}^B(n,k). \qquad (5.6)$$

Therefore we have

$$\Gamma = \sum_{k=1}^{Z-1} \sum_{j=0}^{k} \sum_{n=1}^{Z-1} g_k f_j^A(n,k)(a_{j,k} - b_{k-j,k}).$$ (5.7)

The condition for A to be favoured over B is thus given by

$$\sum_{k=1}^{Z-1} \sum_{j=0}^{k} \sigma_{j,k}(a_{j,k} - b_{k-j,k}) > 0,$$ (5.8)

where

$$\sigma_{j,k} = g_k \sum_{n=1}^{Z-1} f_j^A(n,k)$$ (5.9)

are the structure coefficients. For a fixed group size, $N = k+1$, this reduces to Equation (2.46), with

$$\sigma_j = \sum_{n=1}^{Z-1} f_j^A(n),$$ (5.10)

where we have dropped the explicit dependence on k.

Recall that this derivation is based on the assumption that $f_j^A(n,k)$ is fixed. In cases where this is not true, we set it equal to the expectation of $f_j^A(n)$, taken over a large ensemble of possible configurations under neutral selection, $\delta = 0$. This enables us to approximate the structure coefficients, using Equation (5.10), when $f_j^A(n)$ is not fixed.

The well-mixed population is an example where $f_j^A(n)$ is fixed. It is defined by a hypergeometric distribution:

$$f_j^A(n) = \binom{Z-1}{k}^{-1} \binom{n-1}{j} \binom{Z-n}{k-j}.$$ (5.11)

We can therefore find the structure coefficients [87] by substituting this expression for $f_j^A(n)$ into Equation (5.10):

$$\sigma_j = \binom{Z-1}{k}^{-1} \underbrace{\sum_{n=1}^{Z-1} \binom{n-1}{j} \binom{Z-n}{k-j}}_{S}.$$ (5.12)

It can be shown (see Appendix A in [87]) that

$$S = \begin{cases} \binom{Z}{k+1} & \text{if } 0 \leq j < k \\[2mm] \binom{Z-1}{k+1} & \text{if } j = k. \end{cases} \tag{5.13}$$

Thus the structure coefficients are given by

$$\sigma_j = \begin{cases} \frac{Z}{k+1} & \text{if } 0 \leq j < k \\[2mm] \frac{Z-k-1}{k+1} & \text{if } j = k. \end{cases} \tag{5.14}$$

These are equivalent to Equation (2.48) up to a constant factor. The cycle graph also has a fixed distribution, $f_j^A(n)$, thus the structure coefficients for the shift update rule can also be obtained exactly using Equation (5.10).

For a variable group size, the structure coefficients for the well-mixed population are given by

$$\sigma_{j,k} = g_k \sigma_j(k) = g_k \begin{cases} \frac{Z}{k+1} & \text{if } 0 \leq j < k \\[2mm] \frac{Z-k-1}{k+1} & \text{if } j = k, \end{cases} \tag{5.15}$$

where $\sigma_j(k)$ are defined in Equation (5.14).

Once the structure coefficients have been determined, we can use Equation (2.46) or Equation (5.8) to find the condition under which cooperation is favoured. For a PGG, as defined by Equation (2.41), this is given by

$$\frac{b}{c} > \frac{Z-1}{\sum_{k=1}^{Z-1} \sum_{j=0}^{k} \sigma_{j,k} \left[\beta \left(\frac{j+1}{k+1} \right) - \beta \left(\frac{k-j}{k+1} \right) \right]}. \tag{5.16}$$

5.2.2 Conditions for cooperation to be beneficial

Thus far, we have considered conditions under which a mutant is favoured. However, we recall from Section 2.2.2, that an alternative measure of mutant success can be obtained by considering the conditions under which it is beneficial. Here,

we derive the condition for an A-mutant to be beneficial, i.e. $\rho_A > \rho_0$.

As in the previous section, we make the assumption that the distributions g_k and $f_j^{A/B}(n,k)$ are fixed. Thus, the population averaged fitnesses of A and B players are defined by Equations (5.2) and (5.3) and the transition probabilities by Equation (5.1). The fixation probability for a single A-mutant [77] is then given by

$$\rho_A = \left[1 + \sum_{m=1}^{Z-1} \prod_{n=1}^{m} \frac{T_n^-}{T_n^+} \right]^{-1}. \tag{5.17}$$

Substituting in the transition probabilities and taking the weak selection limit $\delta \ll 1$ we obtain

$$\rho_A = \frac{1}{Z} + \frac{\delta}{Z^2} \sum_{k=1}^{Z-1} \sum_{j=0}^{k} \left(\theta_{j,k}^A a_{j,k} - \theta_{j,k}^B b_{j,k} \right) + \mathcal{O}(\delta^2), \tag{5.18}$$

where we have defined

$$\theta_{j,k}^A = g_k \sum_{m=1}^{Z-1} \sum_{n=1}^{m} f_j^A(n,k) \tag{5.19}$$

$$\theta_{j,k}^B = g_k \sum_{m=1}^{Z-1} \sum_{n=1}^{m} f_j^B(n,k) = g_k \sum_{m=1}^{Z-1} \sum_{n=1}^{m} f_{k-j}^A(Z-n,k). \tag{5.20}$$

The final equality is obtained by symmetry arguments in the weak selection limit.

The condition for A to be a beneficial mutation, $\rho_A > 1/Z$, is therefore given by

$$\sum_{k=1}^{Z-1} \sum_{j=0}^{k} \left(\theta_{j,k}^A a_{j,k} - \theta_{j,k}^B b_{j,k} \right) > 0. \tag{5.21}$$

If we consider a PGG as defined by Equation (2.41), then cooperation is beneficial when

$$\frac{b}{c} > \frac{Z(Z-1)}{2\sum_{k=1}^{Z-1} \sum_{j=0}^{k} \left[\theta_{j,k}^A \beta \left(\frac{j+1}{k+1} \right) - \theta_{j,k}^B \beta \left(\frac{j}{k+1} \right) \right]}. \tag{5.22}$$

For a fixed group size $N = k+1$ these conditions simplify to

$$\sum_{j=0}^{k} \left(\theta_j^A a_j - \theta_j^B b_j \right) > 0 \tag{5.23}$$

and

$$\frac{b}{c} > \frac{Z(Z-1)}{2\sum_{j=0}^{k}\left[\theta_j^A \beta\left(\frac{j+1}{k+1}\right) - \theta_j^B \beta\left(\frac{j}{k+1}\right)\right]}, \tag{5.24}$$

where

$$\theta_j^{A/B} = \sum_{m=1}^{Z-1}\sum_{n=1}^{m} f_j^{A/B}(n,k). \tag{5.25}$$

5.2.3 Antisymmetry-of-invasion property

We saw in Section 2.2.2 that for pairwise games the conditions for a mutant to be beneficial and favoured are equivalent, if the game satisfies a condition known as the equal-gains-from-switching condition. Here, we show that for multiplayer games the conditions for a mutant to be beneficial and favoured are equivalent if the payoffs satisfy a property we call *antisymmetry-of-invasion*. We consider the case where group size is fixed; however, the results can be generalised for variable group size, given certain conditions.

The values θ_j^A and θ_j^B, defined by Equation (5.25), can be written as

$$\begin{aligned}
\theta_j^A &= \sum_{n=1}^{Z-1}(Z-n)f_j^A(n) \\
\theta_j^B &= \sum_{n=1}^{Z-1} n f_{k-j}^A(n).
\end{aligned} \tag{5.26}$$

Thus we have

$$\theta_j^A + \theta_{k-j}^B = Z\sum_{n=1}^{Z-1} f_j^A(n) = Z\sigma_j, \tag{5.27}$$

where the last equality is from the definition of σ_j as stated by Equation (5.10). The condition for A to be beneficial, given by Equation (5.23), thus becomes

$$\sum_{j=0}^{k}\left[\theta_j^A a_j - \left(Z\sigma_j - \theta_j^A\right)b_{k-j}\right] > 0. \tag{5.28}$$

This can be rewritten in the form

$$\sum_{j=0}^{k}\left(\theta_j^A - \frac{Z}{2}\sigma_j\right)(a_j + b_{k-j}) + \frac{Z}{2}\sum_{j=0}^{k}\sigma_j\left(a_j - b_{k-j}\right) > 0. \tag{5.29}$$

If the payoffs satisfy

$$a_j + b_{k-j} = Q, \tag{5.30}$$

where Q is a constant that is independent of j, then the first term in Equation (5.29) vanishes. The condition for A to be beneficial, therefore, becomes

$$\sum_{j=0}^{k} \sigma_j \left(a_j - b_{k-j} \right) > 0, \tag{5.31}$$

which is equivalent to the condition for A to be favoured, as defined by Equation (2.46). Thus the conditions for cooperation to be beneficial and favoured are equivalent when Equation (5.30) holds, which we call the antisymmetry-of-invasion property. If Q is independent of k, this result generalises to variable group size. Note that if we substitute in the payoffs for a two-player matrix game, defined by Equation (2.1), we regain the pairwise equal-gains-from-switching condition: $R + P = S + T = Q$. In Appendix D we discuss the implications of the antisymmetry-of-invasion property for invasion processes.

5.3 Public goods games in an epithelium

A number of studies have considered the evolutionary dynamics of sigmoid PGGs in epithelia, representing the tissue either as a well-mixed population [37], or a fixed graph structure with various local update rules [36, 40]. Here we use the framework introduced in Chapter 4 to consider the evolutionary dynamics of PGGs in the VT model with decoupled update rule. This is a global update rule, therefore we can apply the results derived in Section 5.2.

We start by calculating spatial statistics for the VT model for neutral selection ($\delta = 0$). We then use these to calculate the conditions for cooperation to be favoured and beneficial, according to the theory developed in Section 5.2. We verify theoretical results by running simulations in various parameter regimes. We also compute the gradient of selection to obtain a fuller picture of the dynamics. In all cases we compare VT model results with the well-mixed population, and with results for regular graphs where they are available. Throughout this section, we use C

and D to label the two strategies, rather than A and B, to highlight the fact that this is a PGG played between cooperators and defectors.

5.3.1 Spatial statistics of the Voronoi tessellation model

We use the VT model with decoupled update rule as introduced in Chapters 3 and 4 with parameters defined in Table 4.1. Values for g_k and $f_j^C(n,k)$ are obtained by averaging over a large ensemble of possible states in the weak selection limit. We make the assumption that variation around this mean can be neglected.

Figures 5.1 and 5.2 show the distributions g_k and $f_j^C(n,k)$ for the VT model under neutral selection, calculated by averaging over 500 simulations, each of which starts with a single neutral mutant and is run to fixation. See Appendix E for further discussion on neighbour distributions in the VT model and the validity of assuming g_k is independent of n and cell type.
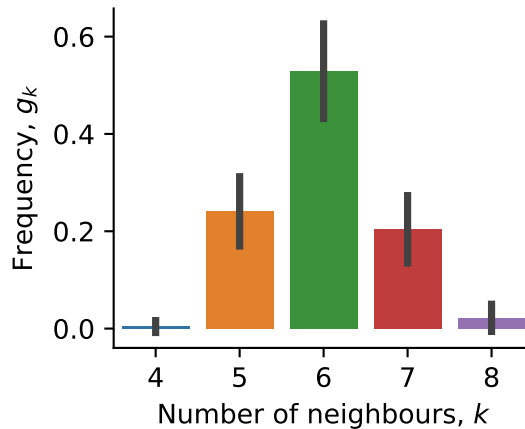
Figure 5.1: Degree distribution for the Voronoi tessellation model. Error bars show standard deviation. Data is obtained from simulations using a decoupled update rule with neutral selection ($\delta = 0$) and population size $Z = 100$.

5.3.2 Favourable cooperation

The condition for cooperation to be favoured can be approximated by calculating the structure coefficients using Equation (5.9). Figure 5.3 plots the VT structure coefficients with those for a well-mixed population as defined by Equation (5.14).

Using the structure coefficients we can derive the condition for cooperation to be favoured for an arbitrary PGG, as defined by Equation (2.41). We define the
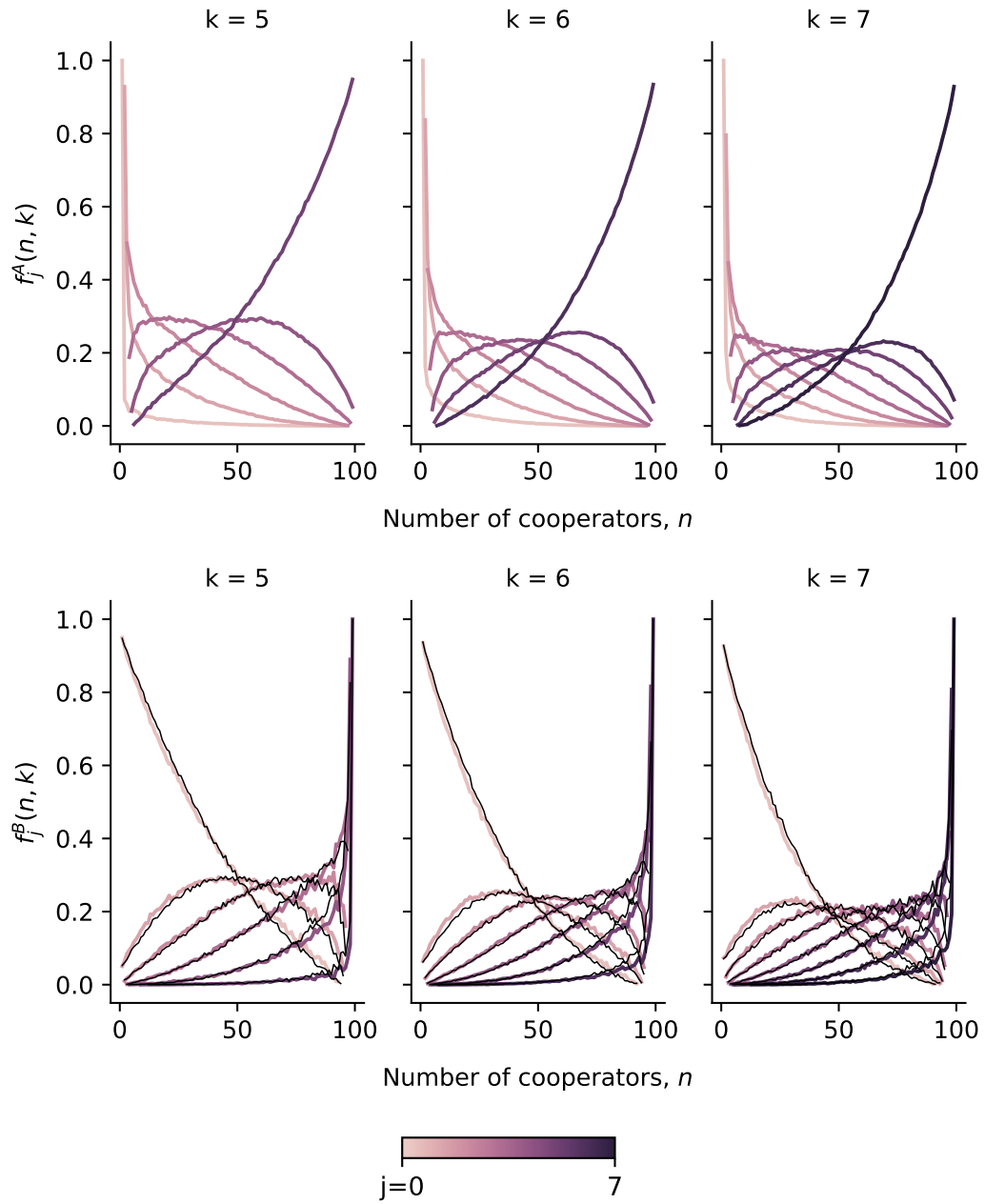
Figure 5.2: Frequency distributions $f_j^A(n,k)$ and $f_j^B(n,k)$ for $Z = 100$. These define the probability that a cell of type A or B, respectively, has j neighbours of type A, given k neighbours total and n cells of type A in the population. The lower panel compares values of $f_j^B(n,k)$ calculated directly through simulation (dashed) with values obtained from the simulated data for A cells defined by $f_j^B(n,k) = f_{k-j}^A(Z-n,k)$.

critical benefit-to-cost ratio $(b/c)_1^*$, such that $\rho_C > \rho_D$ when $b/c > (b/c)_1^*$. Thus
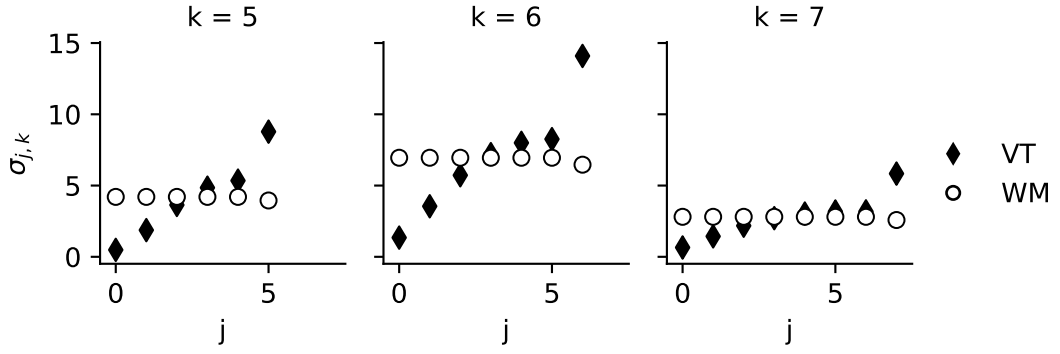
Figure 5.3: Comparing the structure coefficients $\sigma_{j,k}$ for the Voronoi tessellation model with decoupled updating (VT) and for the well-mixed (WM) population. Both have the same neighbour distribution seen in Figure 5.1.

from Equation (5.16) we can write

$$\left(\frac{b}{c}\right)_1^* = \frac{Z-1}{\sum_{k=1}^{Z-1}\sum_{j=0}^{k}\sigma_{j,k}\left[\beta\left(\frac{j+1}{k+1}\right) - \beta\left(\frac{k-j}{k+1}\right)\right]}. \qquad (5.32)$$

For an NPD, defined by Equation (2.42), this becomes

$$\left(\frac{b}{c}\right)_1^* = \frac{Z-1}{\sum_{k=1}^{Z-1}\sum_{j=0}^{k}\sigma_{j,k}\frac{2j+1-k}{k+1}}. \qquad (5.33)$$

Substituting in the structure coefficients we obtain $(b/c)_1^* \approx 2.22$ for the VT model with decoupled update rule and population size $Z = 100$. For a well-mixed population with the same group size distribution we obtain $(b/c)_1^* \approx 7.35$. As we would expect there is a significant increase in the success of cooperative mutants under the VT model. This is due to the high level of assortment in the VT model, which means cooperators are likely to have more cooperator neighbours than defectors.

On average, cells have six neighbours, so the mean group size is seven. We can, therefore, compare the critical benefit-to-cost ratio for a well-mixed population with variable group size, given above, to that of a well-mixed population with fixed group size, $N = 7$. The latter is given by Equation (2.50) to be $(b/c)_1^* = 7.45$. Clearly, incorporating variation in group size has a negligible impact on whether cooperation is favoured in this case.

We note that our model assumes that cells receive a payoff only from the game in which they are the focal player. However, an alternative formulation of multi-player games is to allow individuals to sum or average over the payoffs from all games in which they participate, including those for which their direct neighbours are the focal player. See for example [144]. This approach is more appropriate for social, rather than cellular interactions [36]. However, it could result in non-negligible impact from incorporating variation in group size, e.g. it has been found that heterogeneity in graph structure can promote cooperation [145].
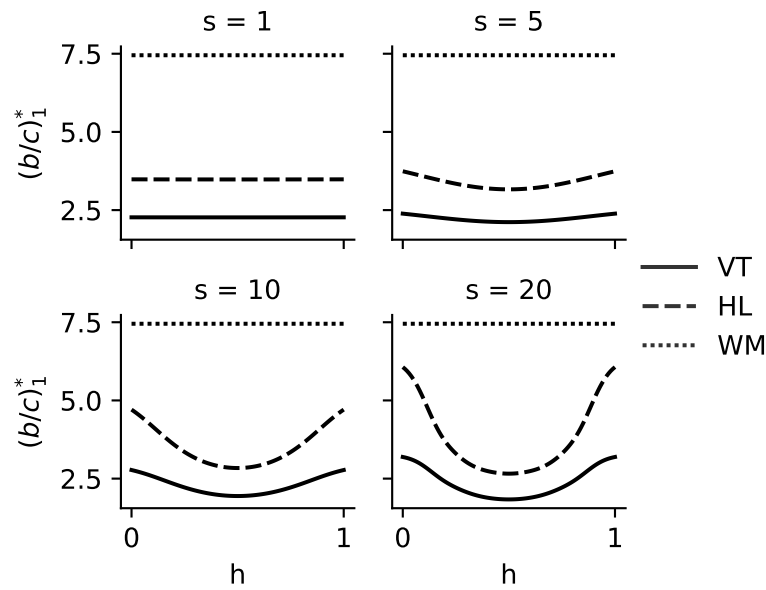
Figure 5.4: Comparing the critical benefit-to-cost ratio $(b/c)_1^*$ at which $\rho_C > \rho_D$, for a sigmoid benefit function. For a well-mixed population with group size $N = 7$ (WM), $(b/c)_1^*$ is highest, and independent of the inflection point h and steepness s. For the Voronoi tessellation model with decoupled update rule (VT) and fixed hexagonal lattice with death-birth update rule (HL), $(b/c)_1^*$ varies with h and s. For small s the benefit function approaches linearity and we regain the results for an NPD. For all values of s and h, $(b/c)_1^*$ is lowest for the VT model with decoupled update rule.

We can also use Equation (5.32) to determine $(b/c)_1^*$ for a sigmoid benefit function. We use a normalised logistic function, defined by Equation (2.44), consistent with previous studies [36, 38, 40]. This function has two parameters: the steepness $s \in (0, \infty)$, and the inflection point $h \in [0, 1]$. Figure 5.4 compares the predicted values of $(b/c)_1^*$ for the VT model, with those for a well-mixed (WM)

population with group size 7, and hexagonal lattice (HL) with death-birth update rule. These are obtained from Equation (5.32) by using the relevant structure coefficients in each case (structure coefficients for death-birth update on regular graphs are derived in [15]).

Values of $(b/c)_1^*$ are symmetric across $h = 0.5$ for all three cases, and minimised at $h = 0.5$ for the hexagonal lattice and VT model. For the well-mixed population, $(b/c)_1^*$ does not vary with either s or h. Furthermore, it is clear for all population types, that as the NPD is approached, i.e. $s \to 0$, $(b/c)_1^*$ becomes independent of h. We will show in Section 5.3.3 that $(b/c)_1^*$ is in fact minimised at $h = 0.5$, so long as the structure coefficients increase with j for $0 \le j < k$.

In all parameter regimes, $(b/c)_1^*$ is highest for the well-mixed population. Both the VT model with decoupled update and HL with death-birth update show similar variation with s and h; however, $(b/c)_1^*$ is always lower for the VT model. Therefore, in terms of thresholds for favourability, we can determine that cooperation is most successful in the VT model with decoupled update, followed by the HL with death-birth update. Cooperation does least well in the well-mixed population. This is consistent with our results for pairwise games in Chapter 4, suggesting that both local interactions and global updating promote cooperation.

Figure 5.5 (right panel) shows the variation of $(b/c)_1^*$ with h and s for the VT model. As we have discussed, these results are based on the approximation that $f_j^C(n,k)$ and g_k are fixed. To verify the accuracy of this approximation, we compare Equation (5.32) with simulation results in Figure 5.6. Simulated values of $(b/c)_1^*$ were obtained for each parameter set (s,h) as follows. We calculated ρ_C (ρ_D) for various b/c values, by running 10^4 simulations of the VT model to fixation, starting with a single C (D) mutant and population size $Z = 100$. In all simulations, we use small selection strength, $\delta = 0.025$, and set $c = 1$. Thus, $(b/c)_1^*$ is determined by the point at which $\rho_C = \rho_D$.

There is a decent fit between simulation and theory. It is possible this could be improved by running larger numbers of simulations, however the model is computationally expensive. In any case, the qualitative behaviour is consistent. For a fixed
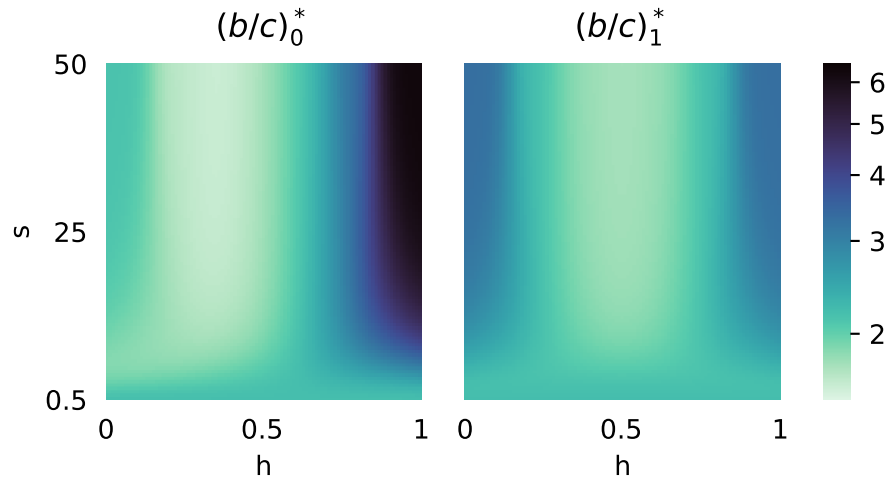
Figure 5.5: Critical benefit-to-cost ratios for the Voronoi tessellation model with decoupled update rule. Cooperation is beneficial when $b/c > (b/c)_0^*$ (left) and favoured when $b/c > (b/c)_1^*$ (right). These are given by Equations (5.32) and (5.39), respectively, for a public goods game with sigmoid benefit function, defined by Equation (2.44). Parameters s and h correspond to the steepness and inflection point of the benefit function, respectively.
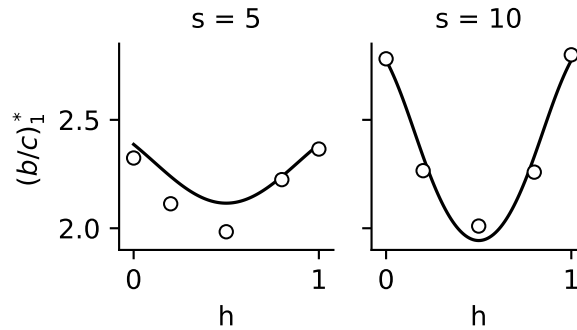
Figure 5.6: Critical benefit-to-cost ratio $(b/c)_1^*$ above which $\rho_C > \rho_D$, for a sigmoid benefit function. The solid line plots Equation (5.32). Circles correspond to simulation data, with each point calculated from 10^4 indiviudal simulations. For both $s = 5$ and $s = 10$ there is symmetry across $h = 0.5$, at which point $(b/c)_1^*$ is minimised. We have set $Z = 100$, $c = 1$ and $\delta = 0.025$.

steepness s, $(b/c)_1^*$ is minimised at $h = 0.5$ and (near) symmetric across this value. The values of $(b/c)_1^*$ are highest when $h = 0$ and $h = 1$, where the benefit function provides diminishing returns or increasing returns respectively.

5.3.3 Minimising the critical benefit-to-cost ratio at which cooperation is favoured

In Section 5.3.2 we considered conditions for cooperation to be favoured for a sigmoid benefit function $\beta(x; h)$, as defined by Equation (2.44). Here, we have made explicit the dependence on the inflection point h. It is clear from Figure 5.4 that the critical benefit-to-cost ratio $(b/c)_1^*$, at which $\rho_C = \rho_D$, is minimised at $h = 0.5$, and symmetric across that point. This appears to hold for both the VT model with decoupled update, and for the death-birth update on a fixed hexagonal lattice. In this section, we show that this is indeed true for any system where $0 < s < \infty$ and the structure coefficients σ_j are increasing for $0 \leq j < k$.

We rewrite Equation (5.32), defining $(c/b)_1^*$, such that cooperation is favoured for $c/b < (c/b)_1^*$:

$$\left(\frac{c}{b}\right)_1^* = \frac{1}{Z-1} \sum_{j=0}^{k} \sigma_j \left[\beta\left(\frac{j+1}{k+1}; h\right) - \beta\left(\frac{k-j}{k+1}; h\right) \right]. \qquad (5.34)$$

We have assumed that the number of neighbours k is fixed, however the results are easily generalisable to variable k. Defining

$$\zeta_j(h) = \beta\left(\frac{j+1}{k+1}; h\right) - \beta\left(\frac{k-j}{k+1}; h\right) \qquad (5.35)$$

we obtain

$$\left(\frac{c}{b}\right)_1^* = \frac{1}{Z-1} \left[\sigma_k + \sum_{k > j \geq k/2} (\sigma_j - \sigma_{k-j-1}) \zeta_j(h) \right]. \qquad (5.36)$$

By taking derivatives with respect to h we show that for $k/2 \leq j < k$, $\zeta_j(h)$ is maximised when $h = 0.5$. In order that this corresponds to a unique maximum of $(c/b)_1^*$, and thus a minimum of the critical benefit-to-cost ratio, certain conditions on σ_j must be satisfied.

First, we show that $\zeta_j(h)$ has one extremum at $h = 0.5$ for $s \in (0, \infty)$. We substitute Equation (2.44) into Equation (5.35) and take the first derivative with

respect to h, letting $r = \frac{j+1}{k+1}$. Thus we obtain

$$
\begin{aligned}
\frac{d\zeta_j}{dh} &= \frac{d}{dh}\left[\frac{(1+e^{s(h-r)})^{-1} - (1+e^{s(h+r-1)})^{-1}}{(1+e^{s(h-1)})^{-1} - (1+e^{sh})^{-1}}\right] \\
&= \frac{d}{dh}\left[\frac{e^{s(r-1)} - e^{-sr}}{1-e^{-s}} \cdot \frac{(1+e^{s(h-1)})(1+e^{sh})}{(1+e^{s(h-r)})(1+e^{s(h+r-1)})}\right] \\
&= s \cdot \frac{e^{s(r-1)} - e^{-sr}}{1-e^{-s}} \cdot \frac{e^{sh}(1+e^{-s}-e^{-sr}-e^{s(r-1)})(1-e^{s(2h-1)})}{(1+e^{s(h+r-1)})^2(1+e^{s(h-r)})^2}.
\end{aligned}
\tag{5.37}
$$

Setting $d\zeta_j/dh = 0$, gives one root at $h = 0.5$ for $0 < s < \infty$. This is a unique stationary point of $(c/b)_1^*$ so long as there is at least one value of $j \in [k/2, k)$ for which $(\sigma_j - \sigma_{k-j-1}) \neq 0$. We can show that this is a maximum by considering the second derivative at $h = 0.5$:

$$
\left.\frac{d^2\zeta_j}{dh^2}\right|_{h=\frac{1}{2}} = -2s^2 \cdot \frac{e^{s/2}(1+e^{-s}-e^{-sr}-e^{s(r-1)})(e^{s(r-1)}-e^{-sr})}{(1-e^{-s})(1+e^{s(r-1/2)})^2(1+e^{-s(r-1/2)})^2},
\tag{5.38}
$$

which is negative given that $1/2 < r < 1$. This corresponds to $(k-1)/2 < j < k$, encompassing all the values of j which we sum over in Equation (5.36). Therefore, in order that $(c/b)_1^*$ is maximised when $h = 0.5$, we require that $(\sigma_j - \sigma_{k-j-1}) \geq 0$ for $k/2 \leq j < k$ and non-zero for at least one value of j in the range. This condition is guaranteed if σ_j is an increasing, but not constant, function for $0 \leq j < k$.

It is clear from Figure 5.3 that $\sigma_{j+1,k} > \sigma_{j,k} \,\forall j,k$ for the VT model with decoupled update, therefore $h = 0.5$ maximises $(c/b)_1^*$ in this case. For k-regular graphs with death-birth update rule, we can verify whether this is true by using the approximate expressions for the structure coefficients derived in [15]. These are plotted for various k values in Figure 5.7. For smaller values of k, we can see that σ_j is strictly increasing for $0 \leq j < k$. However, as k increases, a growing region appears for which σ_j is constant. So long as there is at least one value of $j < k$ for which $(\sigma_j - \sigma_{k-j-1}) > 0$, $(c/b)_1^*$ is maximised at $h = 0.5$. However, as $k \to \infty$, we approach the case where σ_j are constant for $j < k$, and we regain the well-mixed population result that $(c/b)_1^*$ is independent of h.

Thus far we have limited ourselves to cases where $0 < s < \infty$. In the limit
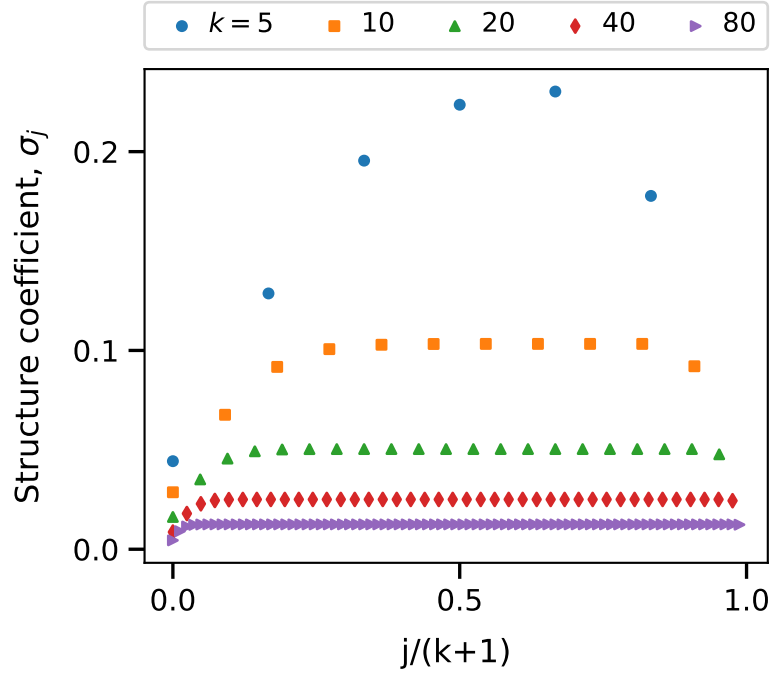
Figure 5.7: Structure coefficients, σ_j, for k-regular graphs with death-birth update rule [15]. It is clear that σ_j is increasing (or constant) for $j < k$.

$s \to 0$, we obtain an NPD game with a linear benefit function which is independent of h. The value of $(c/b)_1^*$ therefore does not depend on h either, as can be seen in Figure 5.4. In the limit $s \to \infty$, the VD game is approached and the benefit function ceases to be continuous. In this case the unique maximum at $h = 0.5$ is maintained only if σ_j are strictly increasing, and therefore $(\sigma_j - \sigma_{k-j-1}) > 0$. This is true for the VT model with decoupled update and for k-regular graphs with death-birth update, if k is sufficiently small. On the other hand, if $(\sigma_j - \sigma_{k-j-1}) = 0$ for some values of $j \in [k/2, k)$, $h = 0.5$ ceases to be an isolated maximum, and there is a region of h values, around $h = 0.5$, which maximise $(c/b)_1^*$.

5.3.4 Beneficial cooperation

Thus far, we have considered conditions for cooperation to be favoured, i.e. where $\rho_C > \rho_D$. We can also define the critical benefit-to-cost ratio $(b/c)_0^*$ above which cooperation is beneficial, i.e. $\rho_C > \rho_0$. From Equation (5.22) this is given by

$$\left(\frac{b}{c}\right)_0^* = \frac{Z(Z-1)}{2\sum_{k=1}^{Z-1}\sum_{j=0}^{k}\left[\theta_{j,k}^C \beta\left(\frac{j+1}{k+1}\right) - \theta_{j,k}^D \beta\left(\frac{j}{k+1}\right)\right]}, \tag{5.39}$$

where $\theta_{j,k}^{C/D}$ are calculated from the distributions $f_j^{C/D}(n,k)$ and g_k according to Equations (5.19) and (5.20) (recall that we have relabelled $A \to C$ and $B \to D$).

Figure 5.5 (left panel) plots $(b/c)_0^*$ against s and h. We can see that for large s, $(b/c)_0^*$ is maximised at $h = 1$ and has a minimum at $h \approx 0.35$. For smaller s this minimum moves towards $h = 0$. As s decreases further, the logistic function approaches linearity and there is negligible variation in $(b/c)_0^*$ with h. In the limit $s \to 0$ the game becomes an NPD, with $(b/c)_0^* = (b/c)_1^* \approx 2.2$. Figure 5.8 compares the simulated values of $(b/c)_0^*$ with the theoretical prediction, finding good agreement between the two for a range of s and h values.
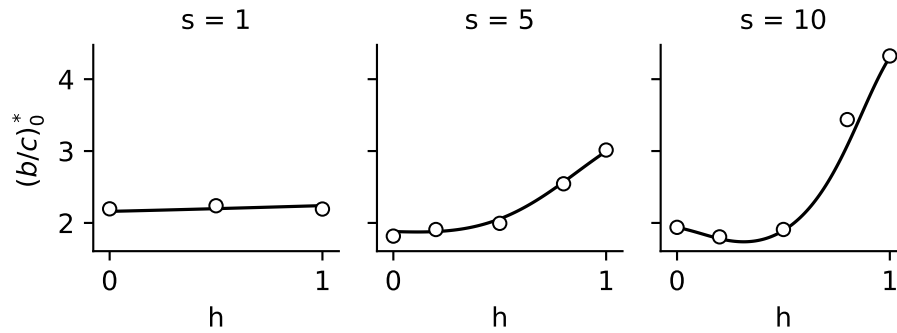
Figure 5.8: Critical benefit-to-cost ratio $(b/c)_0^*$ above which $\rho_C > \rho_0$, for a sigmoid benefit function. The solid line plots Equation (5.39). Circles correspond to simulation data, with each point calculated from 10^4 individual simulations. For small s the sigmoid benefit function becomes near linear and the game approaches an *NPD*, thus there is little variation in $(b/c)_0^*$. For larger s there is strong dependence on the inflection point, h, particularly for $h > 0.5$. We have set $Z = 100$, $c = 1$ and $\delta = 0.025$.

We saw in Figure 5.4 that the critical benefit-to-cost ratios for cooperation to be favoured $(b/c)_1^*$ are lower in the VT model compared to the well-mixed population. Figure 5.9 plots $(b/c)_0^*$ for a well-mixed population with $N = 7$ and the VT model with decoupled update rule, showing clearly that the critical benefit-to-cost ratios for cooperation to be beneficial are also lower for the VT model. Thus, under both measures, cooperation is promoted by the VT model. In contrast to $(b/c)_1^*$, which was independent of the shape of the benefit function for the well-mixed population, $(b/c)_0^*$ is an increasing function of h, so long as s is sufficiently large.
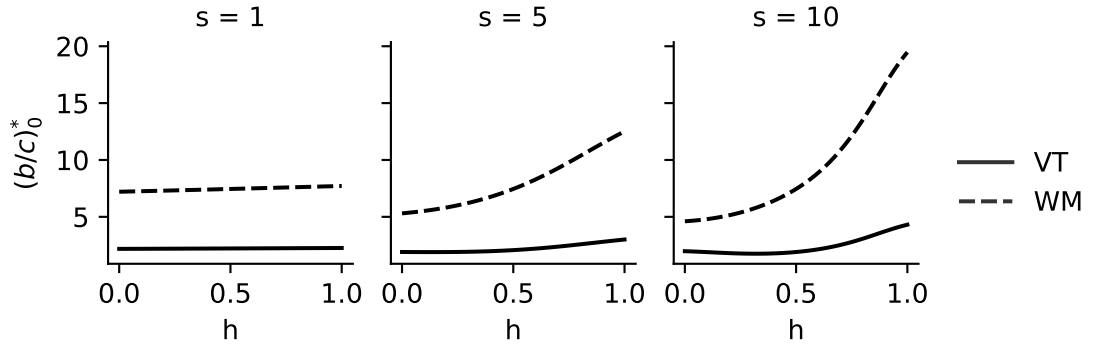
Figure 5.9: Comparing the critical benefit-to-cost ratio $(b/c)_0^*$ at which $\rho_C > \rho_0$, for a public goods game with sigmoid benefit function. The critical ratio is always higher for the well-mixed population with $N = 7$ (WM), than for the Voronoi tessellation model with decoupled update (VT). For small s the benefit function becomes near linear and variation of $(b/c)_0^*$ with h is small. For WM, $(b/c)_0^*$ increases with h, taking its minimum value at $h = 0$. By contrast, for VT, there is a minimum of $(b/c)_0^*$ at $h \approx 0.35$ when s is sufficiently large. For both WM and VT, $(b/c)_0^*$ is maximised at $h = 1$, for any given s.

5.3.5 Beneficial vs. favourable cooperation

In general, the conditions for cooperation to be beneficial are not equivalent to the conditions for cooperation to be favoured. This is evident from Figure 5.10, where we plot $(b/c)_0^*$ and $(b/c)_1^*$ for the sigmoid benefit function. These critical benefit-to-cost ratios are plotted against h, for various values of s. The parameter space can be divided into regions where cooperation is both favoured and beneficial, favoured but not beneficial, beneficial but not favoured, and neither favoured nor beneficial. As s is decreased, the regions where cooperation is beneficial but not favoured, and favoured but not beneficial, get smaller. For sufficiently small s, it appears that $(b/c)_0^* \approx (b/c)_1^*$ for all values of h. This holds for both the VT model and well-mixed population.

We can show that $(b/c)_0^* = (b/c)_1^*$ in the limit $s \to 0$. Recall from Section 5.2.3 that the conditions for cooperation to be beneficial and favoured are equivalent if the payoffs satisfy antisymmetry-of-invasion. When $s \to 0$ we approach the NPD, which has a linear benefit function, given by Equation (2.42). The cooperator and

defector payoffs are thus

$$a_j = b \cdot \left(\frac{j+1}{k+1} \right) - c \quad \text{and} \quad b_j = b \cdot \left(\frac{j}{k+1} \right), \qquad (5.40)$$

respectively. We therefore obtain

$$a_j + b_{k-j} = b - c. \qquad (5.41)$$

As $b - c$ is a constant independent of j, this satisfies the antisymmetry-of-invasion property, defined by equation (5.30). The critical benefit-to-cost ratio above which cooperation is favoured must, therefore, be equal to the critical benefit-to-cost ratio above which cooperation is beneficial.

It also appears from Figure 5.10 that, for both the VT model and well-mixed populations, $(b/c)_0^* = (b/c)_1^*$ when $h = 0.5$. We can again show that this satisfies the antisymmetry-of-invasion property. When $h = 0.5$, the sigmoid benefit function, defined by Equation (2.44), has the symmetry property $\beta(x) = 1 - \beta(1 - x)$. The cooperator and defector payoffs are, therefore, given by

$$a_j = b \cdot \beta \left(\frac{j+1}{k+1} \right) - c = b \cdot \left[1 - \beta \left(\frac{k-j}{k+1} \right) \right] - c$$
$$b_j = b \cdot \beta \left(\frac{j}{k+1} \right), \qquad (5.42)$$

respectively. Once again, we find that $a_j + b_{k-j} = b - c$; thus, there is antisymmetry-of-invasion when $h = 0.5$.

Figure 5.10 shows that $h = 0.5$ divides the parameter space into two regimes. Behaviour where cooperation is beneficial but not favoured, occurs only when $h < 0.5$. Conversely, behaviour where cooperation is favoured but not beneficial occurs only when $h > 0.5$.

We can understand this intuitively by considering the extreme cases ($h = 0, 1$) of the VD game. Recall the benefit function for a VD game is a step function, and it can be obtained as a limiting case of the sigmoid public goods game, by letting $s \to \infty$. When $h = 0$, a cooperator always receives the full benefit, even if it has no

cooperator neighbours. Defectors require a single cooperator neighbour to obtain the benefit. Thus, both cooperators and defectors have higher than average fitness early in the invasion process, when they are most vulnerable to extinction. It is therefore possible, depending on the benefit-to-cost ratio, that both perform better than a neutral invader, and therefore both are beneficial mutations. However, one can still be favoured over the other if its fixation probability is higher.

The converse is true when $h = 1$: defectors will never receive any benefit, and cooperators only obtain the benefit when surrounded by other cooperators. Thus when the number of cooperators/defectors is small, they have lower than average fitness, and there is a high chance they die out early in the invasion process. Therefore, it is possible that neither performs better than a neutral invader.
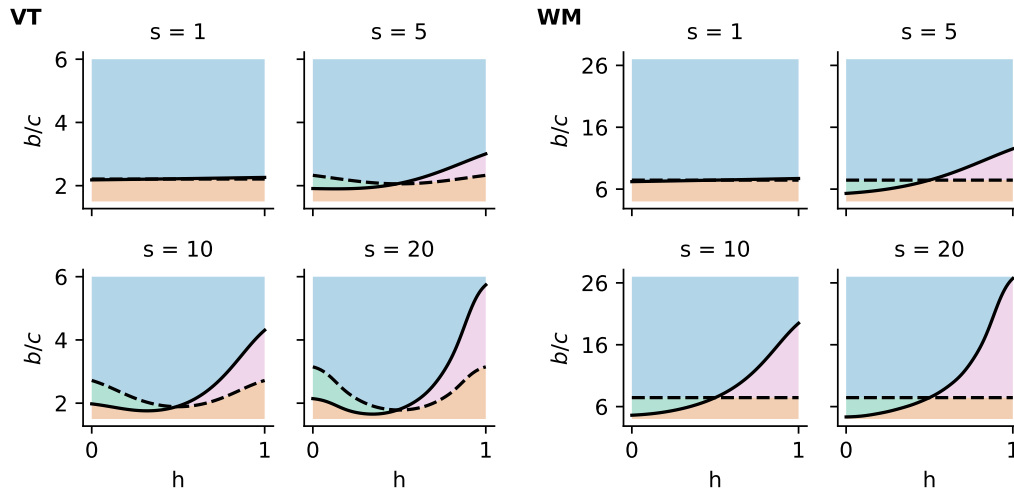
Figure 5.10: Success of cooperator mutants in the Voronoi tessellation model (VT, left) and well-mixed population (WM, right), for a public goods game with sigmoid benefit function. The solid line corresponds to $(b/c)_0^*$, where $\rho_C = \rho_0$. The dashed line corresponds to $(b/c)_1^*$, where $\rho_C = \rho_D$. We have set $Z = 100$, $c = 1$ and $\delta = 0.025$.

Blue region (top): C is beneficial and favoured ($\rho_C > \rho_D$ and $\rho_C > \rho_0$).
Green region (left): C is beneficial but not favoured ($\rho_D > \rho_C > \rho_0$).
Pink region (right): C is favoured but not beneficial ($\rho_0 > \rho_C > \rho_D$).
Orange region (bottom): C is neither beneficial not favoured ($\rho_C < \rho_D$ and $\rho_C < \rho_0$).

5.3.6 Gradient of selection

We can obtain more insight into what is happening in the different parameter regions by looking at the gradient of selection $G(n) = T^+(n) - T^-(n)$. The transition probabilities are defined by Equation (5.1), thus in the weak selection limit, $\delta \ll 1$, the gradient of selection becomes

$$G(n) \approx \frac{Z-n}{Z}\frac{n}{Z}\delta\left\{\sum_{k=1}^{Z-1}\sum_{j=0}^{k} g_k(f_j^A(n,k)a_{j,k} - f_j^B(n,k)b_{j,k})\right\}. \tag{5.43}$$

The sum essentially gives the difference in expected payoffs of A and B players. Thus, the right-hand side is identical to the replicator equation, which describes the deterministic dynamics in the large-population limit (recall Section 2.2.1).

The sign of $G(n)$ indicates the direction of selection, and we can consider the roots of $G(n)$ as 'fixed points'. Of course, for a finite population there are only two absorbing states, $n = 0$ and $n = Z$; however, the location of fixed points is still important. For example, the system may remain for a long time near a stable fixed point, before reaching one of the absorbing states. We can classify the behaviour of the system in different parameter regions based on the fixed points of the gradient of selection.

Figure 5.11 plots $G(n)$ for a sigmoid PGG with various values of h, s and b/c, both for the VT model and well-mixed population. There are four dynamical regimes, consistent with the deterministic results for the well-mixed population [37]:

(i) *Dominance:* there are only two fixed points at $n = 0$ and $n = Z$. Defection dominates if the $n = 0$ fixed point is stable, while cooperation dominates if the $n = Z$ fixed point is stable.

(ii) *Coexistence:* there is an internal stable fixed point, n_R, along with two unstable fixed points at $n = 0$ and $n = Z$. Selection pushes the system towards the stable fixed point, thus it can take a long time to reach one of the absorbing states.

(iii) *Coordination:* there is an internal unstable fixed point, n_L, along with two

stable fixed points at $n = 0$ and $n = Z$.

(iv) *Coexistence & coordination:* In addition to the fixed points at $n = 0$ (stable) and $n = Z$ (unstable), there is both an unstable internal fixed point on the left, n_L, and a stable internal fixed point on the right, n_R. Thus it resembles coexistence, in that there is a stable mixed state; and coordination in that there are two stable fixed points.

These regimes are all familiar in the evolutionary game theory literature for well-mixed populations. The first three correspond to the behaviour of pairwise social dilemma games, outlined in Section 2.2: (i) prisoner's dilemma/harmony game, (ii) snowdrift game, and (iii) stag-hunt game. The final type, coexistence & coordination, arises in both the N-player stag-hunt [146] and N-player snowdrift games [147].

For the well-mixed population, we see dominance when s is sufficiently small, and thus the sigmoid PGG is approximating an NPD. As expected, cooperation is dominant when b/c is sufficiently high. For higher values of s there is a wide range of behaviour. In a region around $h = 0.5$, if b/c is large enough, there are coexistence & coordination dynamics. There is a large basin of attraction for n_R and if the system reaches this fixed point, it will spend a long time in the vicinity. However, a single mutant invader must cross n_L to reach this, against the selection pressure. As b/c is increased, n_L and n_R move further apart, increasing the size of the basin of attraction for n_R. For $h = 0.5$, the gradient of selection is symmetric $(n_L = Z - n_R)$.

Decreasing h from 0.5, causes n_L and n_R to move to the left, eventually entering the coexistence regime. The basin of attraction for the internal stable fixed point is now $0 < n < Z$. The system may spend a large amount of time near this point, although it will ultimately end up in one of the absorbing states. In the coexistence regime, as we discussed in Section 5.3.4 for the VD game with $h = 0$, cooperators and defectors have a selective advantage when they are in sufficiently small numbers. This can lead to the case where both are beneficial mutants, and thus cooperation is able to be beneficial but not favoured.
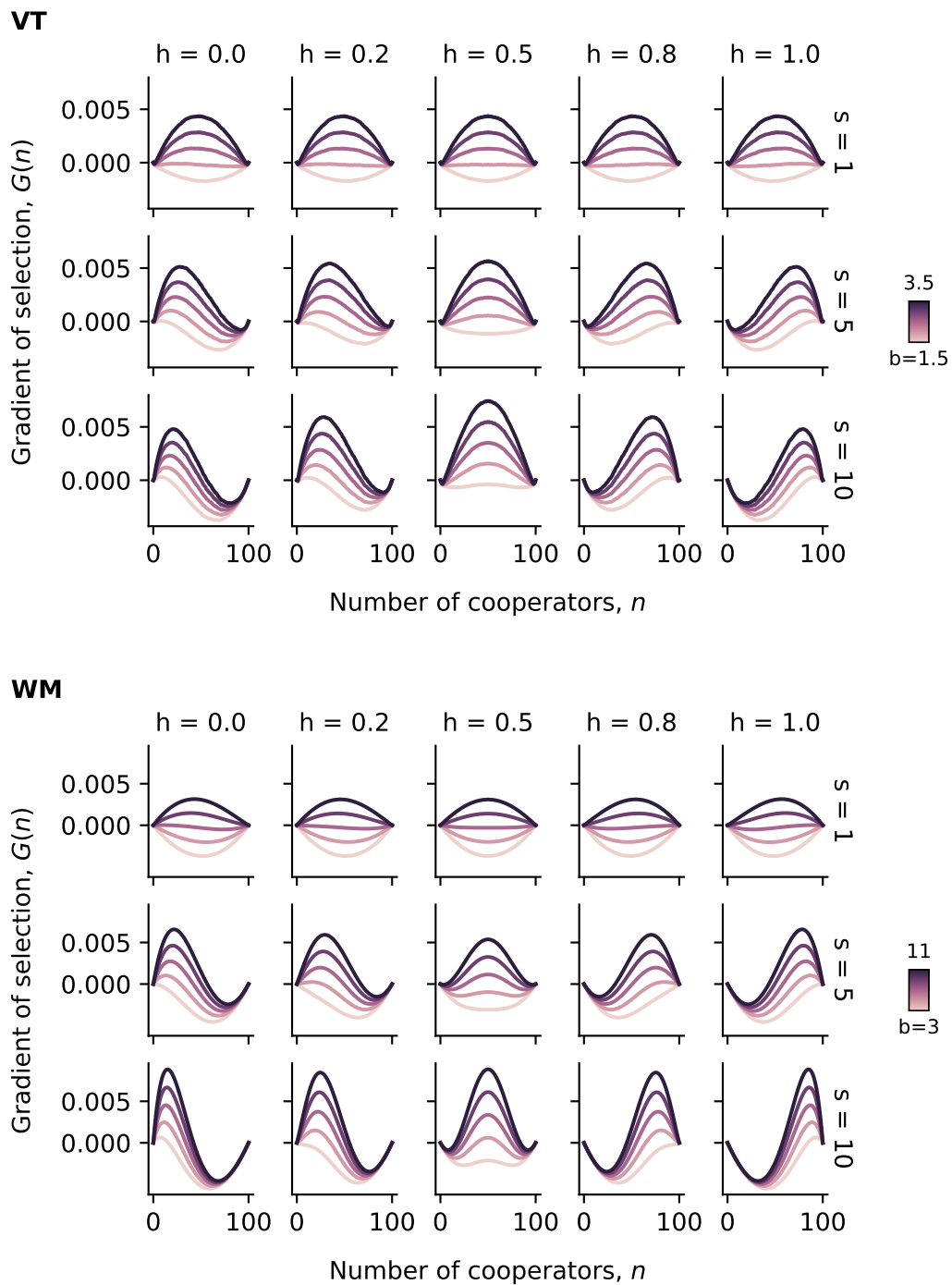
Figure 5.11: Gradient of selection $G(n)$ for a public goods game with sigmoid benefit function in the Voronoi tessellation model with decoupled update (VT, top) and the well-mixed population (WM, bottom). The qualitative behaviour is very similar between the two. However, it occurs at different values of the benefit, b/c. Where $G(n) > 0$, selection is working to increase n, and where $G(n) < 0$ it works to decrease n. The roots of $G(n) = 0$ can be considered as fixed points, and we can use these to classify the behaviour in different parameter regions. We have set $Z = 100$, $c = 1$ and $\delta = 0.025$.

Conversely, as h is increased from 0.5, n_L and n_R move to the right and the dynamics enter the coordination regime. This corresponds to the region in Figure 5.10 where very high values of the benefit-to-cost ratio are required for cooperation to be beneficial, even when cooperation is favoured. We argued in Section 5.3.4, for the VD game with $h == 1$, that this is due to the fact that both cooperators and defectors are at a disadvantage when in small numbers. Indeed, this is the defining feature of the coordination regime, that $n = 0$ and $n = 1$ are stable fixed points. Thus, any invader is at a disadvantage initially, as selection pushes it towards dying out. Therefore it is possible that defectors and cooperators can be at an evolutionary disadvantage compared to a neutral mutant.

The VT model behaviour is qualitatively very similar to that of the well-mixed population. The major difference is that the full spectrum of behaviour is available for a much smaller range of b/c values for the VT model. This means that cooperation is successful at smaller benefit-to-cost ratios, as is consistent with our previous findings. It should be noted, however, that these classifications are often approximate for the VT model. We observe, in a number of cases, additional fixed points very close to $n = 0$ and $n = Z$. An example can be seen in Figure 5.12. It is also clear from Figure 5.11 that the coexistence & coordination behaviour is much less pronounced than it is for the well-mixed case, with the internal fixed points much closer to the boundaries.

5.4   Discussion

This chapter has considered cooperative success in the VT model with spatially decoupled birth and death, where cooperation is defined by a multiplayer public goods game. This extends the work from Chapter 4, which was focused on pairwise games.

We have demonstrated that, for a sigmoid PGG, cooperation is more successful in the VT model compared to a well-mixed population. In both cases, the evolutionary outcomes depend on the parameters s and h of the sigmoid benefit function, as well as the benefit-to-cost ratio. In general, a lower benefit-to-cost ratio is required
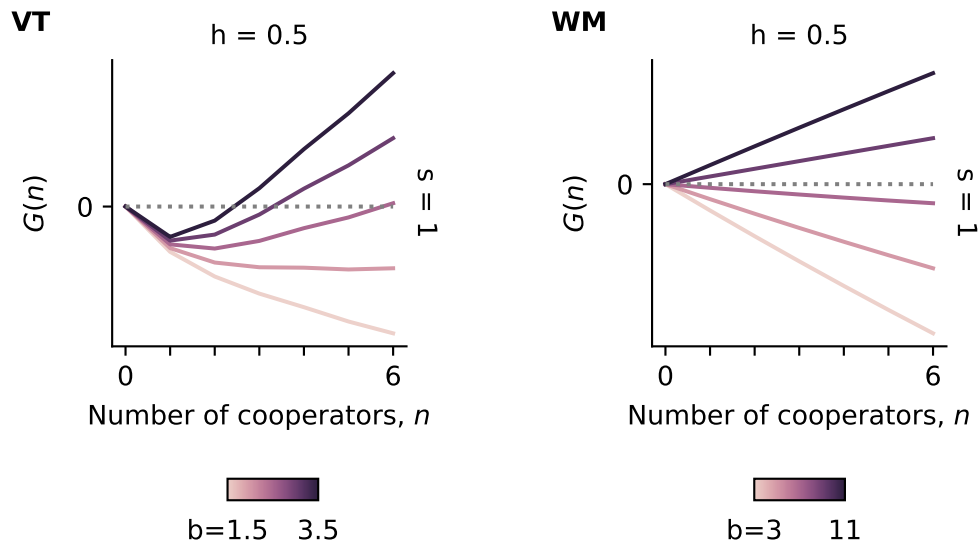
Figure 5.12: Gradient of selection $G(n)$ for a public goods game with sigmoid benefit function in the Voronoi tessellation model with decoupled update (VT) and the well-mixed population (WM). The figure shows results reproduced from Figure 5.11 for $s = 1$ and $h = 0.5$, zooming in on the gradient of selection near $n = 0$. It is clear for WM that the $n = 0$ fixed point can be stable or unstable depending on b. By contrast, for VT, the $n = 0$ fixed point remains stable for all values of b shown. However, for sufficiently high b there is an additional unstable fixed point, close to $n = 0$.

for cooperative success for the VT model than for the well-mixed population. In other words cells need a lower incentive to cooperate. This is consistent with our expectations: both models use global updating, however the population structure in the VT model allows for the positive assortment of cooperators.

Although cooperation is more successful in the VT model than in the well-mixed population, the qualitative behaviour is very similar. We have characterised the evolutionary dynamics by considering conditions for which cooperation is beneficial and/or favourable, as well as calculating the gradient of selection.

As long as the steepness s is large enough, we tend to see coexistence behaviour when the inflection point h is less than half and coordination behaviour when it is greater. These regimes are characterised by the fixed points of the gradient of selection. They also correspond to the regions in the parameter space where cooperation is beneficial but not favourable (coexistence), and favourable but not beneficial (coordination). For small steepness s, the game approaches an NPD and

there is dominance behaviour. In this regime, conditions for cooperation to be beneficial and favoured coincide.

Examining the gradient of selection enables us to identify an additional dynamical regime: mixed coexistence & coordination, which occurs in a region around $h = 0.5$, as long as s and b/c are sufficiently large. This regime is characterised by two stable fixed points, one corresponding to all-defection, and the other to a heterogeneous, majority-cooperator state. This dynamic has been identified previously for both well-mixed populations [37] and graph-structured populations with local updating [40]. We have shown that it can also occur for the VT model, however the internal fixed points tend to be much closer to the boundaries.

It is beyond the scope of this thesis to consider the full dynamics of an epithelial population structure with local update rules. However, we have considered the conditions for cooperation to be favourable on a hexagonal lattice with death-birth update rule, using results from [15]. We found the critical benefit-to-cost ratios to be intermediate between the well-mixed population and VT model. This is consistent with previous results for pairwise games [138]. Taken together, these results suggest not only that population structure is able to promote cooperation, but that global updating also plays a crucial role. Thus, we propose a general rule that cooperation prefers local game play, but global competition for offspring.

It is worth taking a moment to consider the implications of beneficial and favourable mutations for invasion, and how we distinguish between the two concepts. Whether or not a mutation is beneficial is perhaps the most relevant measure for a single invasion event. It essentially tells us that the mutated cell has a higher probability of invasion in a wild-type population, than a wild-type cell would have, and therefore it has an evolutionary advantage. The significance of a mutation being favourable is a little less clear, as it compares two different invasion processes: the probability of invasion of a mutated cell in a wild-type population is higher than the converse scenario, where a wild-type cell invades a population of mutants. However, the condition for a mutant to be favoured is also equivalent to the condition for cooperation to dominate, if mutation is allowed.

These results suggest that there are a number of important considerations which need to be taken into account when modelling the evolution of cooperation in an epithelium: population structure, update rule and benefit function. In particular, the success of cooperation could easily be underestimated, either by ignoring population structure, or by including population structure, but considering only local update rules. If birth and death are decoupled in real epithelia, our results suggest that producers of growth factor can have an evolutionary advantage, even when the cost to themselves is relatively high compared to the benefit.

These local and global update rules represent two extremes: absolute spatial coupling of birth and death, or absolute decoupling, respectively. In reality, the relationship between birth and death in an epithelium is likely somewhere in between the two. Regulatory processes such as contact inhibition [135] and crowding-induced extrusion [136, 137] could lead to a weaker form of spatial coupling, somewhere in between local and global updating. In the following chapter we will introduce contact inhibition into the VT model and consider how it affects the evolutionary success of cooperation.

Chapter 6

The effect of contact inhibition

6.1 Introduction

Throughout this thesis, we have demonstrated the important role which the update dynamics play in determining evolutionary outcomes for structured populations. There are substantive differences depending on whether a global or local update rule is used, and for the latter, how birth and death are coupled. In particular, we have found that using the decoupled update rule within the VT model promotes cooperation compared to a death-birth update rule, which in turn promotes cooperation compared to a birth-death update rule. This result holds for a large spectrum of pairwise and multiplayer games (see Chapters 4 and 5 respectively).

It is therefore necessary to consider the update dynamics of a real epithelium, in particular, the extent to which division and death are spatially coupled. The global and local update rules we have considered thus far, present a binary view, whereby the former has no spatial coupling, and the latter has very strong spatial coupling. There is, however, a spectrum of possible behaviour between these two cases. Furthermore, the update rules we have considered assume that a death is immediately followed by a division, or vice versa, to maintain a fixed population size. In this chapter, we consider how homeostatic population size can be maintained by density-dependent processes within an epithelium, how these can lead to spatial coupling, and how this can affect the evolution of cooperation.

As we discussed in Section 3.4, the regulation of tissue density is vital for

homeostatic epithelia. An increase in density could lead to tumour formation, while a fall could cause a loss of barrier function. Thus to maintain a near constant population size, cell divisions must match cell deaths. It is thought that density-dependence of proliferation and cell death could play an important role in mediating this population control [108, 136, 137]. Density-dependent control of division or death is likely to result in a type of spatial coupling of the two processes. For example if divisions occur only at low density, these are more likely to occur near a recent death.

A recent study of homeostatic epidermal stem cells found that cell division was a downstream result of cell differentiation [110]. This is in contrast to a number of results for immature, developing tissues, which found that population size was controlled by cell delamination induced by overcrowding. The authors suggest a difference in purpose in the two cases. In the developing tissue, proliferation is primary, and cells are removed from the tissue to keep this under control. By contrast, proliferation in the homeostatic tissue is necessary only to replace cells lost by apoptosis or differentiation, thus it could be considered secondary.

For our purposes, we are primarily concerned with homeostatic tissues and thus choose to focus on contact inhibition as the primary mechanism for homeostasis. It should be emphasised, however, that density-dependent apoptosis, extrusion, or delamination may well play a role in homeostatic tissues.

Contact inhibition refers to the observation that cultured cells divide at slower rates as population density increases, eventually leading to proliferative arrest [135, 148]. Thus, it is an excellent candidate as a mechanism for preventing overpopulation, indeed the loss of contact inhibition is one of the hallmarks of cancer [28]. Contact inhibition is a reversible process: cells which are in mitotic arrest can reenter the cell cycle if they are stretched or space becomes available [149, 150].

Due to contact inhibition and other density-dependent processes, there is likely some level of spatial coupling of birth and death in epithelia. This could lead to a type of intermediate update dynamic between a local and global update rule. To examine the effect this has on the evolution of cooperation, we introduce contact

inhibition into the VT model. This also allows us to temporally decouple division and death, as contact inhibition acts to maintain homeostatic population size.

As we did in Chapter 4 for the decoupled update rule, we take the additive prisoner's dilemma (APD) as a starting point for our analysis, as it provides a simple model for cooperation which can be described by a single parameter, the benefit-to-cost ratio. We hypothesise that the success of cooperation in the VT model will be dependent on the strength of contact inhibition. When contact inhibition is very strong, we get closer to a death-birth update. Thus, cooperation is less successful with a higher critical benefit-to-cost ratio. Conversely, when contact inhibition is weak we move towards a decoupled update and cooperation should be promoted.

The remainder of this chapter is set out as follows. We start by outlining how the VT model is extended to incorporate contact inhibition in Section 6.2, before considering how the evolutionary game theory framework is applied within this extended VT model in Section 6.3. We then, in Section 6.4, look at how the success of cooperation depends on the model parameters and compare the outcomes with our previous results for death-birth and decoupled update rules. We find that while stronger contact inhibition does lead to increased spatial coupling, this does not necessarily result in a deleterious effect on cooperation. We consider how this can be explained by differences in the distribution of non-contact inhibited cells. In order to further understand this phenomenon, we introduce a one-dimensional version of the VT model in Section 6.5. Finally, in Section 6.6, we discuss some of the implications of our results for the evolution of cooperation in real epithelia.

6.2 The Voronoi tessellation model with contact inhibition

6.2.1 Model overview

We use the VT model as described in Section 3.3, with the parameters given in Table 6.1. The basic model is the same as has been used throughout Chapters 4 and 5. Here we outline how contact inhibition is incorporated.

Recall from Section 3.3, that the VT model represents cells as points in a fixed

domain which exert spring-like forces on one another. The natural spring length, or preferred cell separation, is given by the parameter s_M. We take the preferred cell area to be the area of a regular hexagon with diameter s_M, such that $A^{(0)} = \frac{\sqrt{3}}{2} s_M^2$.

Contact inhibition is implemented as an area-checkpoint. Cells are only able to proliferate if they exceed a threshold area $\alpha A^{(0)}$, where α is the quiescent area fraction. Cells which satisfy $A_i(t) > \alpha A^{(0)}$ divide with rate γ, such that in a small time interval $(t, t + \Delta t)$, the probability of cell i dividing is given by

$$P_i^{\mathrm{div}}(t, \Delta t) = \gamma \Delta t \Theta \left(A_i(t) - \alpha A^{(0)} \right), \tag{6.1}$$

where $\Theta(x)$ is the Heaviside step function. In simulations we implement this as follows. In each time interval $(t, t + \Delta t)$ a division occurs with probability $Z_{\mathrm{div}}(t) \gamma \Delta t$, where $Z_{\mathrm{div}}(t) = \sum_i \Theta \left(A_i(t) - \alpha A^{(0)} \right)$ is the number of non-contact inhibited cells. The dividing cell is then selected uniformly at random from the set of cells satisfying $A_i(t) > \alpha A^{(0)}$.

Cell deaths occur with a per-cell rate λ, thus the probability of a cell i dying in time interval Δt is

$$P_i^{\mathrm{death}}(\Delta t) = \lambda \Delta t. \tag{6.2}$$

As with division, this is implemented in simulations by defining the probability of a death occurring in the whole population to be $Z(t) \lambda \Delta t$, where $Z(t)$ is the total number of cells at time t. If a death occurs the cell is chosen from the whole population uniformly at random. Dead cells are immediately removed from the tissue. Cell death could refer to a number of processes including apoptosis or differentiation.

This chapter uses a slightly different set of parameters for the VT model, compared to those in Chapters 4 and 5. The original parameters were taken from [151], and are defined in Table 4.1. Parameters for this chapter are defined in Table 6.1. The main difference is that we now assume a smaller death rate, which we have chosen to be in line with differentiation rates for epidermal stem cells [110]. We have then rescaled the parameters μ and Δt, so the resulting dynamics is the same. However, the new death rate is significantly slower than our previous death rate,

and as such we choose to ignore the initial growth phase and assume that $t_M = 0$. New offspring cells are still placed a distance ε apart, but they immediately have a preferred separation of s_M.

Table 6.1: Parameters for the Voronoi tessellation model with contact inhibition used in Chapter 6. Space is measured in units of preferred cell diameter (CD). Explicit units are not given for μ and η, as the dynamics depends only on their ratio μ/η, which has units hour^{-1}. Note that μ has dimensions [mass]/[time]^2 and η has dimensions [mass]/[time]. For values of α, λ/γ and W see Table 6.2. Homeostatic population size depends on these three parameters. We choose W to obtain the desired homeostatic population size, usually $Z^* = 100$.

Symbol	Description	Value
μ	Spring constant	6.25
η	Drag coefficient	1.0
t_M	Growth time for new cells	0.0 hours
s_M	Natural separation of mature cells	1.0 CD
ε	Initial separation of sibling cells	0.1 CD
Δt	Time step	0.04 hours
λ	Death rate	0.25 day^{-1}
γ	Division rate (no contact inhibition)	$(> \lambda)$
α	quiescent area fraction	–
W	Domain width	–
Z^*	Homeostatic population size	100

6.2.2 Homeostasis

We initialise the simulations with a hexagonal lattice of $L \times L = Z_0$ cells, each with diameter W/L. Once the simulation begins, cells are able to divide and die, and the tissue quickly reaches an equilibrium density around which it fluctuates (Figure 6.1a). This homeostatic density decreases as we increase α and λ/γ, as can be seen in Figure 6.1b.

The fraction λ/γ is equal to the expected proportion of proliferating cells. Thus, when λ/γ is large only a small number of cells are expected to be contact inhibited (not able to proliferate) at any given time, and we can interpret this as weak contact inhibition. Conversely, when λ/γ is small, we expect a large number of cells to be contact inhibited, and therefore we can consider that contact inhibition is strong. The strength of contact inhibition is therefore negatively correlated

with λ/γ. Furthermore, stronger contact inhibition implies tighter regulation of population size. It therefore follows that fluctuations in tissue density would be correspondingly smaller. This is clear from Figure 6.1c, which shows the standard deviation of the population density increasing with λ/γ. There is no clear dependence on α.
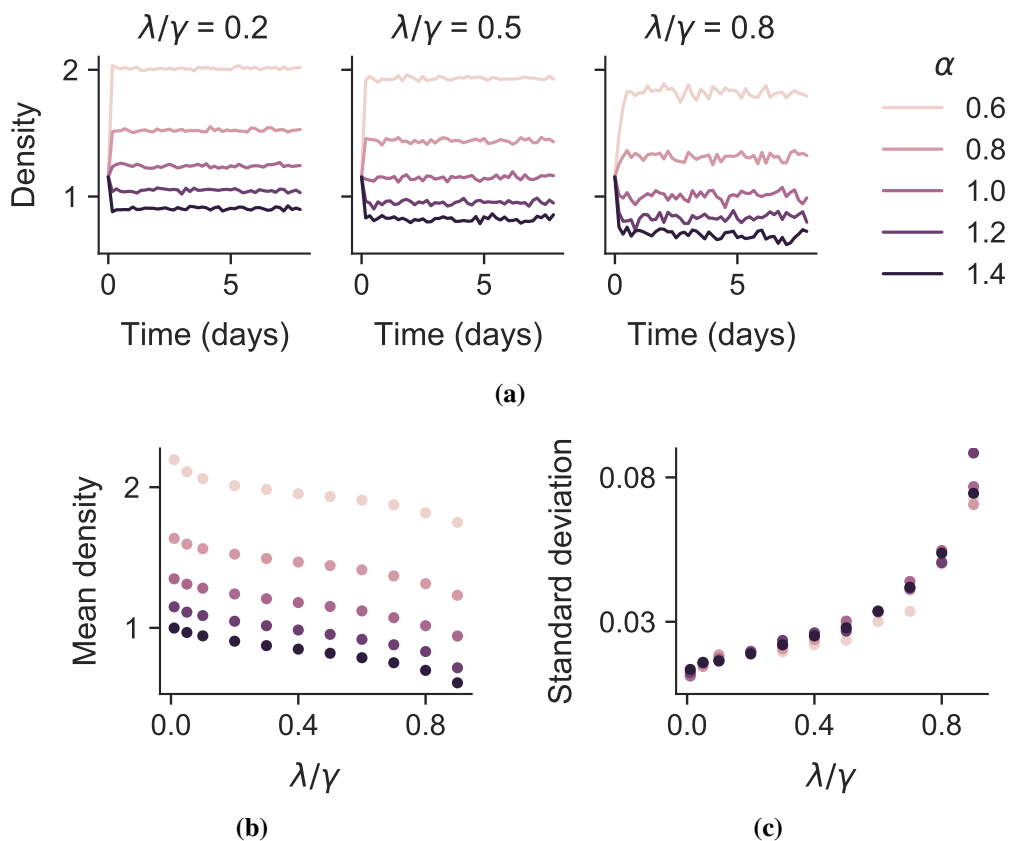
Figure 6.1: Tissue density in the Voronoi tessellation model with contact inhibition. Density is in units of cells per CD^2. Simulations are started with $Z_0 = 196$ cells arranged in a hexagonal grid. Initially all cells have diameter equal to the natural separation $s_M = 1\,CD$ (domain width $W = 14\,CD$). Once the simulation begins, cells are able to divide and die, and the tissue quickly reaches a homeostatic equilibrium density.

(a) Variation in the density over time; (b) and (c) mean and standard deviation, respectively, in the homeostatic tissue density taken as an average over six simulation days, after the tissue has reached equilibrium. All data is taken as an average over three simulated tissues.

We can use the homeostatic density to calculate the domain size required for our desired homeostatic population size. In the remainder of this work, the domain

width W is chosen such that the homeostatic population size is always $Z^* = 100$. These values can be found in Table 6.2.

Table 6.2: Values of domain width, W, for each combination of parameters λ/γ and α used in simulations of the Voronoi tessellation model with contact inhibition. These are chosen so that the homeostatic population size is $Z^* = 100$.

		α	
λ/γ	0.8	1.0	1.2
0.01	8.402	9.253	10.022
0.02	8.444	9.298	10.074
0.06	8.527	9.400	10.222
0.10	8.596	9.488	10.305
0.20	8.706	9.645	10.501
0.30	8.796	9.780	10.663
0.50	8.948	10.016	11.005
0.70	9.177	10.373	11.447

Cell area distributions are dependent on the parameters α and λ/γ. Mean cell area is the inverse of tissue density, thus it increases with both λ/γ and α. This is clear from Figure 6.2, where we plot cell area for various α and λ/γ values. We can also see in Figure 6.2 that both the standard deviation and coefficient of variation of cell area also increase with both parameters. This leads to wider cell area distributions as can be seen in Figure 6.3.

When the mean cell area is less than the preferred cell area, i.e. $\bar{A}/A^{(0)} < 1$, we can consider that the tissue is under compression. This is because cells are exerting spring-like forces on one another, and when they are crowded together the 'springs' are compressed. By contrast, when the mean cell area is greater than the preferred area, i.e. $\bar{A}/A^{(0)} < 1$, the 'springs' are stretched, and thus the tissue is under tension. Areas of the parameter space where the tissue is under tension or stretch can be seen in Figure 6.4.

We see from Figure 6.5 that not all values of α lead to realistic cell shapes, in particular under high compression ($\alpha = 0.4$) we obtain many triangular looking cells. Thus we choose to keep α reasonably close to one. For the remainder of this work we consider $\alpha \in \{0.8, 1.0, 1.2\}$, which gives us a range of behaviour including

(a) Mean

(b) Standard deviation

(c) Coefficient of variation
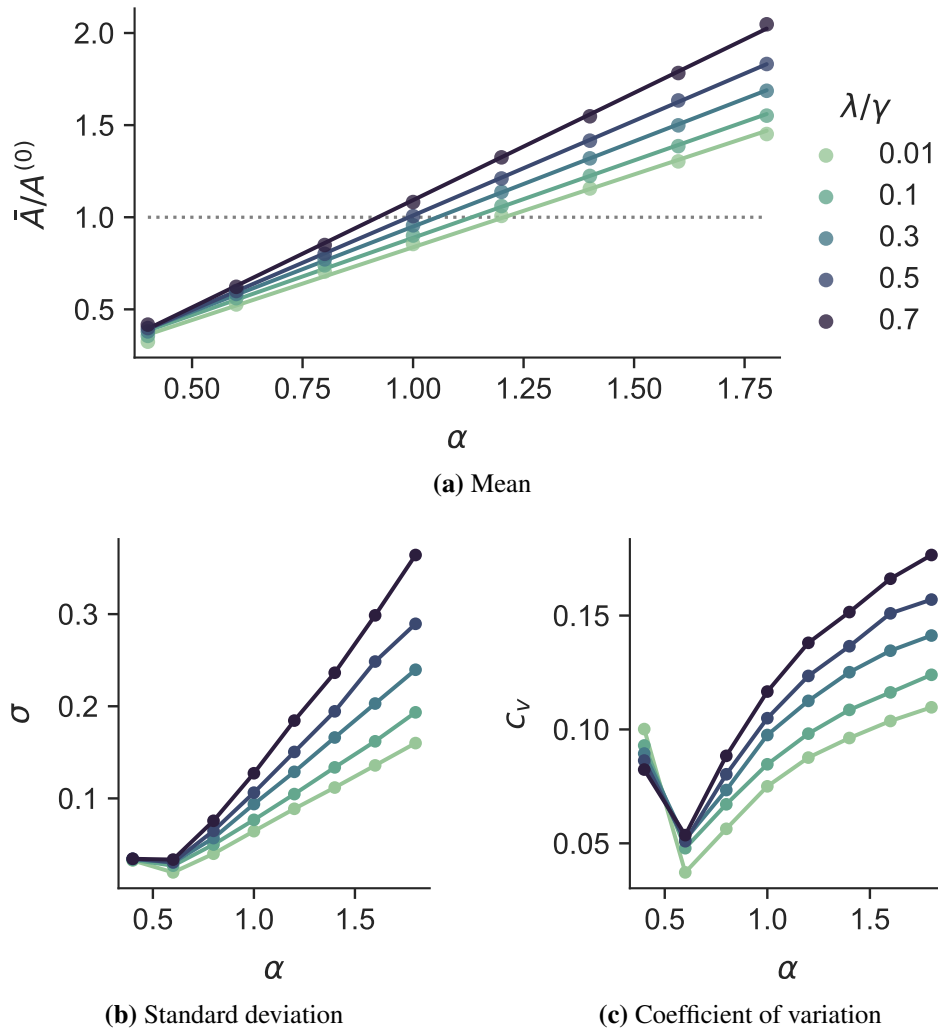
Figure 6.2: Cell area statistics for the Voronoi tessellation model with contact inhibition. We plot the expected values of the (a) mean, (b) standard deviation and (c) coefficient of variation. These are taken as an average over time, after homeostasis is reached, in three distinct simulated tissues. Areas are expressed as a fraction of the preferred area $A^{(0)}$. See Table 6.2 for values of domain width W.
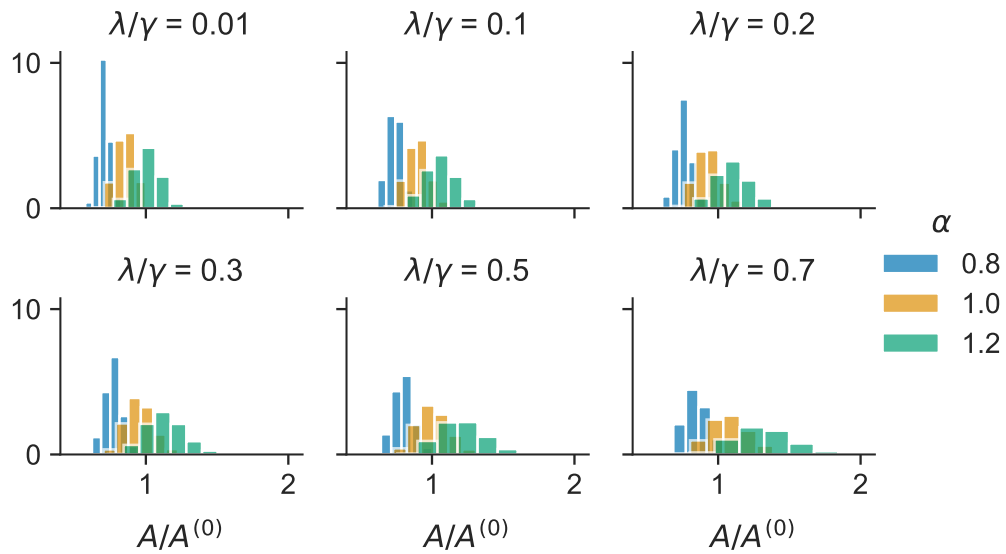
Figure 6.3: Cell area distributions for the Voronoi tessellation model with contact inhi-
bition. Distributions are taken as an average over time, after homeostasis is
reached, in three distinct simulated tissues. See Table 6.2 for values of domain
width W.

tissues under compression and stretch (see Figure 6.4). For the death-to-birth rate
ratio we select $\lambda/\gamma \in \{0.01, 0.02, 0.06, 0.1, 0.2, 0.3, 0.5, 0.7\}$, again these are cho-
sen to give us a broad spectrum of values within a reasonable range. As a reference,
measurements on cultured Madin-Darby canine kidney cells[1] have found prolifer-
ation rates of about $6.7 \times 10^{-2}\,\mathrm{h}^{-1}$ in non-contact inhibited cells and homeostatic
apoptosis rates of about 0.02 per cell per day [109]. These values correspond to
$\lambda/\gamma = 0.012$.

6.3 Evolution of cooperation

We wish to evaluate how the inclusion of contact inhibition in the Voronoi tessella-
tion model affects the success of cooperative mutants. Thus, we extend our frame-
work of evolutionary games within the VT model, as described in Section 4.2, so
that individual cell proliferation rates depend on cell fitnesses, with payoffs defined
by an APD game.

---

[1]Madin-Darby canine kidney cells are an immortalised cell line derived from the kidney epithe-
lium of an adult dog.
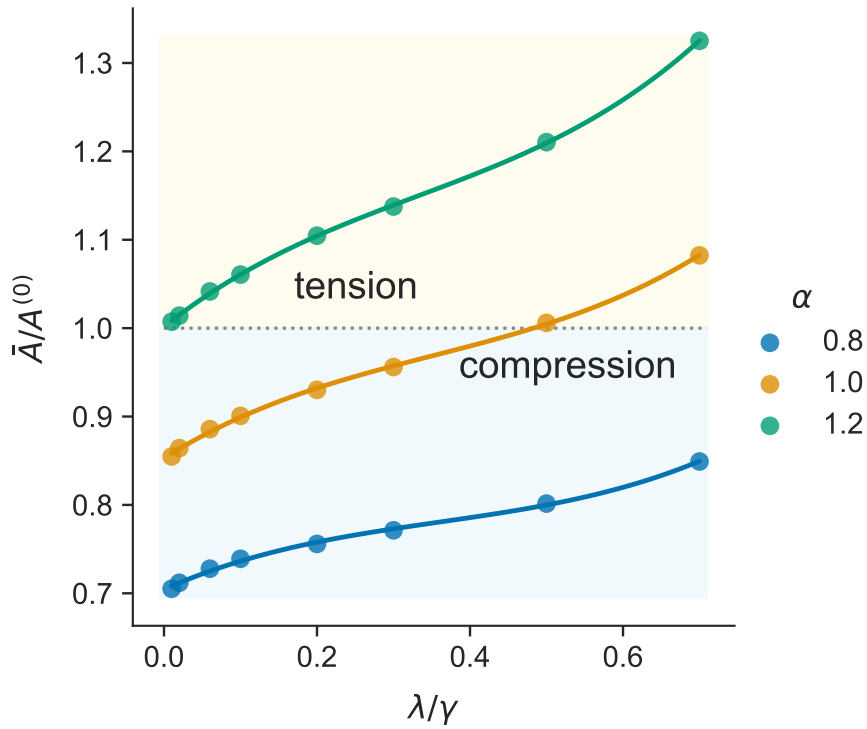
Figure 6.4: Mean cell area as a fraction of preferred cell area for the Voronoi tessellation model with contact inhibition. The figure shows parameter regions where cells in the tissue are, on average, under tension or compression. The plotted circles are simulated data, and correspond to the parameter values we use in simulations of the additive prisoner's dilemma. Lines are obtained by fitting a third degree polynomial. See Table 6.2 for values of domain width W.

The population consists of two types of cells: cooperators and defectors. We denote the type of cell i as $s_i = 0$ (defectors) or $s_i = 1$ (cooperators). Cells derive a payoff through interactions with their neighbours. Cooperators pay a benefit b at a cost c, while defectors pay no benefit and incur no cost. If we denote the connectivity graph of cells as $G(t)$ we can define the total payoff to a cell i as

$$\pi_i(\mathbf{s}, G) = -cs_i + b \sum_{j \in G(t)} \frac{A_{ij} s_j}{k_i} \tag{6.3}$$

where $A_{ij}(t)$ is the adjacency matrix and $k_i(t) = \sum_j A_{ij}(t)$ is the degree of cell i. The fitness of a cell is then defined as

$$F_i = 1 + \delta \pi_i \tag{6.4}$$
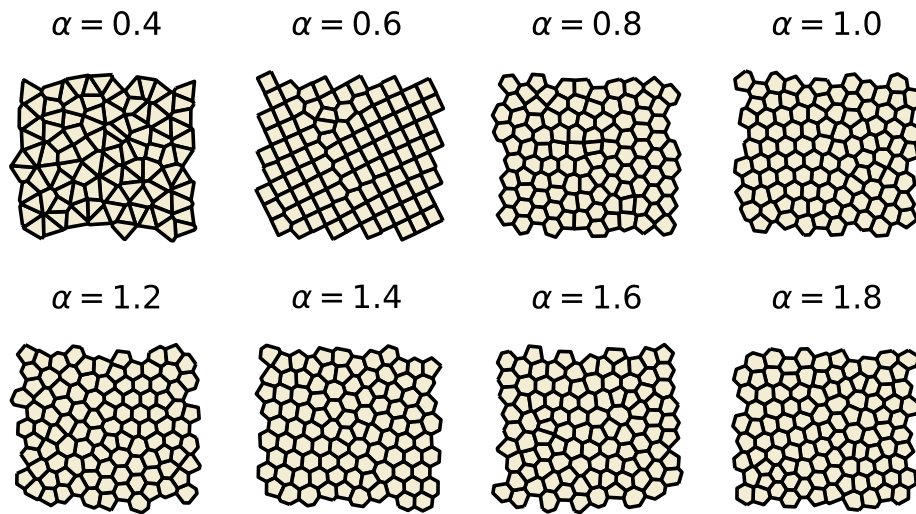
(a) $\lambda/\gamma = 0.01$
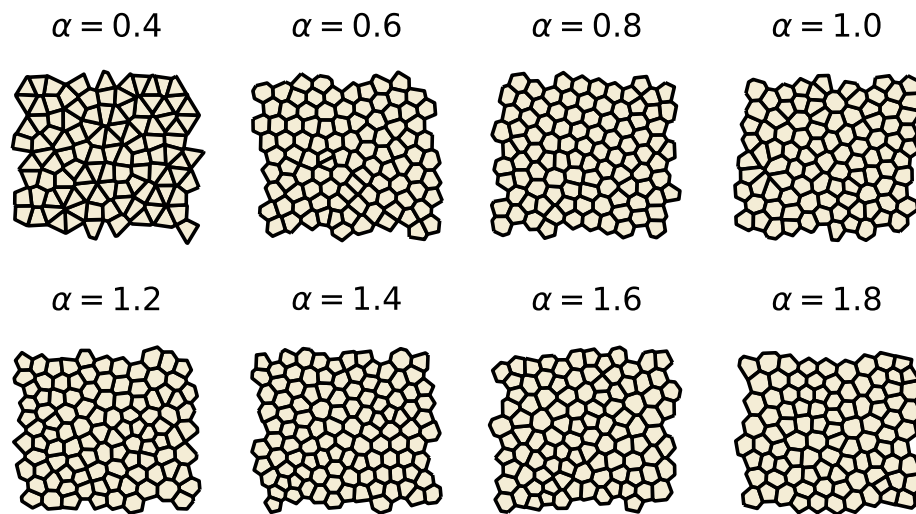
(b) $\lambda/\gamma = 0.7$

Figure 6.5: Snapshots of homeostatic tissues for the Voronoi tessellation model with contact inhibition. Not all parameter regimes give realistic cell shapes. When α is too small, the levels of compression are high, and the cell shapes are no longer realistic. Decreasing λ/γ also leads to higher compression (see Figure 6.4), hence cell shapes cease to be realistic for larger α values, when λ/γ is small. See Table 6.2 for values of domain width W.

where δ is the selection strength parameter. In the following we assume weak selection, setting $\delta = 0.025$. Proliferation rates are now dependent on fitness so Equation (6.1) becomes

$$P_i^{\text{div}}(t, \Delta t) = Z_{\text{div}}(t) \gamma \Delta t \Theta \left(A_i(t) - \alpha A^{(0)} \right) \left[\frac{F_i}{\sum_{j \in G} \Theta(A_j(t) - \alpha A^{(0)}) F_j} \right] . \quad (6.5)$$

This defines the probability that a cell i divides in $(t, t + \Delta t)$, where $\Delta t \ll 1$.

In order to quantify the success of cooperation we calculate the fixation probability ρ_C for a single initial mutant cooperator, varying b and keeping $c = 1$ constant. This can then be compared with the neutral fixation probability $\rho_0 = 1/Z^*$. The critical benefit-to-cost ratio, $(b/c)^*$ occurs when $\rho_C = \rho_0$. For $b/c > (b/c)^*$ cooperation is a beneficial mutation, thus lower values of $(b/c)^*$ imply that cooperation is more successful. As we are using the APD game, which satisfies equal-gains-from-switching, the condition for cooperation to be beneficial is equivalent to the condition for cooperation to be favoured.

6.4 Results

6.4.1 Fixation probabilities

We chose 24 parameter sets $(\lambda/\gamma, \alpha)$, setting the domain width so that the equilibrium population size was $Z^* = 100$ cells (see Table 6.2). For each parameter set we ran simulations to determine how the fixation probability ρ_C varies with b/c. Results are shown in Figure 6.6 and fitted with a linear regression from which we can estimate the critical benefit-to-cost ratio $(b/c)^*$ for each parameter set. This is the value of b/c for which ρ_C exceeds the neutral fixation probability $\rho_0 \approx 1/Z^*$, shown by the dotted line on the plots.

The relationship between $(b/c)^*$ and the parameters α and λ/γ can be seen in Figure 6.7 (see Appendix F.1 for consideration of the error in our $(b/c)^*$ estimates). It is clear that $(b/c)^*$ increases with decreasing λ/γ for all α. This confirms our expectation, that increasing the strength of contact inhibition reduces the success
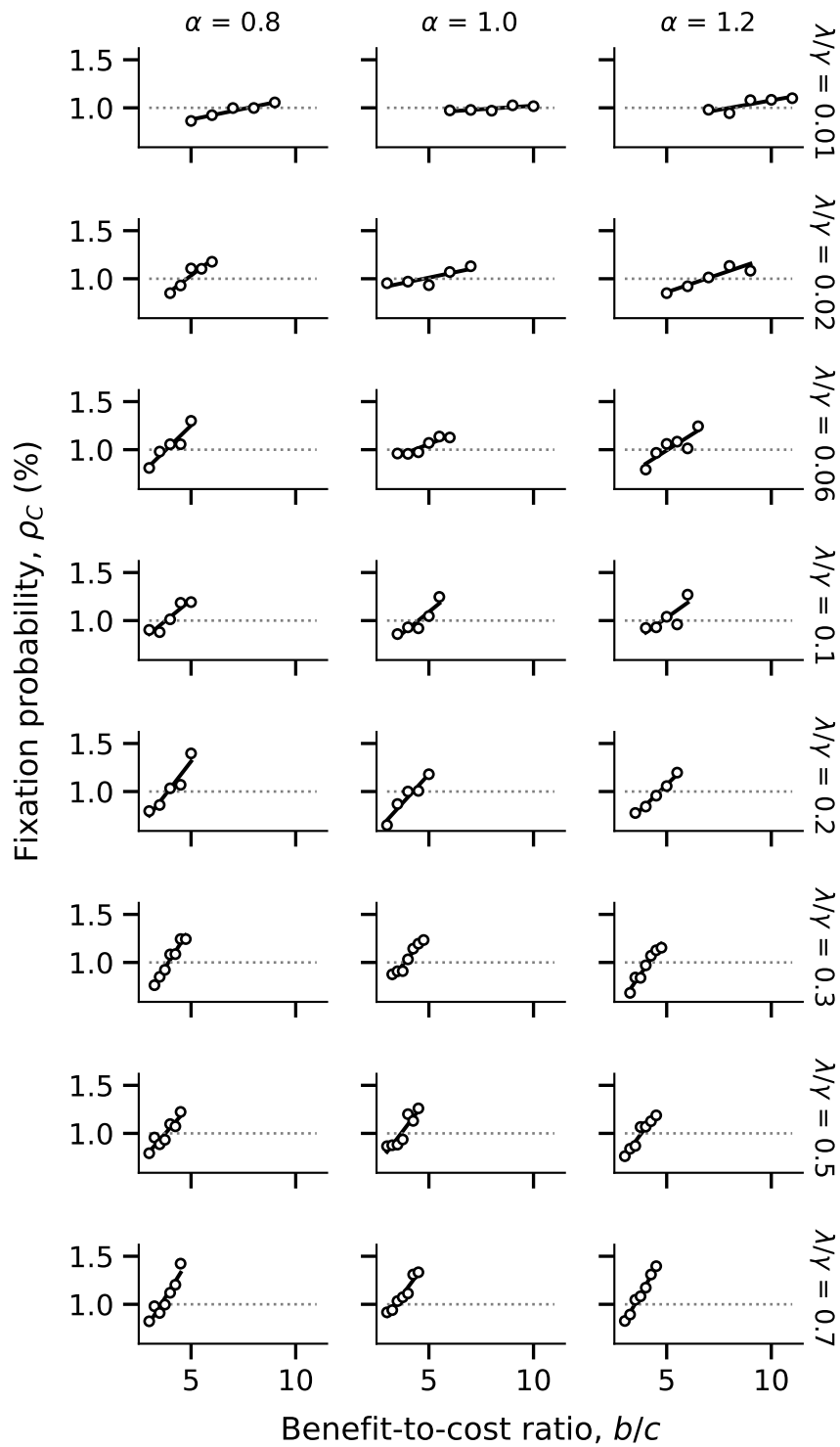
Figure 6.6: Fixation probabilities for the additive prisoner's dilemma in the Voronoi tessellation model with contact inhibition. In all cases, the homeostatic population size is $Z^* = 100$, therefore the critical benefit-to-cost ratio can be approximated as the point at which $\rho_C = 1/Z^*$, shown by the dotted line. Individual data points are calculated from 30,000 simulations, each of which starts with a single cooperator mutant and is run until fixation. We set $c = 1$ and $\delta = 0.025$. See Table 6.2 for values of domain width W, chosen to ensure $Z^* = 100$.

of cooperation. Furthermore, $(b/c)^*$ increases with α for most values of λ/γ. The full behaviour of $(b/c)^*$ and how it varies with the parameters, however, is non-trivial. For larger values of λ/γ, the dependence on α appears to be negligible. In particular, for $\lambda/\gamma > 0.5$, $(b/c)^*$ remains relatively constant for all α. Decreasing λ/γ leads to an increasing divergence of the results for different values of α. For $\alpha = 0.8$, $(b/c)^*$ is relatively constant for $\lambda/\gamma > 0.06$. Reducing λ/γ below 0.06 leads to a rapid increase in $(b/c)^*$. For $\alpha = 1.2$, if we reduce λ/γ, the increase in $(b/c)^*$ is observed sooner, around $\lambda/\gamma = 0.3$. The $\alpha = 1.0$ behaviour is intermediate between the two.
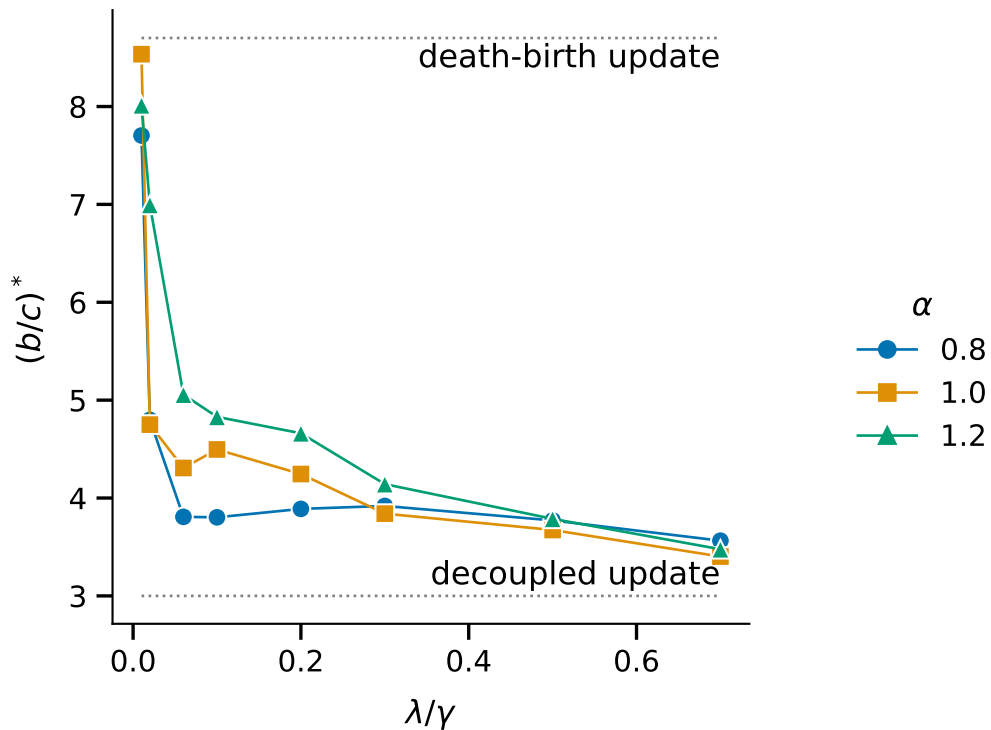
Figure 6.7: Critical benefit-to-cost ratios for additive prisoner's dilemma in the Voronoi tessellation model with contact inhibition. These depend on the quiescent area fraction α and the death-to-birth rate ratio λ/γ. Contact inhibition increases in strength with decreasing λ/γ. The death-birth and decoupled update rules do not explicitly include area-dependent division, however a death-birth update can be interpreted as strong contact inhibition and a decoupled update as no contact inhibition. We set $c = 1$ and $\delta = 0.025$. See Table 6.2 for values of domain width W chosen to ensure $Z^* = 100$.

It is clear from Figure 6.7 that there is a negative relationship between the strength of contact inhibition and the success of cooperation. An intuitive explana-

tion for this is that contact inhibition increases the spatial coupling between birth and death events. When contact inhibition is very strong, we expect that a division can only occur within some neighbourhood of a recent death, as these cells will tend to have more space. Therefore cells are more likely to be competing with cells close to them. As defectors have higher fitness when they neighbour cooperators, and cooperators have lower fitness when they neighbour defectors, this is a disadvantage to cooperators. Cooperators benefit when they are able to compete with distant defectors. Therefore, we can understand how changing λ/γ can impact cooperative success by introducing spatial coupling.

In the next section we will explore the role of spatial coupling, and consider whether it also explains the role of α, or if there is a separate mechanism through which α influences cooperation.

6.4.2 Spatial coupling and cooperative success

To consider the relationship between the spatial coupling of birth and death events, and the parameters α and λ/γ, we calculate the background-corrected fate imbalance (BCFI) [110]. The fate imbalance is given by the number of divisions minus the number of deaths which have occurred within the neighbourhood of a fate event, i.e. a death or division, as a function of time since the event. We correct for background fate imbalance, which is the total number of divisions minus deaths in a given time period, thus obtaining the BCFI. The reason for this correction is to remove global effects. For example, if a death occurs in a tissue at low density, its neighbours are more likely to divide than when a death occurs in a tissue at high density, regardless of local coupling effects.

For a cell i, undergoing a fate event at time t_f, the BCFI is given by

$$\text{BCFI}_i(t) = \sum_{j \in \mathcal{N}_i(t_f)} \text{fate}_j(t) - \frac{|\mathcal{N}_i(t_f)|}{Z(t_f)} \sum_{j=0}^{Z(t_f)} \text{fate}_j(t) \tag{6.6}$$

where $\mathcal{N}_i(t)$ is the set of cells neighbouring i at time t. The quantity, $\text{fate}_j(t) \in \{-1, 0, 1\}$, is defined to be 0 if the cell j is still in the tissue at time t. Otherwise, if j has undergone a fate event, it is given by $+1$ or -1 if the cell has

divided or died, respectively. The second term is the background correction, and the sum is over all cells in the tissue at time t_f.

We find the BCFI around division and death by running a simulation with neutral selection $\delta = 0$, and averaging over $\text{BCFI}_i(t)$ for all cells which undergo division and for all cells that undergo death, respectively. The BCFI depends on the time past since a fate event has occurred. However, after sufficient time it reaches a constant value, once all neighbours have undergone division or death, which we refer to as the final BCFI.

For comparative purposes we first consider the BCFI for the death-birth and decoupled update rules. For the decoupled update rule, divisions and deaths are spatially independent, thus we expect the BCFI around death and division events to be zero. Conversely, for the death-birth update, a death is immediately followed by a neighbouring division event. Therefore, we expect that the BCFI around death is one, while the BCFI around division is zero. These results are both shown to be correct from simulation results in Figure 6.8. The BCFI is not time dependent for these update rules, because the only spatial coupling is for the death-birth update rule, and this occurs instantaneously.

In Figure 6.9 we plot the BCFI for deaths and divisions, averaged over a large number of cells in three simulated tissues over 250 simulation days. In the absence of contact inhibition, and thus spatial coupling, we would expect the BCFI to be zero at all times around both death and division events. When contact inhibition is present we expect a positive BCFI around deaths, which increases with time until it reaches its final, constant value. It is clear from Figure 6.9 that the final BCFI is reached approximately one day after the event, with some small fluctuations.

The final BCFI is plotted against λ/γ in Figure 6.10, averaging over the data from day two onwards. As expected, the final BCFI around death is low when λ/γ is high. Contact inhibition, in this case, is weak and therefore the regime is closer to a decoupled update rule. As λ/γ decreases, and contact inhibition becomes stronger, the final BCFI around death increases. It can be seen in Figure 6.11, that there is positive correlation between $(b/c)^*$ and the final BCFI around death, however, this
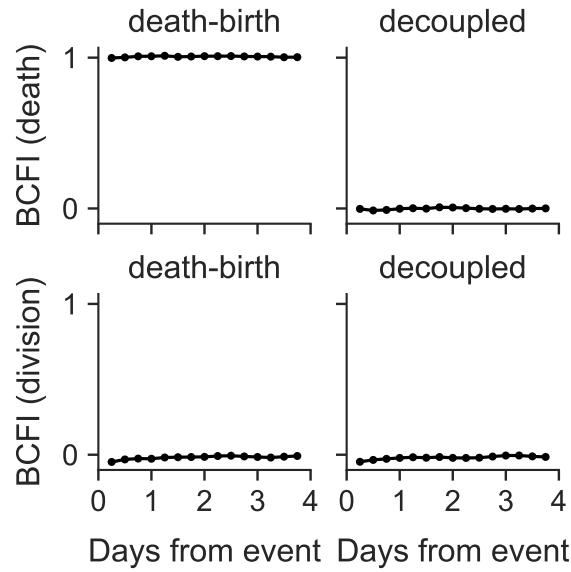
Figure 6.8: Background-corrected fate imbalance (BCFI) around a death (upper) or division (lower) event for the decoupled and death-birth update rules. The BCFI is calculated from Equation (6.6) using simulated data for the Voronoi tessellation model with population size $Z = 100$ and neutral selection $\delta = 0$.

For a death-birth update rule the BCFI is zero around a division, but one around a death. This is consistent with the fact that a death is always followed by a neighbouring division in the death-birth update rule. As expected, the BCFI around death and division is zero for the decoupled update rule, as there is no spatial coupling.

is dependent on α. The values of $(b/c)^*$ show strong dependence on α, particularly for $\lambda/\gamma < 0.2$. While, the final BCFI around death is slightly lower for $\alpha = 0.8$ in this range of λ/γ, Figure 6.11 suggests it is not sufficient to explain the discrepancy in $(b/c)^*$.

There is also clear dependence of the final BCFI around division on λ/γ and α. It is possible that this is having an impact on $(b/c)^*$ and the success of cooperation. Figure 6.10 shows that the final BCFI around division decreases with λ/γ, but increases with α (at least when $\lambda/\gamma < 0.7$). For large enough λ/γ, and small enough α, the final BCFI around division is negative. As deaths occur uniformly at random, this implies that a division is less likely to occur in the neighbourhood of a division. Conversely, the final BCFI around division is positive for lower values of λ/γ, when contact inhibition is stronger, meaning that divisions are more likely to
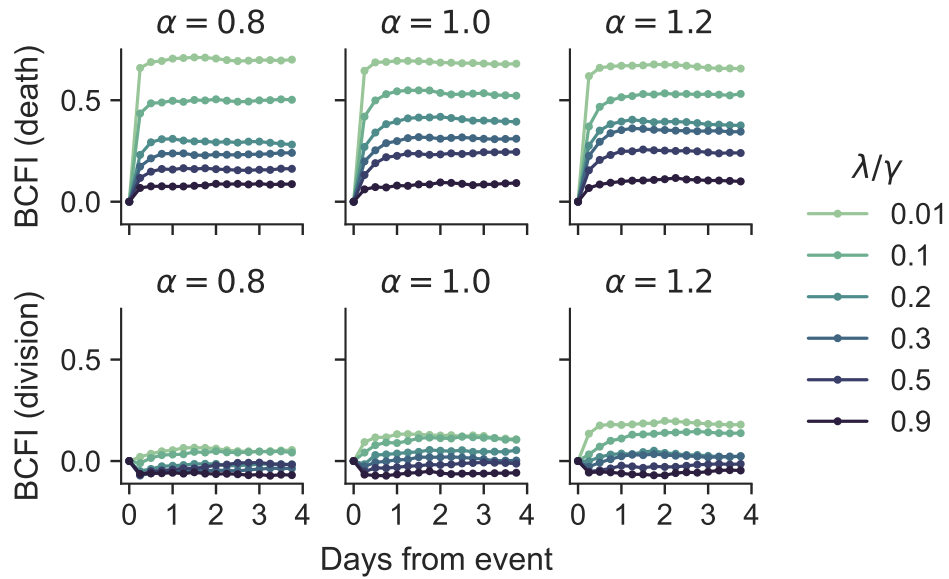
Figure 6.9: Background corrected fate imbalance (BCFI) around a death (upper) or division (lower) in the Voronoi tessellation model with contact inhibition. The BCFI is calculated from Equation (6.6) using simulated data with homeostatic population size $Z^* = 100$ and neutral selection $\delta = 0$. See Table 6.2 for values of domain width W.

The BCFI around death or division quickly reaches a constant value which depends on λ/γ, and to a lesser extent on α.

occur near a recent division. The former case could be explained if a division leads to local competition for space, and therefore a lower likelihood, that neighbouring cells have space to divide. The latter could possibly be explained by a death leading to more than one neighbouring division.

We do not have strong evidence to explain the dependence of $(b/c)^*$ on α. Clearly, the spatial coupling in the contact inhibition model is more complicated than was the case for the death-birth or decoupled update rules. The effects are not immediate, as birth and death are temporally decoupled in the contact-inhibition model. Furthermore, there are downstream effects from divisions which are not seen for the death-birth or decoupled update rule (see Figure 6.8.) However, it is clear that decreasing λ/γ leads to an increase in the final BCFI around death, and that there is a corresponding increase in $(b/c)^*$.

In Appendix F, we verify these results by considering an alternative measure
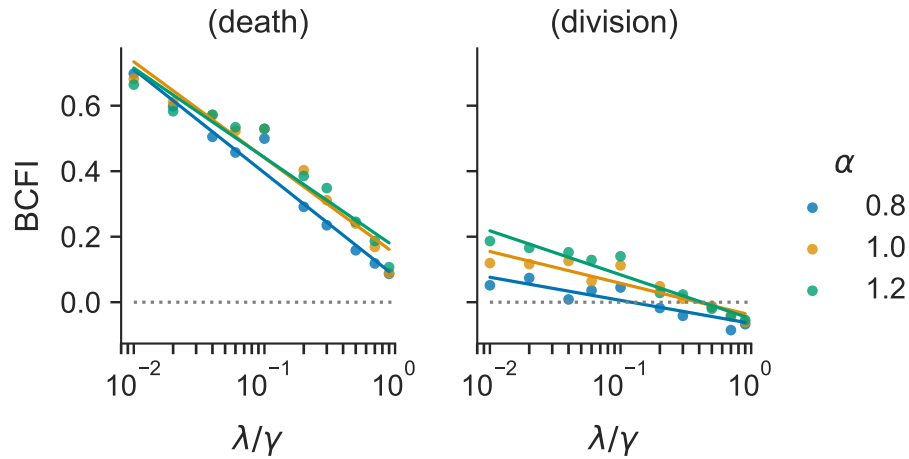
Figure 6.10: Final values of background-corrected fate imbalance (BCFI) around a death or division in the Voronoi tessellation model with contact inhibition. These are calculated by averaging over the data shown in Figure 6.9, 2-7 days from the fate event.

The final BCFI around death decreases quickly with λ/γ, while dependence on α is small. It is always positive for the parameters shown, indicating that division is more likely when a neighbouring cell has died. The final BCFI around division tends to be smaller, but also decreases with λ/γ. When positive, it indicates that division is more likely when a neighbouring cell has divided. Conversely, when negative, division is less likely. The largest value of λ/γ plotted is 0.9.
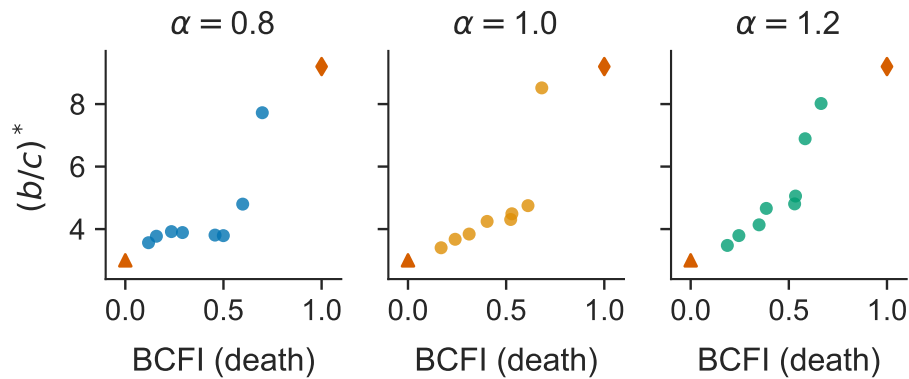
Figure 6.11: Critical benefit-to cost ratio $(b/c)^*$ plotted against the final background-corrected fate imbalance (BCFI) around death, averaged over 2-7 days from the fate event. It is clear that the relationship is dependent on α. The red triangle corresponds to a decoupled update rule (no contact inhibition), while the red diamond represents a death-birth update rule. Critical benefit-to-cost ratios are for the additive prisoner's dilemma with $c = 1$ and $\delta = 0.025$.

for the strength of spatial coupling, the expected distance between a death or division and subsequent division events. Thus, we conclude that changes in the strength of spatial coupling between death and subsequent division events can explain the relationship between λ/γ and the success of cooperation. However, spatial coupling does not provide a decisive explanation for the dependence of cooperative success on α. This is evident from Figure 6.11 which plots $(b/c)^*$ against the final BCFI around death (see also Figure F.3).

We therefore consider whether α has an effect on the fitness of cells, i.e. if cooperators were more clustered for small α this could explain increased cooperative success. We explore this possibility in Appendix F.3, comparing the $\alpha = 0.8$ and $\alpha = 1.2$ regimes with $\lambda/\gamma = 0.1$. Although these have substantially different critical benefit-to-cost ratios (see Figure 6.7), the difference in expected cell fitnesses is negligible. Thus, the dependence of cooperative success on α is not explained by differences in cell fitness.

Some insight can be gained into α dependence by considering the reason for which spatial coupling inhibits cooperative success. When birth and death are spatially independent all cells compete to reproduce. By contrast, when there is spatial coupling, only a subset of cells compete at any given time. In our contact inhibition model, this subset consists of cells which exceed an area threshold. As cell death reduces local cell density, it is likely that cells are able to proliferate if they are close to the site of a recent death. This is especially true when contact inhibition is strong, i.e. λ/γ is small, as demonstrated by Figure 6.9.

If a death occurs and all neighbouring cells cease to be contact-inhibited, they compete with one another to replace the dead cell in a similar way to the death-birth update rule. In contrast to the death-birth update rule, the division of a neighbour is not immediate or guaranteed. Additionally, depending on the strength of contact inhibition, there may be other non-contact inhibited cells which are also competing to divide.

By contrast, if a cell dies and only one of its neighbours ceases to be contact inhibited, there is no local competition between cells. The choice of neighbour

here is not dependent on cell fitness, but on local geometry. Furthermore, this cell will compete to reproduce with other non-contact inhibited cells in the population, which are not necessarily in its close vicinity. Thus, competition occurs across the population, although not all cells are involved at any given time. This situation is closer to a global update. It is feasible in this scenario, therefore, that spatial coupling is strong, but does not inhibit cooperation.

These are two extreme cases, however there is evidence that the latter behaviour is more likely when $\alpha = 0.8$ and the former when $\alpha = 1.2$. In Figure 6.12 we plot the expected number of non-contact inhibited cells which are isolated, i.e. do not neighbour another non-contact inhibited cell. The figure shows that, for $0.06 < \lambda/\gamma < 0.3$, there are more isolated non-contact inhibited cells for $\alpha = 0.8$ than $\alpha = 1.2$. This suggests that the situation where only one neighbour is non-contact inhibited after a death, is more common when $\alpha = 0.8$.

We know from Figure 6.2, that there is more variation in cell area within a tissue when $\alpha = 1.2$, compared to $\alpha = 0.8$. This could explain the above observation, that non-contact inhibited cells are less likely to be isolated when $\alpha = 1.2$. If a cell happens to die in an area of very high density, it could be that no neighbouring cells reach the area-threshold and therefore they all remain contact inhibited. Conversely, in an area of low density they may all reach the threshold. For $\alpha = 0.8$, there is less variation in cell density and we could expect therefore for there to also be less variation in the number of cells which cease to be contact-inhibited after a death.

This also could explain the positive coupling between divisions and subsequent divisions which was evident in the BCFI and normalised distance to division, for sufficiently small λ/γ. This positive coupling implied that a death can sometimes lead to two (or more) divisions. While the effect was very weak for $\alpha = 0.8$, it was significantly stronger for $\alpha = 1.2$. This is consistent with the hypothesis that there is an increased probability for higher α, that following a death, multiple neighbouring cells become non-contact inhibited.
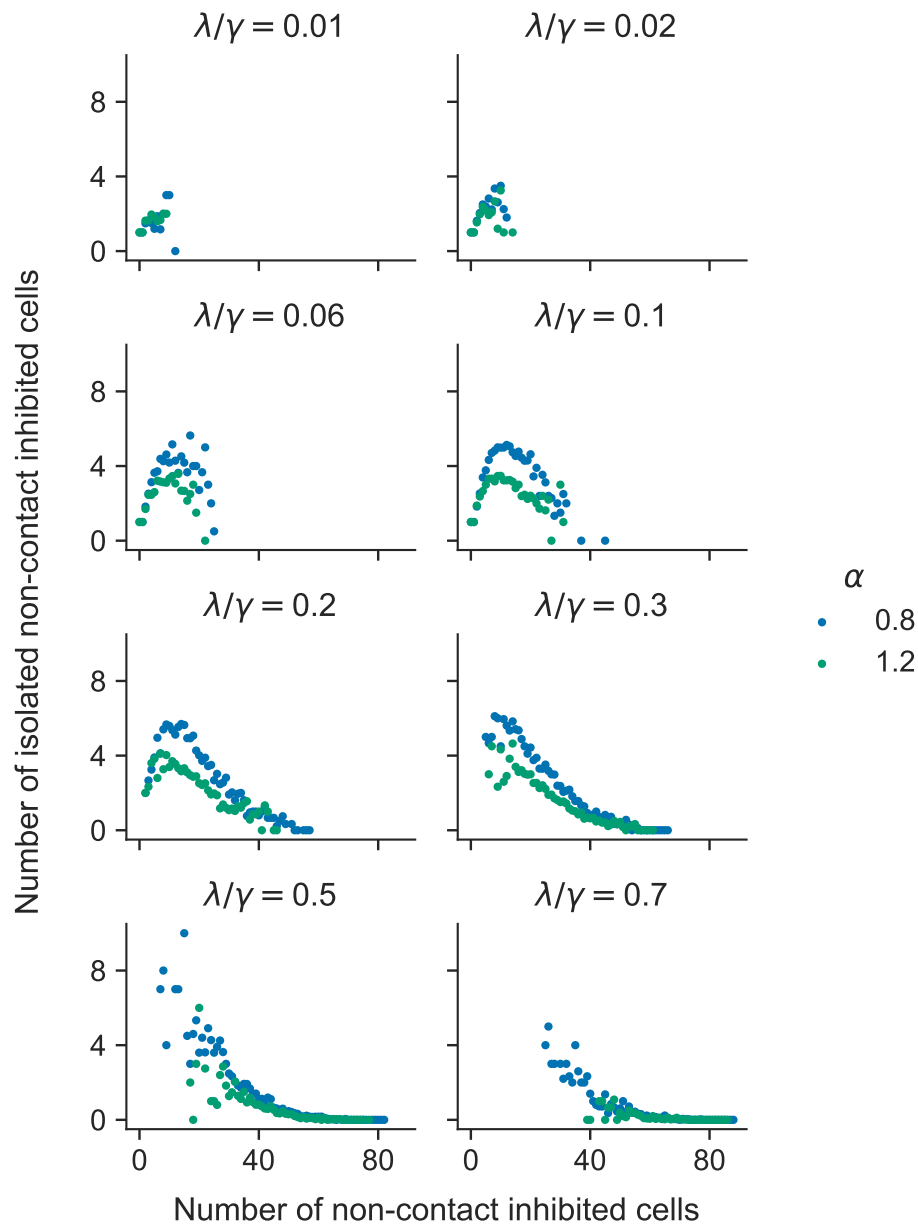
Figure 6.12: Expected number of non-contact inhibited (proliferating) cells that are isolated from other non-contact inhibited cells in the Voronoi tessellation model with contact inhibition. These are obtained from simulations with neutral selection $\delta = 0$. For $0.06 < \lambda/\gamma < 0.3$ it is clear that non-contact inhibited cells are more likely to be isolated when $\alpha = 0.8$ compared to $\alpha = 1.2$. See Table 6.2 for values of domain width W chosen to ensure $Z^* = 100$.

6.5 One-dimensional tissue model

To gain further insight into the effect of the parameters on the evolution of cooperation we consider a simplification of the VT model to one dimension.

In this 1D VT model, cells are represented by points on a line, with periodic boundary conditions, as can be seen in Figure 6.13. As with the VT model, these cell centres are able to move, subject to damping, and exert spring like forces on one another. The length of each cell is obtained by partitioning the domain into segments, whereby each cell boundary falls halfway between two neighbouring cells. This is equivalent to performing a VT in one dimension. Every cell has exactly two neighbours, and its length is equal to half the distance between those neighbours. We take the spring constant, $\mu = 6.25$, and other parameters to be the same as the 2D VT model (see Table 6.1).
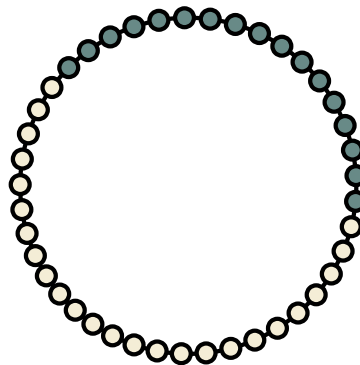
Figure 6.13: Diagram of the one-dimensional Voronoi tessellation model. Cell-centres, represented by circles, are able to move freely along the line and exert forces on their neighbours. The length of a cell is given by half the distance between its two neighbours. A cluster of mutant cells is shown in grey.

Several features of the 2D VT model are lost when we reduce to 1D. For example, there is no longer any variation in neighbour number, nor is there the possibility for rearrangement of neighbours. This means that the death-birth and decoupled update rules in the 1D VT model are indistinguishable from the death-birth and shift update rules on the cycle. We can thus use known results, outlined in Chapter 2, to find the critical benefit-to-cost ratio in these cases.

Although the APD is a pairwise game, it can be expressed as a multiplayer game of the type discussed in Section 2.3, allowing us to use results from that section to find the critical benefit-to-cost ratios. On the cycle, each cell derives its payoff through an interaction with its two nearest neighbours. Thus, we can consider the APD as a three-player game with payoffs:

$$a_0 = -c \qquad\qquad a_1 = b/2 - c \qquad\qquad a_2 = b - c \qquad (6.7)$$

$$b_0 = 0 \qquad\qquad b_1 = b/2 \qquad\qquad b_2 = b. \qquad (6.8)$$

We can therefore use Equation (2.46) to express the critical benefit-to-cost ratios in terms of structure coefficients. These are given by

$$(b/c)^* = \frac{\sigma_0 + \sigma_1 + \sigma_2}{\sigma_2 - \sigma_0}. \qquad (6.9)$$

The structure coefficients σ_i, for the death-birth and shift update rules on a cycle, are given by Equations (2.51) and (2.62), respectively. By plugging these into Equation (6.9), we obtain $(b/c)^* = 2.02$ for the death-birth update rule and $(b/c)^* = 1.11$ for the shift update rule, where we have used population size $Z = 100$.

Contact inhibition is implemented in the same way as for the 2D VT model. We introduce a length-threshold, such that a cell i is only able to divide at time t if its length exceeds the threshold, i.e. $L_i(t) > \alpha L^0$. Here $L_i(t)$ is the length of the cell and $L^{(0)} = s_M$ is the preferred cell length, which is equal to the preferred cell separation (natural spring length). The death-to-birth rate ratio is given by λ/γ. As was the case for the 2D model, the tissue reaches a homeostatic density which depends on α and λ/γ, so long as $\lambda/\gamma < 1$.

Length distributions for fixed domain size and varying α and λ/γ are shown in Figure 6.14. We can see from the figure that the mean cell length increases with α and λ/γ. The width of the distribution also increases with λ/γ, consistent with the 2D model (see Figure 6.3). However, in contrast to the 2D model, there is no clear dependence of the width of the distribution on α. This is as expected, as the only equilibrium state in the 1D model has all cell centres equidistant from one another.

There is no force dependence on the natural spring length, therefore it does not matter whether the tissue is under tension or compression. The observed variation in length is not due to α, but to the difference in time scales over which forces relax and fate events occur. The former is determined by the ratio μ/η, and the latter by λ/γ.
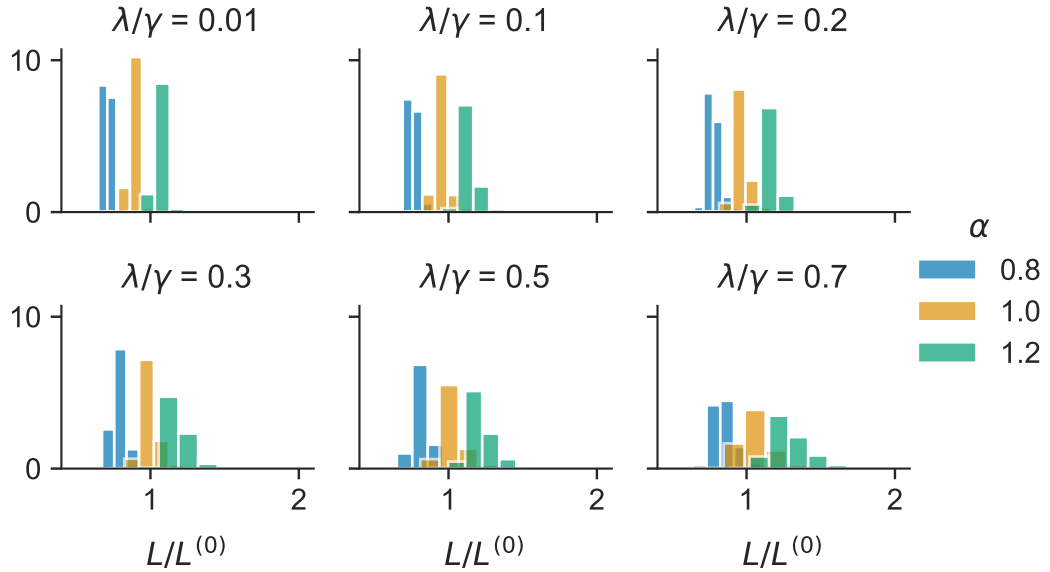
Figure 6.14: Cell length distributions for the one-dimensional Voronoi tessellation model with contact inhibition. Cell lengths are expressed as a fraction of the preferred length $L^{(0)}$. Distributions are taken as an average over time, after homeostasis is reached, in three distinct simulated tissues. See Table 6.3 for values of domain width W, chosen to ensure homeostatic population size $Z^* = 100$.

This is verified in Figure 6.15, which shows the expected values for mean, standard deviation and coefficient of variation of cell length. The mean and standard deviation increase with α and λ/γ, consistent with the 2D model (see Figure 6.2). However, for the 1D model, the coefficient of variation appears to be independent of α, although it does increase with λ/γ.

We use the homeostatic density, equal to $\bar{L}^{-1}$, to calculate the required domain size to obtain an equilibrium population size of $Z^* = 100$. These are summarised in Table 6.3, for a range of α and λ/γ values. We then run simulations to calculate the fixation probabilities for each parameter regime and use these to find the critical benefit-to-cost ratios for an APD game.
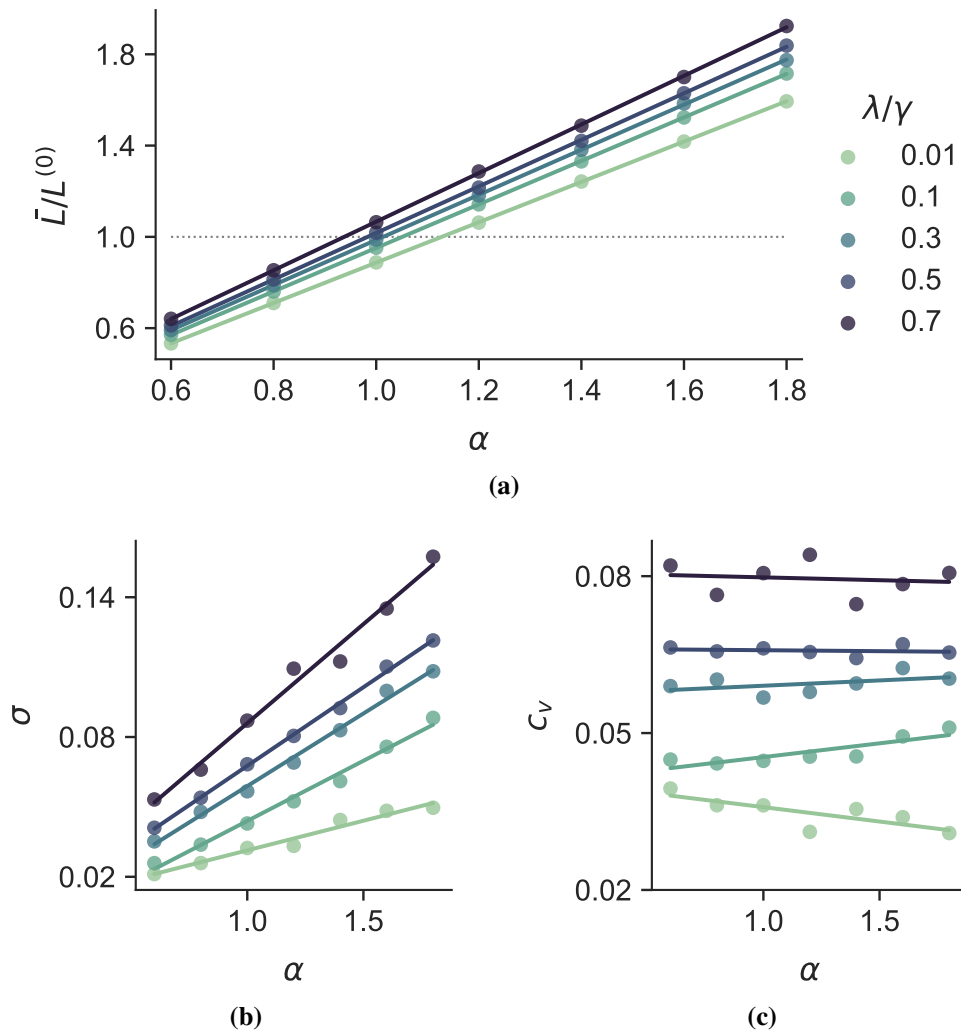
Figure 6.15: Cell length statistics for a one-dimensional tissue. We plot the expected values of the mean, standard deviation and coefficient of variation. These are taken as an average over time, after homeostasis is reached, in three distinct simulated tissues. Cell lengths are expressed as a fraction of the preferred length $L^{(0)}$. The mean and standard deviation both increase with α, however the coefficient of variation remains relatively constant. This is in contrast to the two-dimensional VT model, for which all three statistics increase with α (see Figure 6.2). See Table 6.3 for values of domain width W chosen to ensure homeostatic population size $Z^* = 100$.

Table 6.3: Values of domain width, W, for each combination of parameters λ/γ, α and μ used in simulations of the one-dimensional Voronoi tessellation model with contact inhibition.

| | $\mu = 6.25$ | | | $\mu = 62.5$ |
| | α | | | α |
λ/γ	0.8	1.0	1.2	1.0
0.01	70.894	88.672	106.350	94.383
0.02	72.682	90.934	109.039	95.563
0.06	75.105	93.904	112.612	97.030
0.10	76.099	95.206	114.222	97.761
0.20	77.670	97.194	116.576	98.663
0.30	78.928	98.595	118.320	99.318
0.50	81.045	101.565	122.035	100.582
0.70	85.199	105.035	126.504	102.940

Figure 6.16 plots $(b/c)^*$ against λ/γ for different values of α. It is clear from the figure that $(b/c)^*$ increases with decreasing λ/γ, however there is no variation with α. Thus, the α dependence we observed for the 2D model (Figure 6.7), is not present in 1D. Figure 6.16 also shows $(b/c)^*$ for the shift (decoupled) update rule and death-birth update rule. The decoupled update rule seems to provide a lower bound on $(b/c)^*$, as we would expect due to the fact that there is no spatial coupling. Curiously, the value of $(b/c)^*$ for death-birth update rule is not an upper bound, and is exceeded by the contact inhibition model, when $\lambda/\gamma < 0.06$. It is not immediately obvious why this is the case and requires further investigation.

We argued in Section 6.4.2 that the decreased variation in cell area could explain why cooperation was more successful for smaller α in the 2D model, when λ/γ was sufficiently small. The fact that α does not affect the coefficient of variation for cell lengths in the 1D model, and there is correspondingly no dependence of $(b/c)^*$ on α in 1D, provides further evidence for this. We also plot the number of isolated non-contact inhibited cells against the number of non-contact inhibited cells in Figure 6.17. By contrast to the 2D case, plotted in Figure 6.12, there is no clear relationship with α and λ/γ. In the 1D model, isolated non-contact inhibited cells are rare in all cases, except when there is only a single non-contact inhibited cell in the population.
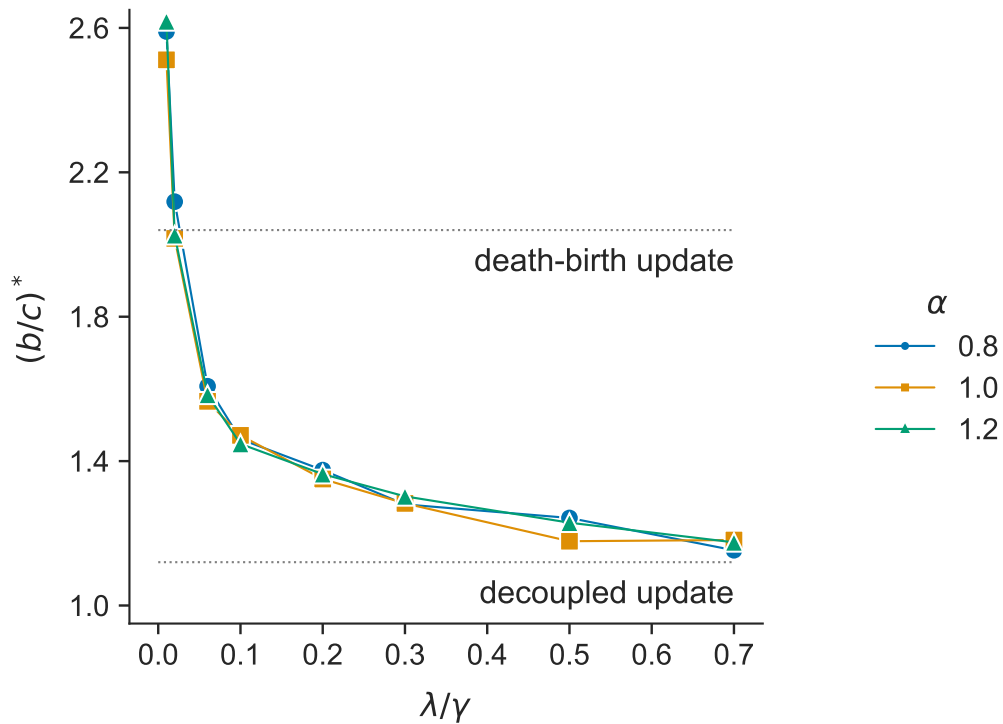
Figure 6.16: Critical benefit-to-cost ratios for the additive prisoner's dilemma in the one-dimensional Voronoi tessellation model with contact inhibition. These depend on the death-to-birth rate ratio λ/γ, but not the quiescent area fraction α. This is in contrast to the two-dimensional Voronoi tessellation model (see Figure 6.7). The death-birth and decoupled update rules do not explicitly include size-dependent division, however a death-birth update can be interpreted as strong contact inhibition and a decoupled update as no contact inhibition. We set $c = 1$ and $\delta = 0.025$. See Table 6.3 for values of domain width W chosen to ensure $Z^* = 100$

In Figure 6.18 we plot the BCFI, calculated according to Equation (6.6), for deaths and divisions in the 1D VT model. Again we observe that, contrary to the 2D model, there is no α dependence. Figure 6.19 plots $(b/c)^*$ against the final BCFI around death. It is clear from the figure that $(b/c)^*$ increases with the final BCFI around death, and this is independent of α. In other words, cooperative success decreases as spatial coupling between death and division increases. Spatial coupling in turn increases with the strength of contact inhibition, i.e. with decreasing λ/γ.

Figure 6.19 also plots results for the shift and death-birth update rules. There is no spatial coupling for the shift update rule, thus the final BCFI around death is zero. By contrast, the death-birth update rule always results in a neighbouring
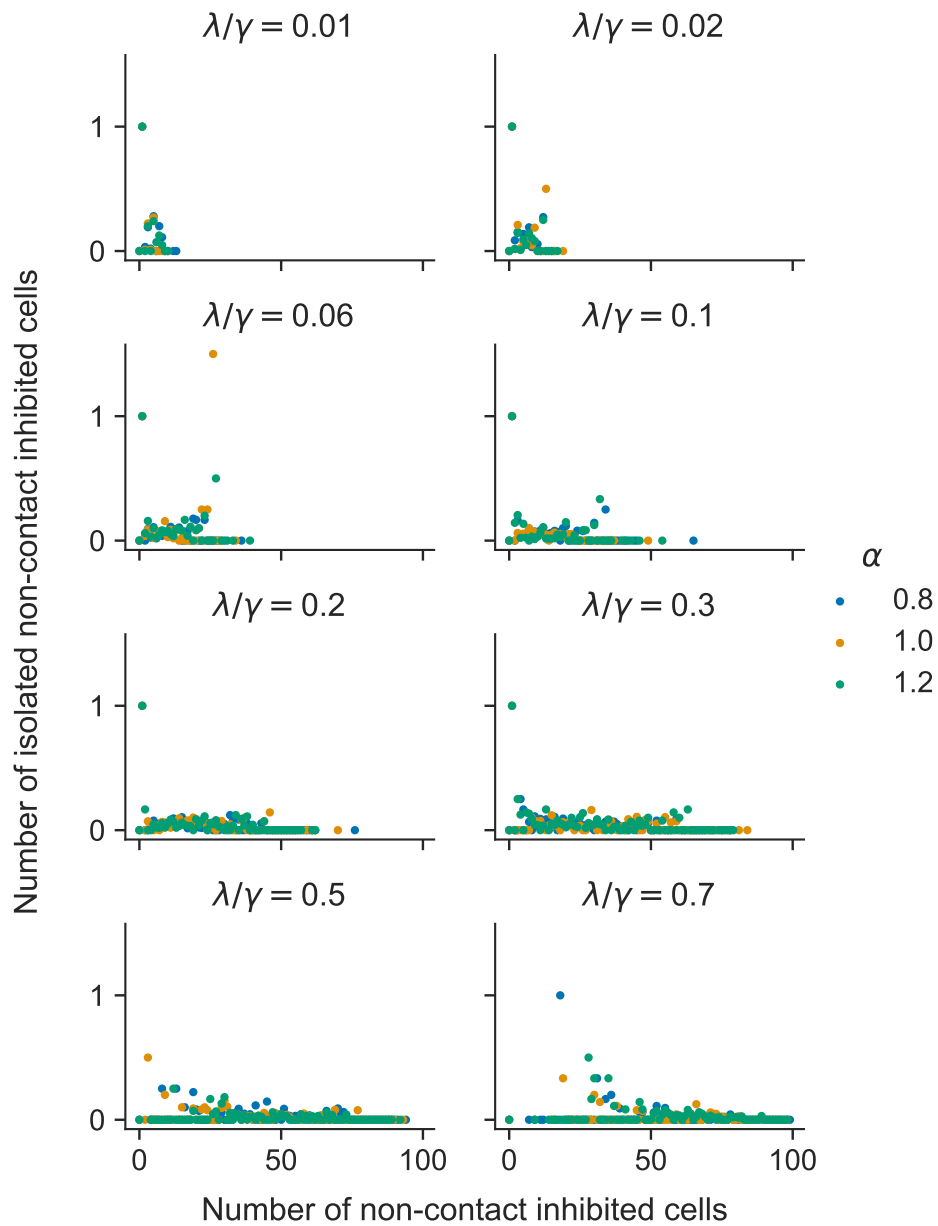
Figure 6.17: Expected number of non-contact inhibited (proliferating) cells that are isolated from other non-contact inhibited cells in the one-dimensional Voronoi tessellation model. These are obtained from simulations with neutral selection $\delta = 0$. There is no clear relationship between α and the number of isolated non-contact inhibited cells of the type we saw in the two-dimensional model (see Figure 6.12). See Table 6.3 for values of domain width W chosen to ensure $Z^* = 100$
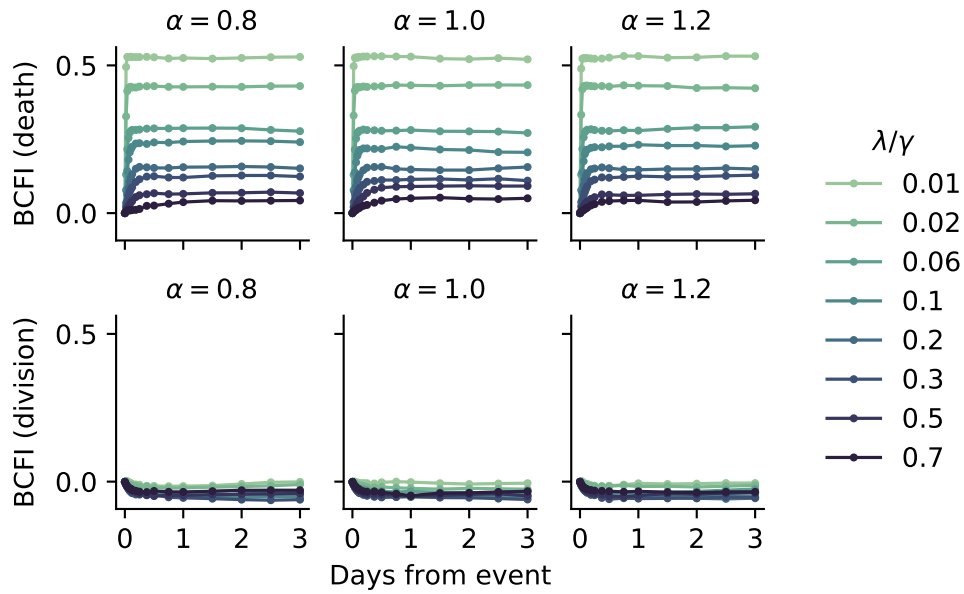
Figure 6.18: Background corrected fate imbalance (BCFI) around a death (upper) or division (lower) in the one-dimensional Voronoi tessellation model with contact inhibition. The BCFI is calculated from Equation (6.6) using simulated data with homeostatic population size $Z^* = 100$ and neutral selection $\delta = 0$. See Table 6.3 for values of domain width W.

The BCFI around death or division quickly reaches a constant value which depends on λ/γ, but not on α.
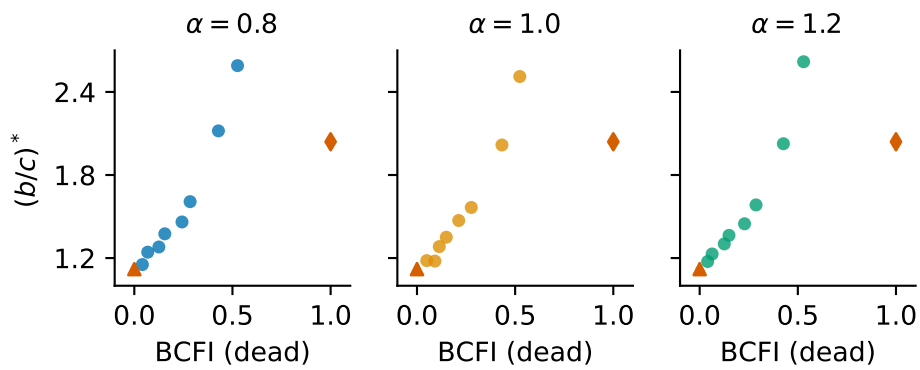
Figure 6.19: Critical benefit-to cost ratio $(b/c)^*$ plotted against the final background corrected fate imbalance (BCFI) around death, averaged over 1-3 days from the fate event. It is clear that the relationship is independent of α. The red triangle corresponds to a decoupled update rule (no contact inhibition), while the red diamond represents a death-birth update rule. Critical benefit-to-cost ratios are for the additive prisoner's dilemma with $c = 1$ and $\delta = 0.025$.

division after a death, thus the final BCFI around death is one. Again, we can see from this figure that the value of $(b/c)^*$ for the death-birth update does not fit into the general trend.

As previously discussed, the 1D VT model has only a single equilibrium state in which all cells are of equal length. This is in contrast to the 2D VT model, and means that for a sufficiently high spring constant μ (or equivalently, low drag coefficient η) the system will return to a state of equally spaced cells between death and division events. The implication, as we discuss in more detail in Appendix F.4, is that for high μ the variation in cell length is negligible, and thus the density-dependence of proliferation will be global rather than local, as either all cells will exceed the length-threshold or none will. Thus, increasing μ will move the system closer to a decoupled update rule.

6.6 Discussion

This chapter has considered how contact inhibition is able to maintain homeostatic population size within an epithelium, and in doing so leads to the spatial coupling of death and division. The strength of this spatial coupling depends primarily on the death-to-birth rate ratio λ/γ, with smaller values of λ/γ indicating both stronger contact inhibition and spatial coupling. Results from Chapters 4 and 5 demonstrated that the spatial coupling of death and division has a deleterious effect on cooperation. Thus, we expected to see a decrease in cooperative success as the strength of contact inhibition is increased.

We have indeed found that there is an inverse relationship between λ/γ and the critical benefit-to-cost ratio $(b/c)^*$, indicating that stronger contact inhibition, and thus spatial coupling, impedes cooperative success. However, we also found that values of $(b/c)^*$ are affected by the quiescent area fraction α, and this dependence cannot be explained by spatial coupling. In the higher α case, cooperation is increasingly suppressed as spatial coupling becomes stronger. In the low α case, spatial coupling must be much stronger for cooperation to be suppressed.

This result is curious, as it means that there is another mechanism promot-

ing cooperation that we have not previously encountered, and that spatial coupling does not necessarily have a strong deleterious effect on cooperation. The reason we expect spatial coupling to oppose cooperation, is that it usually leads to local competition for proliferation. We have, therefore, proposed that this does not always hold, and it is possible in certain cases to have spatial coupling, but still maintain some level of global competition.

This is plausible for smaller values of α, where we have seen that cell death is more likely to result in only a single neighbour reaching the area threshold for proliferation, compared to larger α. This is due to the fact that there is less variation in cell area when α is smaller. The patterning of non-contact inhibited cells, thus, consists more of isolated cells distributed across the tissue, compared to higher α values, where cells tend to be more clustered. As competition for proliferation is between non-contact inhibited cells, it can be characterised as more global when α is smaller and more local when α is larger. The former situation is closer to a decoupled update rule, and the latter to a death-birth update rule.

This phenomenon is likely due to the role α plays in determining the strength of tension or compression within the tissue, which is connected to the distribution of cell areas. Higher α leads to higher tissue tension and wider area distributions, while lower α results in more compression and less variation in area. The dependence of cooperative success on α is not observed in one-dimension, where α does not affect the forces within the tissue or the length distribution of cells. It would be useful to investigate the one-dimensional case more thoroughly, in particular to consider how it is possible that strong contact inhibition leads to worse outcomes for cooperation than the death-birth update rule, which we expect to be an upper limit.

There are clearly important considerations for modelling evolutionary dynamics in epithelia based on this result that contact inhibition, although it leads to spatial coupling, does not necessarily have a detrimental effect on cooperative success. It is worth, therefore, taking a moment to consider the biological significance, particularly with regard to the key parameters.

In order to calculate λ/γ for a real epithelium, we need the proliferation rate of freely dividing (non-contact inhibited) cells and either the proliferation rate or rate of cell loss in a homeostatic tissue (these will be equal). As we discussed in Section 6.2, data for kidney cells suggest a value of $\lambda/\gamma = 0.012$. This is on the very low end of λ/γ values we have considered, suggesting contact inhibition, and thus spatial coupling, is strong. Another experimental study has found strong spatial coupling between cell differentiation (corresponding to "death" in our model) and division in epidermal stem cells [110]. We cannot calculate λ/γ, as there are no reported values for non-contact inhibited proliferation rates. The authors do, however, calculate the BCFI, which appears to reach values in the range 0.4–0.8. Within our model, this corresponds to $\lambda/\gamma < 0.3$.

In general, we expect contact inhibition to be relatively strong to maintain homeostasis within the epithelium. These examples show that this is true for kidney epithelium and epidermal stem cells. We might naively assume, therefore, that this implies poor conditions for cooperation. However, our results indicate that we cannot fully understand the impact of contact inhibition without an estimation for α. Recall that $\alpha A^{(0)}$ is the minimum area at which a cell is able to proliferate. Determining this value for real epithelia would tell us how significant contact inhibition is for the success of cooperation. If a direct measurement of α is difficult, it may be possible to estimate it by considering its effect on the variation in cell area.

There are a number of considerations which could make this result more robust. Firstly, a broader consideration of the parameter space is warranted. We consider, in Appendix B, the implications of varying the spring constant μ for our original formulation of the VT model, used in Chapters 4 and 5. However, it is possible μ could play a more important role within the VT model with contact inhibition. Essentially, μ determines how quickly the intercellular forces reach equilibrium. If μ is sufficiently large, the forces will relax on a much faster time scale than division and death occur. We have seen that this is particularly important for the 1D model and that increasing μ brings the system closer to a decoupled update rule.

Another consideration is that the result depends on how the space occupied by

a dead cell is redistributed amongst its surviving neighbours. Within the VT model, we implement this simply by removing the dead cell, re-performing the VT, and allowing the forces to relax over time. It would be useful to consider how closely this redistribution of area matches the process in a real epithelium. It would also be interesting to see if the results are repeatable using, for example, the vertex model, which we outlined in Chapter 3.

Chapter 7

Conclusions

7.1 Discussion

Evolutionary game theory is increasingly used in cancer modelling [53, 55, 152], both to elucidate tumorigenesis [32, 34, 40, 43, 52], and to inform potential treatment strategies [48, 153–155]. Experimental evidence that malignant cells cooperate to drive tumour growth has been found for breast cancer [156, 157] and glioblastoma [158]. Furthermore, evolutionary games have been explicitly quantified in non-small cell lung cancer [159] and neuroendocrine pancreatic cancer cell cultures [38]. These cancers both originate in epithelial cells, of the lung and pancreas, respectively. Disrupting cooperation could therefore be important for improving cancer treatment [160]. This thesis has sought to explore how the evolutionary success of cooperation is affected by properties of an epithelium, in particular, the population structure and update dynamics.

Game-theoretic cancer models usually rely on the assumption that cell populations are well-mixed or else represent structure as a fixed graph with a local update rule. We have taken an alternative approach, by coupling evolutionary game theory with an explicit model of an epithelium, the VT model. Using this framework we have considered how realistic epithelial structure and update dynamics affect evolutionary outcomes. One of the main restrictions of evolutionary graph theory is that it usually requires local coupling of birth and death. Using the VT model has enabled us to relax this restriction. Initially, in Chapters 4 and 5, we considered

the case where birth and death were spatially independent. Later, in Chapter 6, we incorporated contact inhibition into the VT model, which led to the reintroduction of spatial coupling.

We have proposed that a general rule is that cooperators fare better if they interact locally for game play, but compete for proliferation globally. We can class all the models we have considered in terms of whether interactions and competition are local or global. Thus, the VT model with decoupled update rule (local interaction & global competition) promotes cooperation over the well-mixed population (global interaction & global competition). It also promotes cooperation over the death-birth and birth-death update rules, both within the framework of evolutionary graph theory and when used in the VT model (local interaction & local competition). We have shown that this is true for both pairwise games and multiplayer games in Chapters 4 and 5, respectively.

This rule can be understood intuitively. Local interactions allow cooperators to interact preferentially with other cooperators, meaning a larger proportion of the benefit is retained for the cooperator community. That local interactions, thus, promote cooperation is an established result within evolutionary graph theory [6].

Local competition on the other hand, means that cooperators only directly compete with defectors when they are close to one another. This gives an advantage to the defectors, which have highest fitness when they have cooperator neighbours. Cooperators have highest fitness when they are surrounded by other cooperators, thus prefer competition to occur globally. Again, our result, that cooperators prefer global competition is supported by previous findings for the shift update rule within evolutionary graph theory [62, 63].

These results all consider a binary of local or global update rules, which result in local or global competition, respectively. However, our rule also holds for a more realistic approach to the update dynamics of epithelia. In Chapter 6, we considered how contact inhibition affects cooperative success. We found that stronger contact inhibition, as expected, tends to result in higher levels of spatial coupling and consequently poorer outcomes for cooperation. However, we also uncovered

a curious role for the quiescent area fraction, which affects the natural tension or compression of the tissue, and thus the distribution of cell areas. In some cases where the tissue is under compression and contact inhibition is strong, cooperation can be more successful than in cases where the tissue is under tension, but contact inhibition is weaker.

Although this seems to contradict our rule, it in fact highlights a more complicated picture. It is true that stronger contact inhibition leads to the increased spatial coupling of birth and death. However, as we discussed in Chapter 6, it is possible for there to be a relatively high level of global competition in compressed tissues, even when spatial coupling is strong. Thus, the rule still holds that cooperation prefers local interaction and global competition. We must, however, be wary of the fact that spatial coupling of birth and death does not always lead to correspondingly local competition.

Our use of the VT model to consider evolutionary dynamics within an epithelium has, thus, uncovered a much more nuanced picture of the connection between spatial coupling, competition, and cooperative success. However, this comes with the major drawback that the model is computationally expensive compared to evolutionary graph theory or well-mixed population models. For most of our simulations, we have kept the population size to a hundred cells. This is very small when we consider that the human body is estimated to consist of three trillion cells [161]. Even with this relatively small population size, the model is costly, especially when we consider that to estimate a single fixation probability it is necessary to run tens of thousands of simulations.

In the case where competition is fully global, due to the use of a decoupled update rule, we have derived approximate analytical results for pairwise and multiplayer games, in Chapters 4 and 5, respectively. These give the conditions under which a mutant is beneficial and/or favoured for any two-strategy game. These results rely on spatial statistics derived from the VT model by simulation, and could be extended to larger population sizes. There are also known results from evolutionary graph theory, which allow us to predict evolutionary outcomes for birth-death

and death-birth update rules [14, 15]. The VT model with contact inhibition however, is much harder to analyse, and thus, in Chapter 6, we have relied entirely on simulation results.

It is useful, therefore, to use our insights from the VT model with contact inhibition to consider when a death-birth or decoupled update rule can provide a good approximation. For a compressed tissue, the decoupled update rule is a better fit, except for very strong contact inhibition, when the death-birth update rule would be more appropriate. When the tissue is under tension, the decoupled update rule is the best approximation for weak contact inhibition, and the death-birth update rule for strong contact inhibition. However, the transition between the two is less sharp, meaning there is a significant intermediate regime, where neither is particularly good.

Overall, we have seen that careful consideration of both population structure and population updating is vital for predicting the evolutionary success of cooperation. Cancer models which utilise evolutionary games [54, 162] may therefore underestimate the success of cooperative phenotypes, if they fail to account for population structure, or assume that death and division are more tightly coupled than is realistic. For example, therapeutic strategies that aim to eliminate cooperation by manipulating evolutionary dynamics, rely on accurate predictions of those dynamics [35].

Interestingly, loss of contact inhibition is associated with malignancy [135], suggesting that spatial coupling is weaker, and thus cooperation could be more successful, than in healthy tissues. However, this could also depend on the mechanics of the tumour or tissue. Understanding the nature of spatial coupling in real epithelia, or in cancerous tumours, as well as the mechanical properties, i.e. whether cells are under stretch or strain, could be crucial for predicting evolutionary outcomes.

Our general conclusion that local game play and global competition for offspring favour cooperation has implications beyond applications to cancer, where cooperation unusually may be considered undesirable. In a societal context, where cooperation is desirable, it may be promoted by engineering an environment rich

in local social interactions, which nevertheless allows for imitation of successful strategies more globally.

7.2 Future work

There are several promising avenues for future work following on from this thesis. Firstly, we consider extensions for the VT model with decoupled update rule, analysed in Chapters 4 and 5. We have focused entirely on two-strategy games, however, there are many examples of game-theoretic cancer models which involve multiple strategies. Various studies have, for example, considered three or four strategy games which represent the interdependence of glycolytic, angiogenetic and/or invasive strategies [45, 47, 48]. These models have focused on the deterministic dynamics of well-mixed populations. By considering extensions of the VT model with decoupled update rule to multiple strategies, we could apply our analysis to these types of scenarios.

For both pairwise and multiplayer games, we have assumed that cells interact only with their direct neighbours. Whether this is a realistic assumption will depend on the specific application. For example, for diffusible growth factors, it will depend on their diffusion range. Unfortunately, these are often difficult to measure experimentally [92]. It would, therefore, be useful to consider different ranges within our model, for example cells interacting in groups with their two- or three-step neighbours. This would mean interactions become less local, thus we would expect a detrimental effect on cooperation.

Another extension to our results for the decoupled update rule would be to consider (i) whether our results are consistent with other two-dimensional tissue models, such as the vertex model, and (ii) whether they can be extended to represent three-dimensional tumours. Calculating fixation probabilities through simulation is likely to be computationally infeasible for more complex models or in three-dimensions. However, it should be possible to calculate spatial statistics and, thus, use our approximate analytical results. It would also be possible to consider the effect of explicit cell motility in the VT model.

We have focused on relatively small population sizes, and the stochastic dynamics for which complete defection or complete cooperation are the only two possible outcomes. However, tumours are known to exhibit heterogeneity, with multiple clones coexisting [163]. Extending to larger population sizes would enable us to consider the existence of metastable mixed states, as has been done for well-mixed [37] and graph structured populations [164].

For the VT model with contact inhibition we also propose a number of directions for future work. Firstly, we have touched on the possible importance of the spring constant for the one-dimensional VT model, which determines how quickly forces are relaxed. We suggest (i) considering this parameter in more detail for the one-dimensional model, including the case where there are no forces, thus the spring constant is effectively zero; and (ii) an analysis of the effect of varying the spring constant in two dimensions. In one dimension, the only equilibrium state is where all cells are of equal size, thus there is no spatial coupling if the forces relax sufficiently quickly. This is unlikely to be true for two dimensions.

We also consider that we have used a very simple model of contact inhibition, based on an area threshold for proliferation. It has been found that mechanical measures, such as cell tension or energy, are better indicators for cell cycle duration than geometric ones [165]. Furthermore, cell growth and realistic cell cycles could be incorporated into the VT model.

Another proposal is to consider the evolutionary dynamics of a simple mutation within the VT model with contact inhibition. By simple, we mean a mutation with a given fitness that is independent of interactions with other cells. It is known that population structure can amplify or suppress selection for simple mutations, and that whether a particular graph is an amplifier or a suppressor depends on the update rule [16, 83, 84]. Amplifiers tend to be more common for the birth-death update rule, and suppressors for the death-birth update rule. We did not consider simple mutations for the VT model with decoupled update rule, as it would result in equivalent dynamics to the well-mixed population. For the VT model with contact inhibition, however, there could be an effect in some regimes to suppress selection.

Finally, there are several ways this work could be strengthened by experimental data. This is particularly clear for the contact inhibition model, as we have a wide range of behaviour, dependent on multiple parameters. Obtaining estimates for the death-to-birth rate ratio and quiescent area fraction for different epithelia, could help us understand which regimes are realistic, and to what extent simpler models, such as the decoupled or death-birth update rules, can provide good approximations.

Appendix A

Abbreviations and symbols

A.1   Abbreviations

APD   additive prisoner's dilemma

BCFI   background-corrected fate imbalance

CD   cell diameter

DT   Delaunay triangulation

HL   hexagonal lattice

VT   Voronoi tessellation

NPD N-player prisoner's dilemma

PGG   public goods game

VD   volunteer's dilemma

WM   well-mixed

A.2 Symbols

Symbols are listed in the order that they are first introduced within the thesis.

Chapter 2

R, S, T, P	pairwise game payoffs
π_X	mean payoff to an individual of type X
π_i	payoff to individual i
π	mean payoff for population
F_X	mean fitness of an individual of type X
F	mean fitness taken for population
δ	selection strength parameter
Z	population size
x	frequency of cooperators
n	number of cooperators
$T_n^{\pm}$	transition probabilities
γ_n	ratio of transition probabilities T_n^-/T_n^+
ϕ_n	fixation probability for n initial cooperators
ρ_X	fixation probability for a single initial X mutant
ρ_0	neutral fixation probability
s_i	type of an individual i
G	neighbour connectivity graph
A_{ij}	adjacency matrix for G
k	number of neighbours or co-players
b	benefit or maximum benefit
c	cost paid by a cooperator
$(b/c)^*$	critical benefit-to-cost ratio (pairwise games)
$(b/c)_0^*$	critical benefit-to-cost ratio at which $\rho_C = \rho_0$
$(b/c)_1^*$	critical benefit-to-cost ratio at which $\rho_C = \rho_D$
σ	structure coefficient for a pairwise game
σ_j	j-th structure coefficient for a multiplayer game
$N = k+1$	group size for a multiplayer game

$a_j, a_{j,k}$	payoff to an A-player with j A-type co-players
$b_j, b_{j,k}$	payoff to an B-player with j A-type co-players
$\Theta(x)$	Heaviside step function
$\beta(x)$	normalised benefit function
$\alpha(x)$	logistic function
h	inflection point of logistic function
s	steepness of logistic function

Chapter 3

$\mathbf{F}_{ij}^S$	force exerted on cell i due to j
$\mathbf{F}_i^S$	total force on cell i
$\mathbf{r}_{ij}$	displacement vector pointing from j to i
s_{ij}	natural separation between cells i and j
s_M	natural separation between mature cells
ε	initial separation between new sibling cells
t_M	time over which natural separation grows from ε to s
$\mathcal{N}_i$	set of cells which are neighbours of i
η	drag coefficient
μ	spring constant
Δt	small time step

Chapter 4

λ	per cell death rate
Λ_n^{CC}	expected proportion of cooperator neighbours for a cooperator
m	probability of migration

Chapter 5

g_k	probability of having k co-players/neighbours
$f_j^{A/B}(n,k)$	probability that an A/B player interacts with j co-players of type A
$G(n)$	gradient of selection

Chapter 6

$A^{(0)} = \frac{\sqrt{3}}{2}s_M^2$	preferred cell area
α	quiescent area fraction
$A_i(t)$	area of cell i
$\bar{A}$	population mean cell area
γ	per cell division rate of non-contact inhibited cells
λ/γ	death to birth rate ratio
Z_{div}	number of non-cotact inhibited cells
Z^*	homeostatic population size
Z_0	initial population size
$P_i^{\mathrm{div}}(t,\Delta t)$	probability cell i divides in $(t,\Delta t)$
$P_i^{\mathrm{death}}(t,\Delta t)$	probability cell i dies in $(t,\Delta t)$
W	domain width
$\mathrm{BCFI}_i(t)$	background-corrected fate imbalance for cell i
$L_i(t)$	length of cell i
$L^{(0)}$	preferred cell length

Appendix B

Varying the spring constant in the Voronoi tessellation model with decoupled update rule

In Chapters 4 and 5 we used parameter values for the Voronoi tessellation (VT) model taken from [151] as shown in Table 2. Here we show that our main result of Chapter 2, that the decoupling of birth and death promotes cooperation under the additive prisoner's dilemma (APD), is robust to changes in these values. In particular, we look at changes in the spring constant to drag coefficient ratio μ/η, which determines how quickly relaxation occurs when the system is out of equilibrium (i.e. birth or death has occurred). Varying this ratio while keeping the birth and death rates λ constant, will alter the tissue dynamics and topology. This is clear from Figure B.1, which shows the polygon (neighbour number) distributions for different values of μ, while keeping $\eta = 1$ constant. Decreasing μ leads to more variation in neighbour number.

To consider the effect of varying μ we calculate the fixation probability for a range of values using the approximate analytical technique described in Section 4.2.2 of the main text. We calculate Λ_n^{CC}, defined by Equation (4.10), computationally by running 500 simulations for each μ. The fixation probabilities are then calculated using Equation (4.12) and the critical benefit-to-cost ratios, $(b/c)^*$, using Equation (4.13). The critical benefit-to-cost ratios are plotted in Figure B.2.
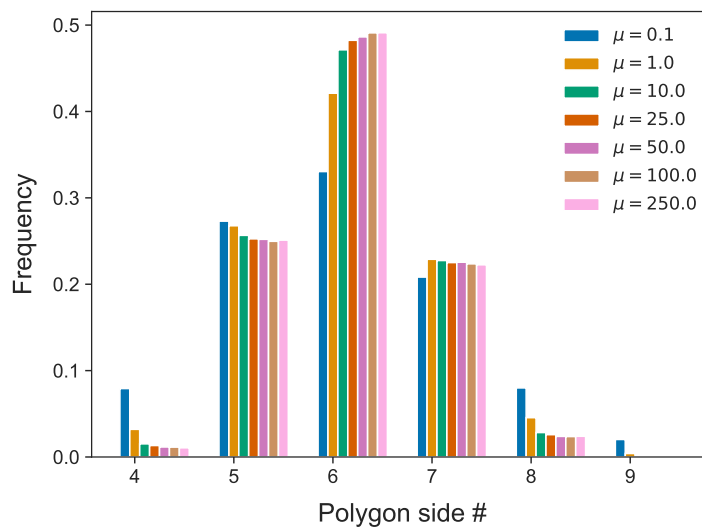
Figure B.1: Polygon distributions for various values of spring constant μ. In the main text we use $\mu = 50$. Decreasing μ below this value leads to increased variation in side number around the mean. Each distribution is calculated from data collected from three simulation runs of 100 hours simulation time.

We keep all other parameters constant, except for Δt, which is set to be

$$\Delta t = 0.005 \times \min\left(1, \frac{50}{\mu}\right) .$$
(B.1)

This ensures that when μ is increased, Δt remains small enough for numerical stability.

Figure B.2 shows that $(b/c)^*$ increases with μ. Increasing μ above 50 (the value used in the main text) leads to small increases in $(b/c)^*$, but it remains well below the values for death-birth updating (see Table 1). Decreasing μ below 50 leads to fast decreases in $(b/c)^*$, thus the success of cooperation is increased. It is not possible without further investigation to ascertain whether this is due to the changes in graph topology, or whether there are other effects to the tissue dynamics which are promoting cooperation. Note that we do not claim this range of μ to be biologically reasonable, indeed for low values of μ the forces will act so slowly that it certainly is not realistic. We have chosen to show this large range of μ in order to demonstrate the robustness of our result that decoupling birth and death promotes cooperation in the Voronoi Tessellation model.
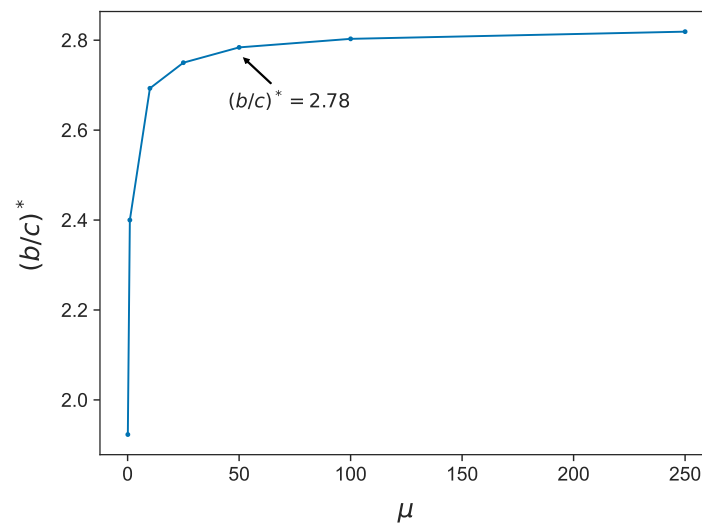
Figure B.2: Critical benefit-to-cost ratio $(b/c)^*$ against the spring constant μ, for a cooperative mutant in the Voronoi Tessellation model with decoupled update rule. The labelled point corresponds to the value of μ used in simulations in the main text. Lower values of $(b/c)^*$ imply that cooperation is more successful, thus cooperative success is decreasing with μ.

Appendix C

The additive prisoner's dilemma with strong selection

Throughout this thesis we have primarily analysed evolutionary games within the limit of weak selection. This limit is commonly employed in order to obtain analytical results, e.g. [10, 14, 81]. Essentially, weak selection implies that the payoffs obtained by playing the game are only a small contribution to overall fitness. It allows expansion of fixation probabilities in powers of the selection strength parameter.

While analytical results are difficult to obtain for arbitrary selection strength, we can use simulation to explore the behaviour of our models beyond weak selection. To do this we consider an exponential fitness mapping [166]:

$$F_i = \exp\{\delta \pi_i\}. \tag{C.1}$$

This ensures that the fitnesses cannot be negative. For small δ we regain the linear fitness mapping: $F_i \approx 1 + \delta \pi_i$, which was introduced in Chapter 2, and used throughout this thesis.

In Figure C.1 we plot the fixation probabilities ρ_C for a single initial cooperator, playing the additive prisoner's dilemma, for various non-small values of the selection strength parameter δ. These are calculated by simulation for both the VT model with decoupled update rule, and a fixed hexagonal lattice with death-birth

update rule. We see from the figure that for arbitrary selection strength, the fixation probabilities are non-linear functions of the benefit-to-cost ratio b/c. We also plot the theoretical results for weak selection ($\delta = 0.025$) discussed in the main text, i.e. Equation (4.12) for the VT model, which was derived in Chapter 4, and Equation (2.37) for the hexagonal lattice [14], which we introduced in Chapter 2.

For the Voronoi tessellation model, we can see a range of behaviour in Figure C.1, depending on the value of δ. Firstly, for $0.025 < \delta < 0.2$, it appears that increasing δ leads to higher fixation probabilities for all values of b/c we consider. However, if we continue to increase δ beyond 0.2, we start to see the fixation probabilities fall. This is particularly clear for higher values of b/c. For example, at $\delta = 1$ the fixation probability is maximised at $b/c \approx 7$.

Once δ is sufficiently large, e.g. for $\delta = 2$ in Figure C.1, it appears that we enter a regime where $\rho_C < 1/Z$ for all b/c. This implies that if selection is too strong, cooperation is never favoured.

We can understand this observation, because strong selection implies much weaker stochasticity. Cells with high payoffs have a very high probability that they are chosen to divide, compared to cells with low payoffs. Thus, this choice is near-deterministic. As the system is always started with a single initial mutant cooperator, which has lower payoffs than all other cells, there is a very low probability of that cell dividing, and thus reaching a state which favours cooperators.
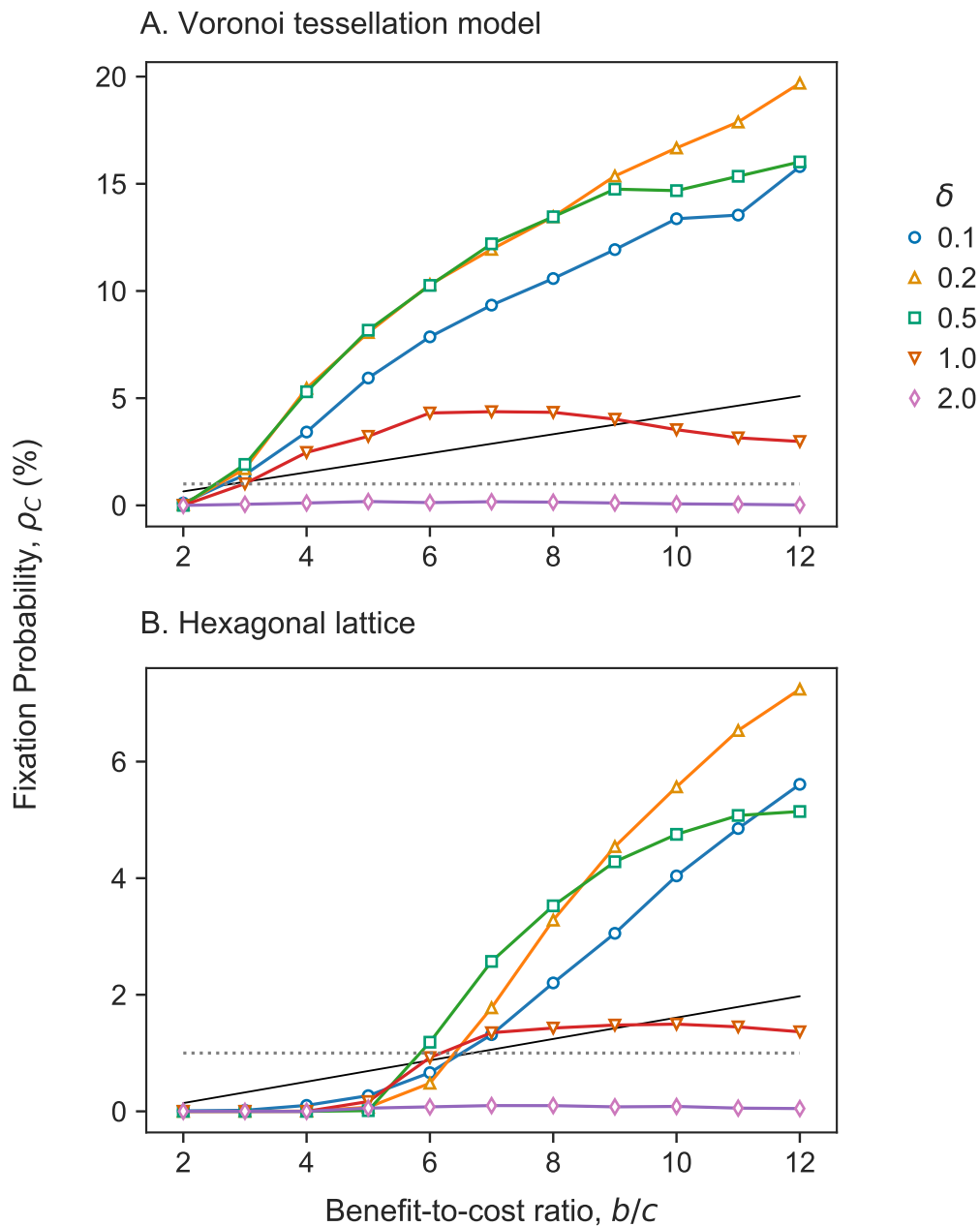
Figure C.1: Fixation probability ρ_C for the additive prisoner's dilemma game with varying selection strength δ. Simulation results are shown for the Voronoi tessellation model with decoupled update rule (A) and the hexagonal lattice with death-birth update rule (B). In both cases population size is $Z = 100$. The dotted line is the neutral fixation probability $\rho_0 = 1/Z$ and the solid line corresponds to theoretical results for ρ_C calculated in the weak selection limit, where we have set $\delta = 0.025$. These are given by Equation (4.12) (A) and Equation (2.37) (B).

Appendix D

Implications of the antisymmetry-of-invasion property

In Section 5.2.3 we showed that the conditions for a mutant to be beneficial and favoured are equivalent for games which satisfy the antisymmetry-of-invasion property, defined by Equation (5.30). Here, we explore further some of the implications of this property.

For games which satisfy antisymmetry-of-invasion, there is a fixed total payoff which can be obtained when equal numbers of A and B co-players are distributed between an A and B player. By this we mean that the A-player has j other A-players in its group and $k - j$ B-players, whilst the B-player has j other B-players, and $k - j$ A-players. Regardless of how the co-players are distributed (the value of j), the sum of the payoffs to the A and B player are the same.

The implications of this property can be better understood if we consider symmetric invasion processes. Consider, for example an arbitrary evolutionary path through the state space. This path can be represented by a sequence of states

$$S = (G_0, \mathbf{s}_0) \rightarrow (G_1, \mathbf{s}_1) \rightarrow \cdots \rightarrow (G_L, \mathbf{s}_L), \tag{D.1}$$

where G_q are graphs representing the population structure at time t_q and $\mathbf{s}_q$ are Z-dimensional vectors giving the type of each individual at time t_q. Thus, $[\mathbf{s}_q]_i = 1$ if the ith individual is an A-player and $[\mathbf{s}_q]_i = 0$ if it is a B-player. Recall Z is the

population size. There are L transitions between states, each of which is caused by an update event (i.e. a death and a division).

The symmetric invasion process $\tilde{S}$ is obtained by flipping the type of each individual ($A \to B$ and $B \to A$), as illustrated in Figure D.1. Thus

$$\tilde{S} = (G_0, \tilde{\mathbf{s}}_0) \to (G_1, \tilde{\mathbf{s}}_1) \to \cdots \to (G_L, \tilde{\mathbf{s}}_L), \qquad (D.2)$$

where $[\tilde{\mathbf{s}}_q]_i = 1 - [\mathbf{s}_q]_i$.
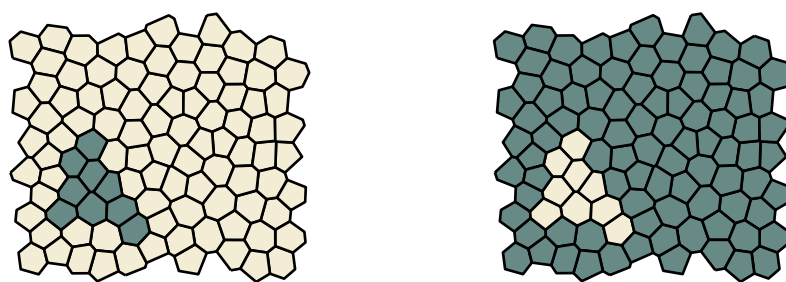
(a) Original state S.   **(b)** Symmetric state $\tilde{S}$.

Figure D.1: Symmetric states. (a) a mutant clone of A-players is invading a population of B-players. (b) a mutant clone of B-players is invading a population of A-players. If the antisymmetry-of-invasion property holds a given A-player in state (a) has payoff a_j, the equivalent B-player in state (b) will have payoff $b_{k-j} = Q - a_j$.

Given any evolutionary path S and a symmetric path $\tilde{S}$ we can show that, if the antisymmetry-of-invasion property holds, the probabilities of each occurring are related in the following way:

$$P(S) - P(S_0) = P(S_0) - P(\tilde{S}), \qquad (D.3)$$

at least to $\mathscr{O}(\delta)$. Here, S_0 is the evolutionary path with neutral selection $\delta = 0$, i.e. all individuals have the same fitness. Thus, if any given path has an advantage over the neutral process, the symmetric path must have an equivalent disadvantage.

We can further show that the following relation between the fixation probability for an A-player and the fixation probability of a B-player, denoted by ρ_A and ρ_B,

respectively, must hold:

$$\rho_A - 1/Z = 1/Z - \rho_B \,, \tag{D.4}$$

again to $\mathscr{O}(\delta)$. Recall that $\rho_0 = 1/Z$ is the fixation probability for a neutral mutant. Thus, antisymmetry-of-invasion ensures that $\rho_A > \rho_0$ implies $\rho_B < \rho_0$, and hence that the conditions for *A* or *B* to be favourable are the same as to be beneficial.

Proof of Equation (D.3). Consider a path *S* as described by Equation (D.1). The transition probability from state $(G_q, \mathbf{s}_q)$ to $(G_{q+1}, \mathbf{s}_{q+1})$ is given by

$$
\begin{aligned}
P((G_q, \mathbf{s}_q) \to (G_{q+1}, \mathbf{s}_{q+1})) &= P(\mathbf{s}_q \to \mathbf{s}_{q+1}) \cdot P(G_q \to G_{q+1} | \mathbf{s}_q \to \mathbf{s}_{q+1}) \\
&= \frac{1}{Z^2} \left\{ 1 + \delta \left[\pi_{\text{birth}}(G_q, \mathbf{s}_q) - \pi(G_q, \mathbf{s}_q) \right] \right\} \cdot \psi_q \,,
\end{aligned}
\tag{D.5}
$$

where π_{birth} is the payoff of the proliferating individual and π is the average payoff in the population. The probabilities for transitions between graphs are given by $P(G_q \to G_{q+1} | \mathbf{s}_q \to \mathbf{s}_{q+1}) = \psi_q$.

The probability of *S* occurring, given initial state $(G_0, \mathbf{s}_0)$, is given by multiplying the transition probabilities, i.e.

$$P(S) = \prod_{q=0}^{L-1} P((G_q, \mathbf{s}_q) \to (G_{q+1}, \mathbf{s}_{q+1})) \,, \tag{D.6}$$

which in the weak selection limit $\delta \to 0$ becomes

$$P(S) = \frac{1}{Z^{2L}} (1 + \delta X(S)) \Psi(S) + \mathscr{O}(\delta^2) \,. \tag{D.7}$$

Here,

$$X(S) = \sum_{q=0}^{L-1} \left(\pi_{\text{birth}}(G_q, \mathbf{s}_q) - \pi(G_q, \mathbf{s}_q) \right) \tag{D.8}$$

and

$$\Psi(S) = \prod_{q=0}^{L-1} \psi_q \,. \tag{D.9}$$

The symmetric evolutionary path $\tilde{S}$ is equivalent to *S*, except that every individual has flipped its type. We assume that, in the weak selection limit at least, graph

transitions do not depend on type, and thus, $\Psi(\tilde{S}) = \Psi(S)$. The payoffs of course do depend on type, thus we write

$$X(\tilde{S}) = \sum_{q=0}^{L-1} \left(\pi_{\text{birth}}(G_q, \tilde{\mathbf{s}}_q) - \pi(G_q, \tilde{\mathbf{s}}_q) \right) . \tag{D.10}$$

If the antisymmetry-of-invasion property, defined by Equation (5.30), holds then

$$X(\tilde{S}) = \sum_{q=0}^{L-1} \left((Q - \pi_{\text{birth}}(G_q, \mathbf{s}_q)) - (Q - \pi(G_q, \mathbf{s}_q)) \right) \ = -X(S). \tag{D.11}$$

Therefore, substituting into Equation (D.7), we obtain

$$P(\tilde{S}) = \frac{1}{Z^{2L}}(1 - \delta X(S))\Psi(S) + \mathcal{O}(\delta^2). \tag{D.12}$$

Setting $\delta = 0$ gives $P(S_0) = \Psi(S)/Z^{2L}$. Therefore, by summing Equations (D.7) and (D.12), we obtain $P(S) + P(\tilde{S}) = 2P(S_0)$, from which Equation (D.3) follows.

Proof of Equation (D.4). The fixation probability for a single initial A-player is obtained by summing $P(S_i)$ over all paths S_i that start with a single initial A-player, and end with fixation for A-players. Summing over Equation (D.7), we obtain

$$\begin{aligned} \rho_A &= \sum_i \frac{\Psi(S_i)}{Z^{2L(S_i)}} + \sum_i \frac{\delta\Psi(S_i)}{Z^{2L(S_i)}} X(S_i) + \mathcal{O}(\delta^2) \\ &= \frac{1}{Z} + \sum_i \frac{\delta\Psi(S_i)}{Z^{2L(S_i)}} X(S_i) + \mathcal{O}(\delta^2), \end{aligned} \tag{D.13}$$

where we have used the fact that the fixation probability for neutral selection ($\delta = 0$) is $\rho_0 = 1/Z$. The fixation probability for B-players can similarly be obtained by summing $P(\tilde{S}_i)$ over all paths $\tilde{S}_i$ that start from a single B-player and end with B-player fixation. Thus,

$$\rho_B = \frac{1}{Z} - \sum_i \frac{\delta\Psi(S_i)}{Z^{2L(S_i)}} X(S_i) + \mathcal{O}(\delta^2). \tag{D.14}$$

Summing Equations (D.13) and (D.14) gives us $\rho_A + \rho_B = 2/Z$, and thus Equation (D.4).

Appendix E

Neighbour distributions in the Voronoi tessellation model

In Sections 5.2.1 and 5.2.2 we derived conditions under which cooperation is favoured and beneficial, given by Equations (5.16) and (5.22) respectively. These derivations are based on the assumption that the frequency of cells with k neighbours is a fixed distribution g_k, independent of the cell type or the number of cooperators in the population, n.

Figure E.1 plots neighbour distributions from simulations of the VT model for cooperators and defectors at different values of n. It is clear from the plot that the assumption is a reasonable one. The neighbour distributions are approximately equal for different values of n and for the two cell types. The exception is when there are either very few cooperators or very few defectors, i.e. near $n = 1$ and $n = 99$ respectively. In the case where there is only one or very few cooperators, the cooperator neighbour distribution becomes slightly more narrow. Similarly, the defector neighbour distribution becomes more narrow when there are few defectors.
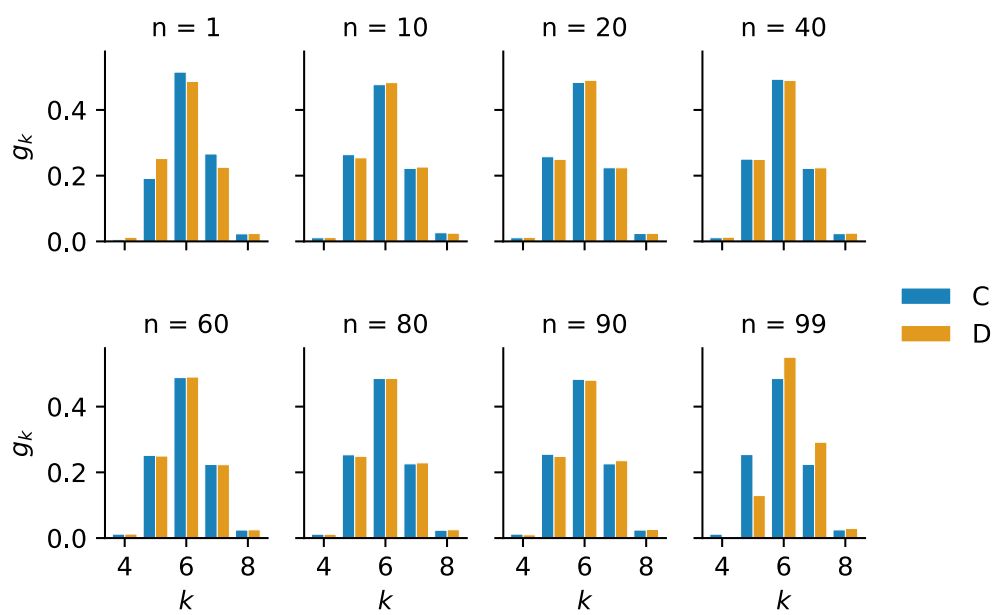
Figure E.1: Neighbour distributions in the Voronoi tessellation model for cooperators (C) and defectors (D), for varying cooperator population size n. Data is generated from simulations with total population size $Z = 100$ and neutral selection $\delta = 0$.

Appendix F

The Voronoi tessellation model with contact inhibition

This appendix contains supplemental results for the Voronoi tessellation model with contact inhibition, introduced in Chapter 6.

F.1   Error in the critical benefit-to-cost ratios

In Figure 6.7 we plotted the critical benefit-to-cost ratios $(b/c)^*$ for the Voronoi tessellation model with contact inhibition for various values of λ/γ and α. Each value of $(b/c)^*$ was obtained by running 3×10^4 simulations for a range of b/c values, fitting a best fit line by linear regression, and finding the intersection with $b/c = 1/Z^*$.

Ideally, to find a measure of the error we would repeat this process a number of times and calculate the standard deviation of our predicted values of $(b/c)^*$. However, this is computationally unfeasible. Alternatively, we have divided our data into ten separate batches, each of which contains the results of 3000 simulations. For each batch, we have calculated $(b/c)^*$ by fitting a best fit line and finding the intersection with $b/c = 1/Z^*$. We have then taken the mean and standard deviation of these estimates and plotted the results in Figure F.1.

We find that the error bars are very large, particularly for small λ/γ. We attribute this to the fact that 3000 simulations is not sufficient to obtain an accurate estimate for the fixation probabilities which are in the order of 10^{-2}. It is clear

from Figure 6.6 that in some parameter regimes, fixation probabilities increase very slowly with $(b/c)^*$. These cases, in particular, require large numbers of simulations per data point, in order to obtain a reasonable estimate of the slope.
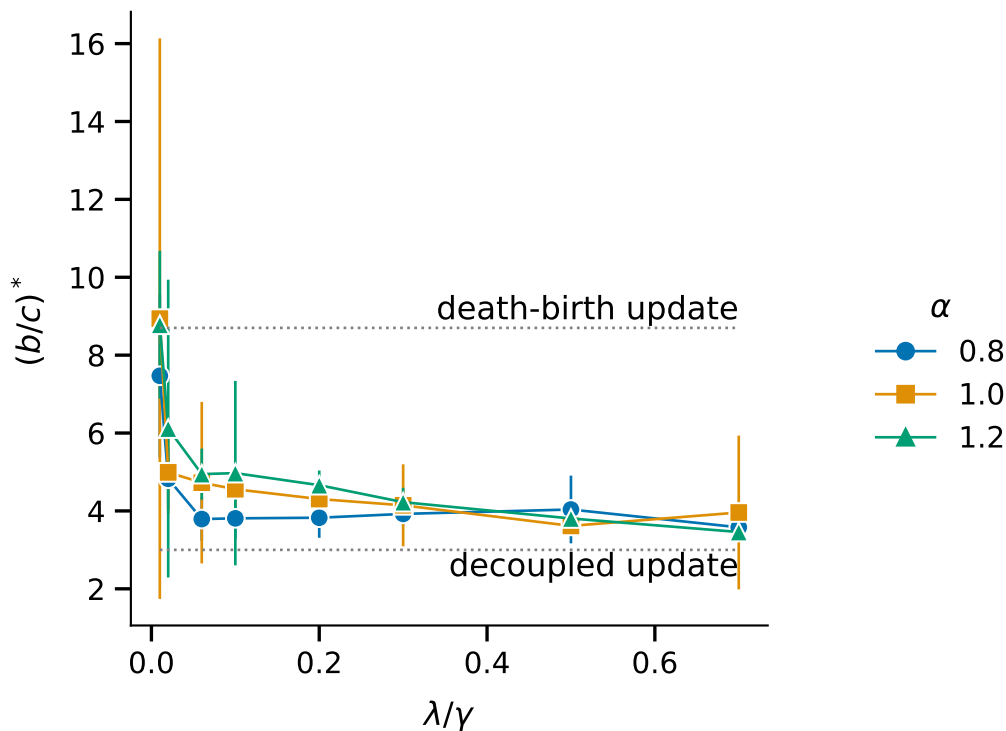
Figure F.1: Error bars are plotted for the critical-benefit-to-cost ratios $(b/c)^*$. Data is the same as for Figure 6.7 in the main text. However, here we have calculated ten separate estimates for $(b/c)^*$ for each set of $(\lambda/\gamma, \alpha)$. Points are the mean values and error bars show standard deviations.

F.2 Average distance between fate events

In Section 6.4.2 we considered the extent to which spatial coupling of death and division events was dependent on key parameters of the Voronoi tessellation model with contact inhibition by calculating the background corrected fate imbalance (BCFI) around deaths and divisions. We found that spatial coupling between death and division was stronger for smaller values of λ/γ, and that there was only a small effect from varying α.

Here, we verify these results by considering the distance between a death or division and the n-th subsequent division. Average distances are plotted in Figure F.2.

These are normalised to be in units of expected cell separation, which depends on the parameters α and λ/γ. It is clear from the figure that the expected distance between a death and the next division decreases when λ/γ is decreased (upper panel), as does the expected distance between a division and the next division (lower panel). This is consistent with the results for the BCFI, as it implies that the level of spatial coupling between death and a subsequent division is negatively correlated with the value of λ/γ. Thus, stronger contact inhibition implies stronger spatial coupling.
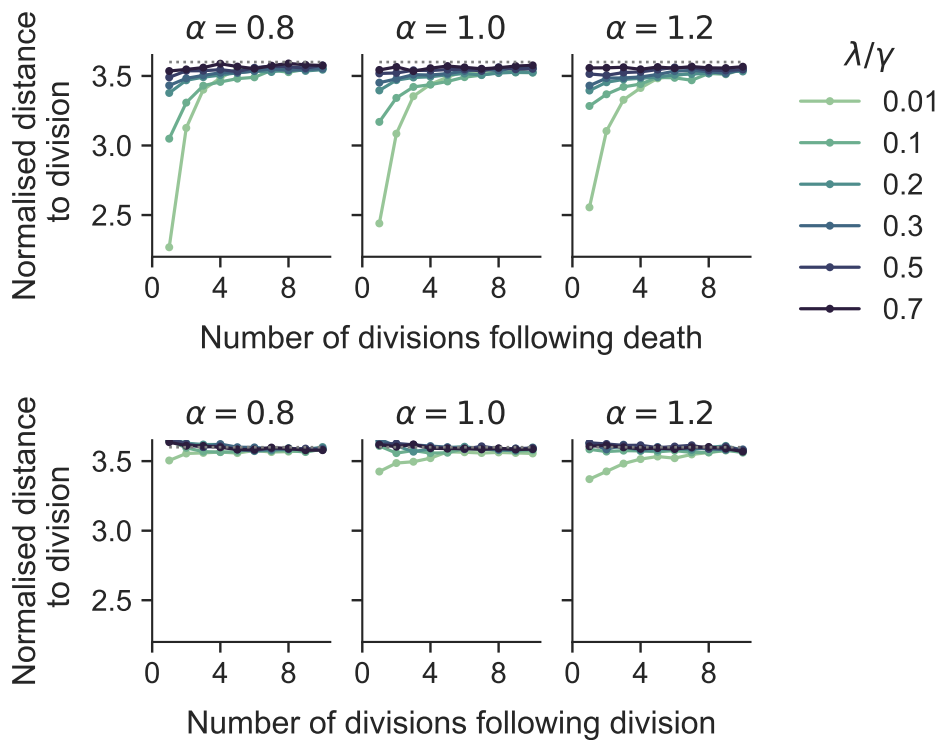
Figure F.2: Mean distance between the location of a death (upper panel) or division (lower panel), and subsequent divisions, in the Voronoi tessellation model with contact inhibition. Distances are normalised to be in units of the time-averaged mean cell separation which is different for each parameter set. The dotted line is the average distance between two cells. In the absence of contact inhibition or other form of spatial coupling, this value would be the expected distance between a division/death and any subsequent division.

There is also some small dependence on α, again consistent with the results for the BCFI. However, this does not appear to be sufficient to explain the fact that smaller α values promote cooperation (at least when λ/γ is sufficiently small). This is clear from Figure F.3, which plots the critical benefit-to-cost ratio $(b/c)^*$ against

the expected distance between death and the next division, for different values of α.
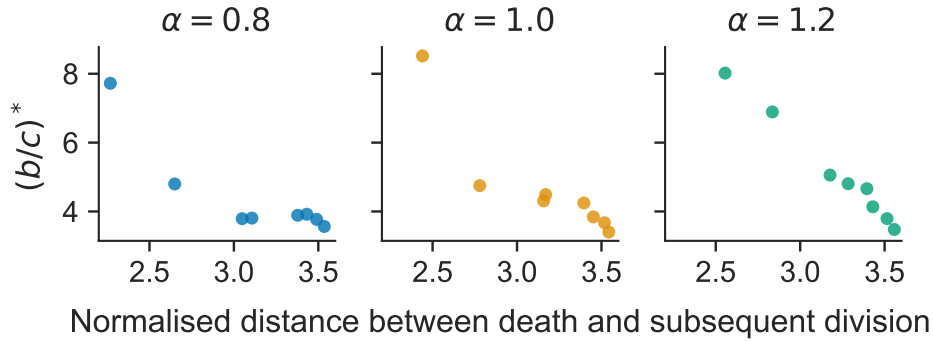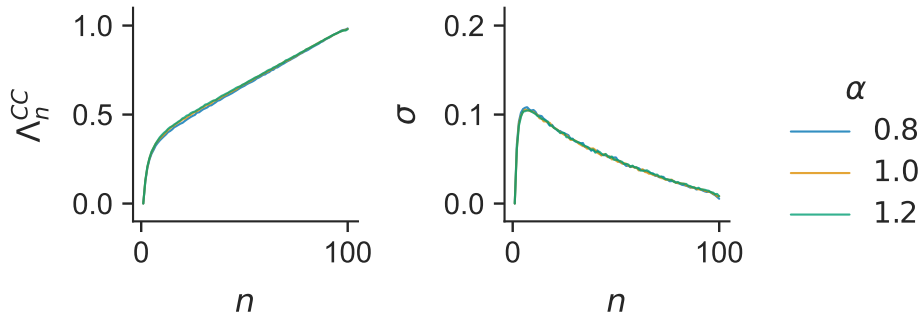

Figure F.3: Critical benefit-to-cost ratio $(b/c)^*$ plotted against the average normalised distance between the location of a death and the next division. The value of $(b/c)^*$ is negatively correlated to the normalised distance, but also depends on the quiescent area fraction α. Critical benefit-to-cost ratios are for the additive prisoner's dilemma with $c = 1$ and $\delta = 0.025$.

F.3 Dependence of cell fitness on the critical area fraction

In this section we consider whether the dependence of the critical benefit-to-cost ratio $(b/c)^*$ on the critical area fraction α can be explained by differences in cell fitness. We look at the case where $\lambda/\gamma = 0.1$ and compare $\alpha = 0.8$ and $\alpha = 1.2$, which have $(b/c)^* = 3.8$ and 4.8, respectively. For both regimes, we generate simulation data with neutral selection $\delta = 0$. Figure F.4a plots the proportion of cooperator neighbours that are cooperators Λ_n^{CC}, calculated for all cells in the population. The higher the value of Λ_n^{CC} for a given number of cooperators n in the population, the higher the expected cooperator fitness. When birth and death are spatially decoupled, Λ_n^{CC} can be used to calculate the fixation probabilities directly [138]. It is clear there is negligible difference in the expectation and standard deviation of Λ_n^{CC} for $\alpha = 0.8$ and $\alpha = 1.2$. We also plot Λ_n^{CC} calculated only for cells which are able to proliferate (i.e. non-contact inhibited cells) in Figure F.4b. Again, there is negligible difference between the $\alpha = 0.8$ and $\alpha = 1.2$ cases. We therefore conclude that the dependence of cooperative success on α cannot be explained by differences in expected fitness.

(a) all cells

(b) proliferating cells only

Figure F.4: Expected proportion of cooperator neighbours which are cooperators Λ_n^{CC} and the standard deviation σ, for the Voronoi tessellation model with contact inhibition. Results are for $\lambda/\gamma = 0.1$ and show negligible difference for $\alpha = 0.8$ and $\alpha = 1.2$. Panel (a) takes the mean and SD over all cells in the tissue, while panel (b) includes only cells which are able to proliferate, i.e. are not contact inhibited. Results are calculated by running 500 tissue simulations to fixation, with neutral selection $\delta = 0$, and tracking clones which are defined as cells with a common ancestor. Each clone gives us a potential cooperator cluster of size n and we assume the cluster shapes are independent of the game.

F.4 Varying the spring constant in the one-dimensional Voronoi tessellation model

The one-dimensional VT model, described in Section 6.5 has a single equilibrium state. In this state all cells are of equal length. Therefore, if the ratio of spring constant to drag coefficient (μ/η) is sufficiently high, the system will return to a state of equally spaced cells on a faster time scale than death and division events

occur. This can be seen in Figure F.5, where we plot the coefficient of variation for cell length against μ, while keeping $\eta = 1$ constant. For high μ, there is very little variation in the length of cells.
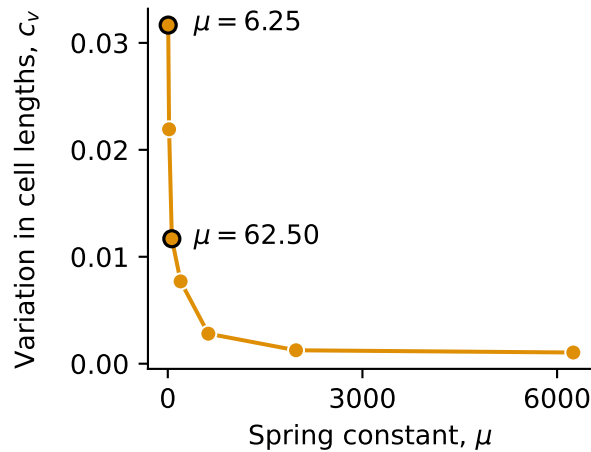
Figure F.5: Coefficient of variation for cell lengths c_v in the one-dimensional Voronoi tessellation model varies with spring constant μ. The value of c_v is taken as an average over time, in three distinct simulations, with $\alpha = 1.0$, $\lambda/\gamma = 0.01$ and $W = 88.672$.

For larger values of μ the intercellular forces reach equilibrium on a much faster time scale than division and death occur. The only equilibrium for the one-dimensional spring system is the state with all cells of equal length, thus c_v is very small. For smaller μ relaxation is slower, thus we observe greater variation in cell lengths. Labelled values of μ indicate those used in simulations of the additive prisoner's dilemma.

When variation in cell length is very small, the density-dependence of proliferation will be global rather than local, as either all cells will exceed the length threshold or none will. Thus, we expect that increasing μ will move the system closer to a decoupled update rule, with cooperation becoming increasingly successful. For sufficiently high μ we expect $(b/c)^*$ to be independent of λ/γ. It is computationally expensive to consider very high values of μ, because it requires a correspondingly small timestep Δt to maintain numerical stability when using the forward Euler method (see Section 3.3). We have considered a value of $\mu = 62.5$, which is ten times larger than the original value and correspondingly set $\Delta t = 0.004$. Simulation results for $(b/c)^*$ with this increased value of μ are shown in Figure F.6. As expected we see $(b/c)^*$ is reduced for all values of λ/γ and closer to the decou-

pled update result, when compared with the results for $\mu = 6.25$ in Figure 6.16.
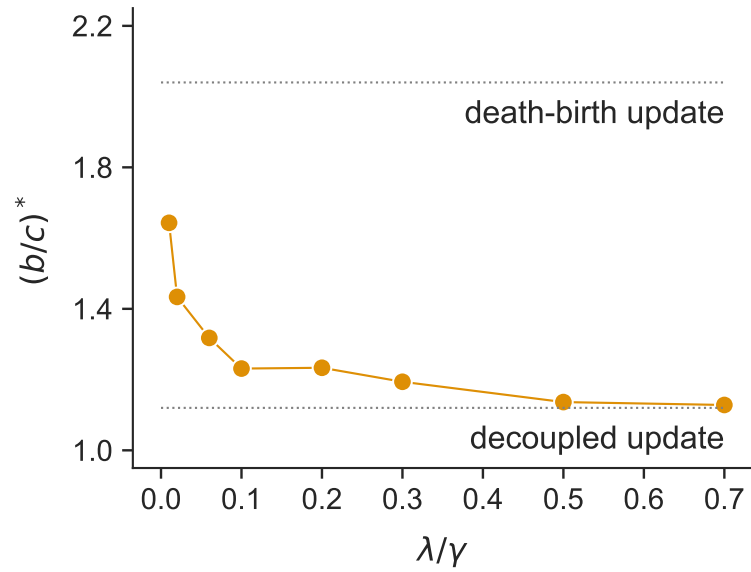
Figure F.6: Critical benefit-to-cost ratios $(b/c)^*$ obtained for $\mu = 62.5$ and $\alpha = 1.0$ in the one-dimensional Voronoi tessellation model, with those for death-birth and decoupled update rules. Values of $(b/c)^*$ increase with decreasing λ/γ, however they remain smaller than the equivalent values for $\mu = 6.25$ (see Figure 6.16). Cooperation is, therefore, more successful when μ is higher.

Appendix G

Implementation of Voronoi tessellation model

We have written bespoke code *VTdyn* to run simulations of the Voronoi tessellation (VT) model in Python 2.7.15. The general code for running VT model simulations is available at https://github.com/jessierenton/VTdyn. Specific code and data for Chapters 4 and 5 can be accessed at:

https://github.com/jessierenton/evo_epithelium and

https://github.com/jessierenton/pgg_epithelium, respectively.

The file structure is shown in Figure G.1. The main code is divided into two subdirectories: structure and libs. Structure contains modules which define Tissue, Mesh and Force objects. These store information for the tissue at a single timestep, as defined by the VT model, and contain methods for updating the tissue, both according to the force law at incremental time steps, and after a cell division or death. The Mesh object contains all spatial information and is stored as an attribute of the Tissue object. It also has methods for performing VT (or Delaunay triangulation) when necessary to redetermine cellular neighbourhoods. The Force object determines the force law used to determine cell movement, and is also an attribute of the Tissue. Other cell information, such as cell type, age and ancestry, can be stored as Tissue attributes.

The libs subdirectory contains various modules with functions for running simulations, such as pd_lib.py (used in Chapter 4), public_goods_lib.py (used in Chap-

ter 5) and contact_inhibition_lib.py in Chapter 6. For simulations with neutral selection, pd_lib_neutral.py is used.

In general these lib files contain a 'run_simulation' function which sets up the simulation and various 'simulation . . . ' functions which define different types of simulations (e.g. for different update rules). These always take a Tissue object, a (small) timestep, and a maximum number of steps as arguments. The simulation loops through incremental timesteps, with the Tissue updating according to the force law. Update events (or separate birth and death events) occur at each timestep δt, with probability $\lambda Z \delta t$, where λ is the per cell event rate and Z is the population size.

Also in the libs subdirectory are plot.py, which defines plotting functions (torus_plot and animate_torus are the most useful), and data.py which contains helpful functions for data handling.

Finally, various files for running single simulations or multiple simulations are in the main VTdyn directory. These import functions from a given lib file. We use the python multiprocessing package to run simulations in parallel.

Most of the simulations in this thesis were run on a high performance computing cluster. As an indicator of run time, it takes approximately 10 hours to run 10,000 simulations of the prisoner's dilemma with decoupled updating on a cluster machine, using 40 cores (i.e. running 40 simulations in parallel). These simulations start with a single mutant and run to fixation. Note that this is a rough estimate, and that the time will depend on the exact parameters.

```
VTdyn
├── structure
│   ├── __init__.py
│   ├── cell.py
│   ├── global_constants.py
│   ├── initialisation.py
│   └── mesh.py
├── libs
│   ├── __init__.py
│   ├── contact_inhibition_lib.py
│   ├── data.py
│   ├── density_dep_lib.py
│   ├── pd_lib.py
│   ├── pd_lib_neutral.py
│   ├── plot.py
│   └── public_goods_lib.py
├── run_file1.py
├── run_file2.py
└── ⋮
```

Figure G.1: Directory tree for VTdyn code.

Bibliography

[1] P. Lindenfors, *For Whose Benefit?: The Biological and Cultural Evolution of Human Cooperation*, Springer International Publishing, 2017.

[2] A. Aktipis, *The Cheating Cell: How Evolution Helps Us Understand and Treat Cancer*, Princeton University Press, 2020.

[3] J. Maynard Smith and G. R. Price, "The logic of animal conflict," *Nature*, vol. 246, no. 5427, pp. 15–18, 1973.

[4] J. Maynard Smith, "The theory of games and the evolution of animal conflicts," *Journal of Theoretical Biology*, vol. 47, no. 1, pp. 209–221, 1974.

[5] N. L. Kerr, "Social dilemmas," *Group Processes*, vol. 31, no. 1, pp. 85–110, 2012.

[6] M. A. Nowak, "Five rules for the evolution of cooperation," *Science*, vol. 314, no. 5805, pp. 1560–1563, 2006.

[7] M. A. Nowak and R. M. May, "Evolutionary games and spatial chaos," *Nature*, vol. 359, no. 6398, pp. 826–829, 1992.

[8] H. Ohtsuki, C. Hauert, E. Lieberman, and M. A. Nowak, "A simple rule for the evolution of cooperation on graphs and social networks," *Nature*, vol. 441, no. 7092, pp. 502–505, 2006.

[9] A. Szolnoki, M. Perc, and Z. Danku, "Towards effective payoffs in the prisoner's dilemma game on scale-free networks," *Physica A: Statistical Mechanics and its Applications*, vol. 387, no. 8-9, pp. 2075–2082, 2008.

[10] C. E. Tarnita, H. Ohtsuki, T. Antal, F. Fu, and M. A. Nowak, "Strategy selection in structured populations," *Journal of Theoretical Biology*, vol. 259, no. 3, pp. 570–581, 2009.

[11] M. A. Nowak, C. E. Tarnita, and T. Antal, "Evolutionary dynamics in structured populations," *Philosophical Transactions of the Royal Society B: Biological Sciences*, vol. 365, no. 1537, pp. 19–30, 2010.

[12] M. Broom and J. Rychtář, "A general framework for analysing multiplayer games in networks using territorial interactions as a case study," *Journal of Theoretical Biology*, vol. 302, pp. 70–80, 2012.

[13] B. Allen, M. A. Nowak, and U. Dieckmann, "Adaptive dynamics with interaction structure," *American Naturalist*, vol. 181, no. 6, pp. E139–63, 2013.

[14] B. Allen, G. Lippner, Y. T. Chen, B. Fotouhi, N. Momeni, S. T. Yau, and M. A. Nowak, "Evolutionary dynamics on any population structure," *Nature*, vol. 544, no. 7649, pp. 227–230, 2017.

[15] J. Peña, B. Wu, J. Arranz, and A. Traulsen, "Evolutionary Games of Multiplayer Cooperation on Graphs," *PLoS Computational Biology*, vol. 12, no. 8, pp. 1–15, 2016.

[16] E. Lieberman, C. Hauert, and M. A. Nowak, "Evolutionary dynamics on graphs," *Nature 2004 433:7023*, vol. 433, no. 7023, pp. 312–316, 2005.

[17] H. Ohtsuki, C. Hauert, E. Lieberman, and M. A. Nowak, "A simple rule for the evolution of cooperation on graphs and social networks," *Nature*, vol. 441, no. 7092, pp. 502–505, 2006.

[18] H. Ohtsuki and M. A. Nowak, "The replicator equation on graphs," *Journal of Theoretical Biology*, vol. 243, no. 1, pp. 86–97, 2006.

[19] G. Szabó and G. Fáth, "Evolutionary games on graphs," *Physics Reports*, vol. 446, no. 4-6, pp. 97–216, 2007.

[20] P. D. Taylor, T. Day, and G. Wild, "Evolution of cooperation in a finite homogeneous graph," *Nature*, vol. 447, no. 7143, pp. 469–472, 2007.

[21] H. Ohtsuki and M. A. Nowak, "Evolutionary stability on graphs," *Journal of Theoretical Biology*, vol. 251, no. 4, pp. 698–707, 2008.

[22] M. S. Krieger, A. McAvoy, and M. A. Nowak, "Effects of motion in structured populations," *Journal of the Royal Society Interface*, vol. 14, no. 135, p. 20170509, 2017.

[23] J. Tkadlec, A. Pavlogiannis, K. Chatterjee, and M. A. Nowak, "Population structure determines the tradeoff between fixation probability and fixation time," *Communications Biology*, vol. 2, no. 1, pp. 1–8, 2019.

[24] A. Traulsen, M. A. Nowak, and J. M. Pacheco, "Stochastic dynamics of invasion and fixation," *Physical Review E - Statistical, Nonlinear, and Soft Matter Physics*, vol. 74, no. 1, p. 011909, 2006.

[25] M. Archetti and I. Scheuring, "Review: Game theory of public goods in one-shot social dilemmas without assortment," *Journal of Theoretical Biology*, vol. 299, pp. 9–20, 2012.

[26] S. Hummert, K. Bohl, D. Basanta, A. Deutsch, S. Werner, G. Theißen, A. Schroeter, and S. Schuster, "Evolutionary game theory: Cells as players," *Molecular BioSystems*, vol. 10, no. 12, pp. 3044–3065, 2014.

[27] D. Hanahan and R. A. Weinberg, "The hallmarks of cancer," *Cell*, vol. 100, pp. 57–70, 2000.

[28] D. Hanahan and R. A. Weinberg, "Hallmarks of cancer: The next generation," *Cell*, vol. 144, no. 5, pp. 646–674, 2011.

[29] E. Witsch, M. Sela, and Y. Yarden, "Roles for Growth Factors in Cancer Progression," *Physiology*, vol. 25, no. 2, pp. 85–101, 2010.

[30] J. Jouanneau, G. Moens, Y. Bourgeois, M. F. Poupon, and J. P. Thiery, "A minority of carcinoma cells producing acidic fibroblast growth factor induces a community effect for tumor progression," *Proceedings of the National Academy of Sciences of the United States of America*, vol. 91, no. 1, pp. 286–290, 1994.

[31] R. Axelrod, D. E. Axelrod, and K. J. Pienta, "Evolution of cooperation among tumor cells," *Proceedings of the National Academy of Sciences of the United States of America*, vol. 103, no. 36, pp. 13474–13479, 2006.

[32] I. P. M. Tomlinson and W. F. Bodmer, "Modelling the consequences of interactions between tumour cells," *British Journal of Cancer*, vol. 75, no. 2, pp. 157–160, 1997.

[33] L. A. Bach, S. M. Bentzen, J. Alsner, and F. B. Christiansen, "An evolutionary-game model of tumour-cell interactions: Possible relevance to gene therapy," *European Journal of Cancer*, vol. 37, no. 16, pp. 2116–2120, 2001.

[34] L. A. Bach, D. J. Sumpter, J. Alsner, and V. Loeschcke, "Spatial evolutionary games of interaction among generic cancer cells," *Journal of Theoretical Medicine*, vol. 5, no. 1, pp. 47–58, 2003.

[35] M. Archetti, "Evolutionarily stable anti-cancer therapies by autologous cell defection," *Evolution, Medicine, and Public Health*, vol. 2013, no. 1, pp. 161–172, 2013.

[36] M. Archetti, "Dynamics of growth factor production in monolayers of cancer cells and evolution of resistance to anticancer therapies," *Evolutionary Applications*, vol. 6, no. 8, pp. 1146–1159, 2013.

[37] M. Archetti, "Evolutionary game theory of growth factor production: Implications for tumour heterogeneity and resistance to therapies," *British Journal of Cancer*, vol. 109, no. 4, pp. 1056–1062, 2013.

[38] M. Archetti, D. A. Ferraro, and G. Christofori, "Heterogeneity for IGF-II production maintained by public goods dynamics in neuroendocrine pancreatic cancer," *Proceedings of the National Academy of Sciences of the United States of America*, vol. 112, no. 6, pp. 1833–1838, 2015.

[39] B. Allen, J. Gore, and M. A. Nowak, "Spatial dilemmas of diffusible public goods," *eLife*, vol. 2013, no. 2, 2013.

[40] M. Archetti, "Cooperation among cancer cells as public goods games on Voronoi networks," *Journal of Theoretical Biology*, vol. 396, pp. 191–203, 2016.

[41] O. Warburg, "On the origin of cancer cells," *Science*, vol. 123, no. 3191, pp. 309–314, 1956.

[42] R. A. Gatenby, E. T. Gawlinski, A. F. Gmitro, B. Kaylor, and R. J. Gillies, "Acid-mediated tumor invasion: A multidisciplinary study," *Cancer Research*, vol. 66, no. 10, pp. 5216–5223, 2006.

[43] D. Basanta, M. Simon, H. Hatzikirou, and A. Deutsch, "Evolutionary game theory elucidates the role of glycolysis in glioma progression and invasion," *Cell Proliferation*, vol. 41, no. 6, pp. 980–987, 2008.

[44] I. Kareva, "Prisoner's dilemma in cancer metabolism," *PLoS ONE*, vol. 6, no. 12, p. e28576, 2011.

[45] D. Basanta, J. G. Scott, R. Rockne, K. R. Swanson, and A. R. Anderson, "The role of IDH1 mutated tumour cells in secondary glioblastomas: An evolutionary game theoretical view," *Physical Biology*, vol. 8, no. 1, 2011.

[46] M. Archetti, "Evolutionary dynamics of the Warburg effect: Glycolysis as a collective action problem among cancer cells," *Journal of Theoretical Biology*, vol. 341, pp. 1–8, 2014.

[47] M. Archetti, "Heterogeneity and proliferation of invasive cancer subclones in game theory models of the Warburg effect," *Cell Proliferation*, vol. 48, no. 2, pp. 259–269, 2015.

[48] A. Kaznatcheev, R. Vander Velde, J. G. Scott, and D. Basanta, "Cancer treatment scheduling and dynamic heterogeneity in social dilemmas of tumour acidity and vasculature," *British Journal of Cancer*, vol. 116, no. 6, pp. 785–792, 2017.

[49] A. R. Anderson, M. Hassanein, K. M. Branch, J. Lu, N. A. Lobdell, J. Maier, D. Basanta, B. Weidow, A. Narasanna, C. L. Arteaga, A. Reynolds, V. Quaranta, L. Estrada, and A. M. Weaver, "Microenvironmental independence associated with tumor progression," *Cancer Research*, vol. 69, no. 22, pp. 8797–8806, 2009.

[50] D. Basanta, J. G. Scott, M. N. Fishman, G. Ayala, S. W. Hayward, and A. R. Anderson, "Investigating prostate cancer tumour-stroma interactions: Clinical and biological insights from an evolutionary game," *British Journal of Cancer*, vol. 106, no. 1, pp. 174–181, 2012.

[51] I. P. M. Tomlinson, "Game-theory models of interactions between tumour cells," *European Journal of Cancer Part A*, vol. 33, no. 9, pp. 1495–1500, 1997.

[52] D. Basanta, H. Hatzikirou, and A. Deutsch, "Studying the emergence of invasiveness in tumours using game theory," *European Physical Journal B*, vol. 63, no. 3, pp. 393–397, 2008.

[53] R. C. Rockne, A. Hawkins-Daarud, K. R. Swanson, J. P. Sluka, J. A. Glazier, P. Macklin, D. A. Hormuth, A. M. Jarrett, E. A. Lima, J. Tinsley Oden, G. Biros, T. E. Yankeelov, K. Curtius, I. Al Bakir, D. Wodarz, N. Komarova, L. Aparicio, M. Bordyuh, R. Rabadan, S. D. Finley, H. Enderling, J. Caudell, E. G. Moros, A. R. Anderson, R. A. Gatenby, A. Kaznatcheev, P. Jeavons, N. Krishnan, J. Pelesko, R. R. Wadhwa, N. Yoon, D. Nichol,

A. Marusyk, M. Hinczewski, and J. G. Scott, "The 2019 mathematical oncology roadmap," *Physical Biology*, vol. 16, no. 4, p. 41005, 2019.

[54] R. A. Gatenby and J. S. Brown, "Integrating evolutionary dynamics into cancer therapy," *Nature Reviews Clinical Oncology*, vol. 17, no. 11, pp. 675–686, 2020.

[55] B. Wölfl, H. te Rietmole, M. Salvioli, F. Thuijsman, J. S. Brown, B. Burgering, and K. Staňková, "The contribution of evolutionary game theory to understanding and treating cancer," *medRxiv*, 2020, 2020.12.02. 20241703.

[56] J. Zukewich, V. Kurella, M. Doebeli, and C. Hauert, "Consolidating birth-death and death-birth processes in structured populations," *PLoS ONE*, vol. 8, no. 1, p. e54639, 2013.

[57] J. M. Pacheco, A. Traulsen, and M. A. Nowak, "Active linking in evolutionary games," *Journal of Theoretical Biology*, vol. 243, no. 3, pp. 437–443, 2006.

[58] F. C. Santos, J. M. Pacheco, and T. Lenaerts, "Cooperation prevails when individuals adjust their social ties," *PLoS Computational Biology*, vol. 2, no. 10, pp. 1284–1291, 2006.

[59] B. Wu, D. Zhou, F. Fu, Q. Luo, L. Wang, and A. Traulsen, "Evolution of cooperation on stochastic dynamical networks," *PLoS ONE*, vol. 5, no. 6, p. e11187, 2010.

[60] F. L. Pinheiro, F. C. Santos, and J. M. Pacheco, "Linking Individual and Collective Behavior in Adaptive Social Networks," *Physical Review Letters*, vol. 116, no. 12, p. 128702, 2016.

[61] J. A. Moreira, J. M. Pacheco, and F. C. Santos, "Evolution of collective action in adaptive social structures," *Scientific Reports*, vol. 3, no. 1521, 2013.

[62] B. Allen and M. A. Nowak, "Evolutionary shift dynamics on a cycle," *Journal of Theoretical Biology*, vol. 311, pp. 28–39, 2012.

[63] A. Pavlogiannis, K. Chatterjee, B. Adlam, and M. A. Nowak, "Cellular cooperation with shift updating and repulsion," *Scientific Reports*, vol. 5, no. 17147, 2015.

[64] A. Csikász-Nagy, M. Cavaliere, and S. Sedwards, "Combining game theory and graph theory to model interactions between cells and the tumor microenvironment," in A. D'Onofrio, P. Cerrai, and A. Gandolfi, eds., *New challenges for cancer systems biomedicine*, pp. 3–18, Milano: Springer, 2012.

[65] A. Csikász-Nagy, L. M. Escudero, M. Guillaud, S. Sedwards, B. Baum, and M. Cavaliere, "Cooperation and competition in the dynamics of tissue architecture during homeostasis and tumorigenesis," *Seminars in Cancer Biology*, vol. 23, no. 4, pp. 293–298, 2013.

[66] S. Duvdevani-Bar and S. Lee, "On topological simulations in developmental biology," *Journal of Theoretical Biology*, vol. 166, no. 1, pp. 33–50, 1994.

[67] F. A. Meineke, C. S. Potten, and M. Loeffler, "Cell migration and organization in the intestinal crypt using a lattice-free model," *Cell Proliferation*, vol. 34, no. 4, pp. 253–266, 2001.

[68] I. M. M. Van Leeuwen, G. R. Mirams, A. Walter, A. Fletcher, P. Murray, J. Osborne, S. Varma, S. J. Young, J. Cooper, B. Doyle, J. Pitt-Francis, L. Momtahan, P. Pathmanathan, J. P. Whiteley, S. J. Chapman, D. J. Gavaghan, O. E. Jensen, J. R. King, P. K. Maini, S. L. Waters, and H. M. Byrne, "An integrative computational model for intestinal tissue renewal," *Cell Proliferation*, vol. 42, no. 5, pp. 617–636, 2009.

[69] M. Perc and A. Szolnoki, "Coevolutionary games—A mini review," *BioSystems*, vol. 99, no. 2, pp. 109–125, 2010.

[70] M. W. Macy and A. Flache, "Learning dynamics in social dilemmas," *Proceedings of the National Academy of Sciences of the United States of America*, vol. 99, no. SUPPL. 3, pp. 7229–7236, 2002.

[71] F. C. Santos, J. M. Pacheco, and T. Lenaerts, "Evolutionary dynamics of social dilemmas in structured heterogeneous populations," *Proceedings of the National Academy of Sciences of the United States of America*, vol. 103, no. 9, pp. 3490–3494, 2006.

[72] C. Hauert, S. De Monte, J. Hofbauer, and K. Sigmund, "Volunteering as Red Queen mechanism for cooperation in public goods games," *Science*, vol. 296, no. 5570, pp. 1129–1132, 2002.

[73] P. D. Taylor and L. B. Jonker, "Evolutionary stable strategies and game dynamics," *Mathematical Biosciences*, vol. 40, no. 1-2, pp. 145–156, 1978.

[74] J. Hofbauer, P. Schuster, and K. Sigmund, "A note on evolutionary stable strategies and game dynamics," *Journal of Theoretical Biology*, vol. 81, no. 3, pp. 609–612, 1979.

[75] S. Holmes, J. Hofbauer, and K. Sigmund, *Evolutionary Games and Population Dynamics*, vol. 95, Cambridge University Press, 2000.

[76] C. Taylor, D. Fudenberg, A. Sasaki, and M. A. Nowak, "Evolutionary game dynamics in finite populations," *Bulletin of Mathematical Biology*, vol. 66, no. 6, pp. 1621–1644, 2004.

[77] A. Traulsen and C. Hauert, "Stochastic Evolutionary Game Dynamics," in H. G. Schuster, ed., *Reviews of nonlinear dynamics and complexity*, vol. 2, chap. 1, pp. 25–61, Wiley-VCH, 2009.

[78] P. A. Moran, "Random processes in genetics," *Mathematical Proceedings of the Cambridge Philosophical Society*, vol. 54, no. 1, pp. 60–71, 1958.

[79] W. Maciejewski, F. Fu, and C. Hauert, "Evolutionary Game Dynamics in Populations with Heterogenous Structures," *PLOS Computational Biology*, vol. 10, no. 4, p. e1003567, 2014.

[80] C. E. Tarnita, T. Antal, H. Ohtsuki, and M. A. Nowak, "Evolutionary dynamics in set structured populations," *Proceedings of the National Academy of Sciences of the United States of America*, vol. 106, no. 21, pp. 8601–8604, 2009.

[81] C. G. Nathanson, C. E. Tarnita, and M. A. Nowak, "Calculating evolutionary dynamics in structured populations," *PLoS Computational Biology*, vol. 5, no. 12, p. e1000615, 2009.

[82] T. Antal, H. Ohtsuki, J. Wakeley, P. D. Taylor, and M. A. Nowak, "Evolution of cooperation by phenotypic similarity," *Proceedings of the National Academy of Sciences of the United States of America*, vol. 106, no. 21, pp. 8597–8600, 2009.

[83] L. Hindersin and A. Traulsen, "Most undirected random graphs are amplifiers of selection for birth-death dynamics, but suppressors of selection for death-birth dynamics," *PLoS Computational Biology*, vol. 11, no. 11, pp. 1–14, 2015.

[84] B. Allen, C. Sample, R. Jencks, J. Withers, P. Steinhagen, L. Brizuela, J. Kolodny, D. Parke, G. Lippner, and Y. A. Dementieva, "Transient amplifiers of selection and reducers of fixation for death-Birth updating on graphs," *PLoS Computational Biology*, vol. 16, no. 1, p. e1007529, 2020.

[85] N. Masuda, "Directionality of contact networks suppresses selection pressure in evolutionary dynamics," *Journal of Theoretical Biology*, vol. 258, no. 2, pp. 323–334, 2009.

[86] M. Broom, C. Cannings, and G. T. Vickers, "Multi-player matrix games," *Bulletin of Mathematical Biology*, vol. 59, no. 5, pp. 931–952, 1997.

[87] C. S. Gokhale and A. Traulsen, "Evolutionary games in the multiverse," *Proceedings of the National Academy of Sciences of the United States of America*, vol. 107, no. 12, pp. 5500–5504, 2010.

[88] B. Wu, A. Traulsen, and C. S. Gokhale, "Dynamic properties of evolutionary multi-player games in finite populations," *Games*, vol. 4, no. 2, pp. 182–199, 2013.

[89] J. Penã, B. Wu, and A. Traulsen, "Ordering structured populations in multi-player cooperation games," *Journal of the Royal Society Interface*, vol. 13, no. 114, p. 20150881, 2016.

[90] F. C. Santos, M. D. Santos, and J. M. Pacheco, "Social diversity promotes the emergence of cooperation in public goods games," *Nature*, vol. 454, no. 7201, pp. 213–216, 2008.

[91] A. Li, M. Broom, J. Du, and L. Wang, "Evolutionary dynamics of general group interactions in structured populations," *Physical Review E - Statistical, Nonlinear, and Soft Matter Physics*, vol. 93, no. 2, pp. 1–18, 2016.

[92] M. Archetti, I. Scheuring, and D. W. Yu, "The non-tragedy of the non-linear commons," *Preprints*, 2020, 2020040226.

[93] L. A. Bach, T. Helvik, and F. B. Christiansen, "The evolution of n-player cooperation - Threshold games and ESS bifurcations," *Journal of Theoretical Biology*, vol. 238, no. 2, pp. 426–434, 2006.

[94] M. Archetti, "The volunteer's dilemma and the optimal size of a social group," *Journal of Theoretical Biology*, vol. 261, no. 3, pp. 475–480, 2009.

[95] M. Archetti, "Cooperation as a volunteer's dilemma and the strategy of conflict in public goods games," *Journal of Evolutionary Biology*, vol. 22, no. 11, pp. 2192–2200, 2009.

[96] A. McAvoy and C. Hauert, "Asymmetric evolutionary games," *PLoS Computational Biology*, vol. 11, no. 8, 2015.

[97] T. Antal, A. Traulsen, H. Ohtsuki, C. E. Tarnita, and M. A. Nowak, "Mutation-selection equilibrium in games with multiple strategies," *Journal of Theoretical Biology*, vol. 258, no. 4, pp. 614–622, 2009.

[98] N. Champagnat, R. Ferrière, and G. B. Arous, "The canonical equation of adaptive dynamics: a mathematical view," *Selection*, vol. 2, no. 1-2, pp. 73–83, 2002.

[99] G. Aguadé-Gorgorió and R. Solé, "Adaptive dynamics of unstable cancer populations: the canonical equation," *Evolutionary Applications*, vol. 11, no. 8, pp. 1283–1292, 2018.

[100] P. Gerlee and P. M. Altrock, "Persistence of cooperation in diffusive public goods games," *Physical Review E - Statistical, Nonlinear, and Soft Matter Physics*, vol. 99, no. 6, 2019.

[101] M. C. Gibson, A. B. Patel, R. Nagpal, and N. Perrimon, "The emergence of geometric order in proliferating metazoan epithelia," *Nature*, vol. 442, no. 7106, pp. 1038–1041, 2006.

[102] W. T. Gibson and M. C. Gibson, "Cell Topology, Geometry, and Morphogenesis in Proliferating Epithelia," *Current Topics in Developmental Biology*, vol. 89, pp. 87–114, 2009.

[103] H. Honda, "Description of cellular patterns by Dirichlet domains: the two-dimensional case," *Journal of Theoretical Biology*, vol. 72, no. 3, pp. 523–543, 1978.

[104] D. Sánchez-Gutiérrez, M. Tozluoglu, J. D. Barry, A. Pascual, Y. Mao, and L. M. Escudero, "Fundamental physical cellular constraints drive self-organization of tissues," *The EMBO Journal*, vol. 35, no. 1, pp. 77–88, 2016.

[105] G. Voronoi, "Nouvelles applications des paramètres continus à la théorie des formes quadratiques. Deuxième mémoire. Recherches sur les parallélloèdres

primitifs." *Journal für die reine und angewandte Mathematik*, , no. 134, pp. 198–287, 1908.

[106] F. Aurenhammer, "Voronoi diagrams—a survey of a fundamental geometric data structure," *ACM Computing Surveys*, vol. 23, no. 3, pp. 345–405, 1991.

[107] A. M. Marchiando, W. V. Graham, and J. R. Turner, "Epithelial barriers in homeostasis and disease," *Annual Review of Pathology: Mechanisms of Disease*, vol. 5, pp. 119–144, 2010.

[108] S. A. Gudipaty, J. Lindblom, P. D. Loftus, M. J. Redd, K. Edes, C. F. Davey, V. Krishnegowda, and J. Rosenblatt, "Mechanical stretch triggers rapid epithelial cell division through Piezo1," *Nature*, vol. 543, no. 7643, pp. 118–121, 2017.

[109] A. Puliafito, L. Primo, and A. Celani, "Cell-size distribution in epithelial tissue formation and homeostasis," *Journal of the Royal Society Interface Interface*, vol. 14, no. 128, p. 20170032, 2017.

[110] K. R. Mesa, K. Kawaguchi, K. Cockburn, D. Gonzalez, J. Boucher, T. Xin, A. M. Klein, and V. Greco, "Homeostatic epidermal stem cell self-renewal is driven by local differentiation," *Cell Stem Cell*, vol. 23, no. 5, pp. 677–686, 2018.

[111] Y. A. Miroshnikova, H. Q. Le, D. Schneider, T. Thalheim, M. Rübsam, N. Bremicker, J. Polleux, N. Kamprad, M. Tarantola, I. Wang, M. Balland, C. M. Niessen, J. Galle, and S. A. Wickström, "Adhesion forces and cortical tension couple cell proliferation and differentiation to drive epidermal stratification," *Nature Cell Biology*, vol. 20, no. 1, pp. 69–80, 2018.

[112] P. Van Liedekerke, M. M. Palm, N. Jagiella, and D. Drasdo, "Simulating tissue mechanics with agent-based models: concepts, perspectives and some novel results," *Computational Particle Mechanics*, vol. 2, no. 4, pp. 401–444, 2015.

[113] Y. Lee, S. Kouvroukoglou, L. V. McIntire, and K. Zygourakis, "A cellular automaton model for the proliferation of migrating contact-inhibited cells," *Biophysical Journal*, vol. 69, no. 4, pp. 1284–1298, 1995.

[114] M. Block, E. Schöll, and D. Drasdo, "Classifying the expansion kinetics and critical surface dynamics of growing cell populations," *Physical Review Letters*, vol. 99, no. 24, pp. 3–6, 2007.

[115] M. Radszuweit, M. Block, J. G. Hengstler, E. Schöll, and D. Drasdo, "Comparing the growth kinetics of cell populations in two and three dimensions," *Physical Review E - Statistical, Nonlinear, and Soft Matter Physics*, vol. 79, no. 5, pp. 1–12, 2009.

[116] C. A. Yates, A. Parker, and R. E. Baker, "Incorporating pushing in exclusion-process models of cell migration," *Physical Review E - Statistical, Nonlinear, and Soft Matter Physics*, vol. 91, no. 5, pp. 1–12, 2015.

[117] F. Graner and J. A. Glazier, "Simulation of biological cell sorting using a two-dimensional extended Potts model," *Physical Review Letters*, vol. 69, no. 13, pp. 2013–2016, 1992.

[118] P. Hogeweg, "Evolving mechanisms of morphogenesis: On the interplay between differential adhesion and cell differentiation," *Journal of Theoretical Biology*, vol. 203, no. 4, pp. 317–333, 2000.

[119] T. Hirashima, E. G. Rens, and R. M. Merks, "Cellular Potts modeling of complex multicellular behaviors in tissue morphogenesis," *Development Growth and Differentiation*, vol. 59, no. 5, pp. 329–339, 2017.

[120] M. Scianna, E. Bassino, and L. Munaron, "A cellular Potts model analyzing differentiated cell behavior during in vivo vascularization of a hypoxic tissue," *Computers in Biology and Medicine*, vol. 63, pp. 143–156, 2015.

[121] E. L. Stott, N. F. Britton, J. A. Glazier, and M. Zajac, "Stochastic simulation

of benign avascular tumour growth using the Potts model," *Mathematical and Computer Modelling*, vol. 30, no. 5-6, pp. 183–198, 1999.

[122] A. Szabó and R. M. Merks, "Cellular Potts modeling of tumor growth, tumor invasion, and tumor evolution," *Frontiers in Oncology*, vol. 3, no. 87, 2013.

[123] J. Galle, M. Loeffler, and D. Drasdo, "Modeling the effect of deregulated proliferation and apoptosis on the growth dynamics of epithelial cell populations in vitro," *Biophysical Journal*, vol. 88, no. 1, pp. 62–75, 2005.

[124] P. Pathmanathan, J. Cooper, A. Fletcher, G. Mirams, P. Murray, J. Osborne, J. Pitt-Francis, A. Walter, and S. J. Chapman, "A computational study of discrete mechanical tissue models," *Physical Biology*, vol. 6, no. 3, p. 036001, 2009.

[125] D. Drasdo, R. Kree, and J. S. McCaskill, "Monte Carlo approach to tissue-cell populations," *Physical Review E - Statistical, Nonlinear, and Soft Matter Physics*, vol. 52, no. 6, pp. 6635–6657, 1995.

[126] D. P. Germano and J. M. Osborne, "A mathematical model of cell fate selection on a dynamic tissue," *Journal of Theoretical Biology*, vol. 514, p. 110535, 2021.

[127] T. Nagai and H. Honda, "A dynamic cell model for the formation of epithelial tissues," *Philosophical Magazine B: Physics of Condensed Matter; Statistical Mechanics, Electronic, Optical and Magnetic Properties*, vol. 81, no. 7, pp. 699–719, 2001.

[128] R. Farhadifar, J. C. Röper, B. Aigouy, S. Eaton, and F. Jülicher, "The influence of cell mechanics, cell-cell interactions, and proliferation on epithelial packing," *Current Biology*, vol. 17, no. 24, pp. 2095–2104, 2007.

[129] A. G. Fletcher, M. Osterfield, R. E. Baker, and S. Y. Shvartsman, "Vertex models of epithelial morphogenesis," *Biophysical Journal*, vol. 106, no. 11, pp. 2291–2304, 2014.

[130] S. Alt, P. Ganguly, and G. Salbreux, "Vertex models: from cell mechanics to tissue morphogenesis," *Philosophical Transactions of the Royal Society B: Biological Sciences*, vol. 372, no. 1720, 2017.

[131] J. M. Osborne, "Multiscale model of colorectal cancer using the cellular Potts framework," *Cancer Informatics*, vol. 14, pp. 83–93, 2015.

[132] E. M. Purcell, "Life at low Reynolds number," *American Journal of Physics*, vol. 45, no. 1, pp. 3–11, 1977.

[133] G. M. Odell, G. Oster, P. Alberch, and B. Burnside, "The mechanical basis of morphogenesis. I. Epithelial folding and invagination," *Developmental Biology*, vol. 85, no. 2, pp. 446–462, 1981.

[134] J. C. Dallon and H. G. Othmer, "How cellular movement determines the collective force generated by the Dictyostelium discoideum slug," *Journal of Theoretical Biology*, vol. 231, no. 2, pp. 203–222, 2004.

[135] A. I. McClatchey and A. S. Yap, "Contact inhibition (of proliferation) redux," *Current Opinion in Cell Biology*, vol. 24, no. 5, pp. 685–694, 2012.

[136] G. T. Eisenhoffer, P. D. Loftus, M. Yoshigi, H. Otsuna, C. B. Chien, P. A. Morcos, and J. Rosenblatt, "Crowding induces live cell extrusion to maintain homeostatic cell numbers in epithelia," *Nature*, vol. 484, no. 7395, pp. 546–549, 2012.

[137] R. Fernandez-Gonzalez and J. A. Zallen, "Feeling the squeeze: live-cell extrusion limits cell density in epithelia," *Cell*, vol. 149, no. 5, pp. 965–967, 2012.

[138] J. Renton and K. M. Page, "Evolution of cooperation in an epithelium," *Journal of the Royal Society Interface*, vol. 16, no. 152, p. 20180918, 2019.

[139] F. L. Pinheiro, J. M. Pacheco, and F. C. Santos, "From local to global dilemmas in social networks," *PLoS ONE*, vol. 7, no. 2, p. e32114, 2012.

[140] A. D. Cliff and J. K. Ord, *Spatial processes, models & applications*, London: Pion, 1981.

[141] J. Renton and K. M. Page, "Cooperative success in epithelial public goods games," *Journal of Theoretical Biology*, vol. 528, p. 110838, 2021.

[142] D. Basanta and A. Deutsch, "A game theoretical perspective on the somatic evolution of cancer," in *Selected topics in cancer modeling: Genesis, evolution, immune competition, and therapy*, pp. 1–16, Birkhäuser Boston, 2008, 0810.4738.

[143] M. Archetti and I. Scheuring, "Coexistence of cooperation and defection in public goods games," *Evolution*, vol. 65, no. 4, pp. 1140–1148, 2011.

[144] M. Perc, J. Gómez-Gardeñes, A. Szolnoki, L. M. Floría, and Y. Moreno, "Evolutionary dynamics of group interactions on structured populations: A review," *Journal of the Royal Society Interface*, vol. 10, no. 80, 2013, 1301.2247.

[145] F. C. Santos, M. D. Santos, and J. M. Pacheco, "Social diversity promotes the emergence of cooperation in public goods games," *Nature*, vol. 454, no. 7201, pp. 213–216, 2008.

[146] J. M. Pacheco, F. C. Santos, M. O. Souza, and B. Skyrms, "Evolutionary dynamics of collective action in N-person stag hunt dilemmas," *Proceedings of the Royal Society B: Biological Sciences*, vol. 276, no. 1655, pp. 315–321, 2009.

[147] M. O. Souza, J. M. Pacheco, and F. C. Santos, "Evolution of cooperation under N-person snowdrift games," *Journal of Theoretical Biology*, vol. 260, no. 4, pp. 581–588, 2009.

[148] H. Eagle and E. M. Levine, "Growth regulatory effects of cellular interaction," *Nature*, vol. 213, no. 5081, pp. 1102–1106, 1967.

[149] B. W. Benham-Pyle, B. L. Pruitt, and W. J. Nelson, "Mechanical strain induces E-cadherin-dependent Yap1 and β-catenin activation to drive cell cycle entry," *Science*, vol. 348, no. 6238, pp. 1024–1027, 2015.

[150] M. Aragona, T. Panciera, A. Manfrin, S. Giulitti, F. Michielin, N. Elvassore, S. Dupont, and S. Piccolo, "A mechanical checkpoint controls multicellular growth through YAP/TAZ regulation by actin-processing factors," *Cell*, vol. 154, no. 5, pp. 1047–1059, 2013.

[151] J. M. Osborne, A. G. Fletcher, J. M. Pitt-Francis, P. K. Maini, and D. J. Gavaghan, "Comparing individual-based approaches to modelling the self-organization of multicellular tissues," *PLoS Computational Biology*, vol. 13, no. 2, p. e1005387, 2017.

[152] M. Archetti and K. J. Pienta, "Cooperation among cancer cells: applying game theory to cancer," *Nature Reviews Cancer*, vol. 19, no. 2, pp. 110–117, 2019.

[153] D. Basanta, R. A. Gatenby, and A. R. Anderson, "Exploiting evolution to treat drug resistance: Combination therapy and the double bind," *Molecular Pharmaceutics*, vol. 9, no. 4, pp. 914–921, 2012.

[154] J. Zhang, J. J. Cunningham, J. S. Brown, and R. A. Gatenby, "Integrating evolutionary dynamics into treatment of metastatic castrate-resistant prostate cancer," *Nature Communications*, vol. 8, no. 1, 2017.

[155] J. West, Y. Ma, and P. K. Newton, "Capitalizing on competition: An evolutionary model of competitive release in metastatic castration resistant prostate cancer treatment," *Journal of Theoretical Biology*, vol. 455, pp. 249–260, 2018.

[156] A. Marusyk, D. P. Tabassum, P. M. Altrock, V. Almendro, F. Michor, and K. Polyak, "Non-cell-autonomous driving of tumour growth supports subclonal heterogeneity," *Nature*, 2014.

[157] A. S. Cleary, T. L. Leonard, S. A. Gestl, and E. J. Gunther, "Tumour cell heterogeneity maintained by cooperating subclones in Wnt-driven mammary cancers," *Nature*, vol. 508, no. 1, pp. 113–117, 2014.

[158] M. D. M. Inda, R. Bonavia, A. Mukasa, Y. Narita, D. W. Sah, S. Vandenberg, C. Brennan, T. G. Johns, R. Bachoo, P. Hadwiger, P. Tan, R. A. DePinho, W. Cavenee, and F. Furnari, "Tumor heterogeneity is an active process maintained by a mutant EGFR-induced cytokine circuit in glioblastoma," *Genes and Development*, vol. 24, no. 16, pp. 1731–1745, 2010.

[159] A. Kaznatcheev, J. Peacock, D. Basanta, A. Marusyk, and J. G. Scott, "Fibroblasts and alectinib switch the evolutionary games played by non-small cell lung cancer," *Nature Ecology and Evolution*, vol. 3, no. 3, pp. 450–456, 2019.

[160] H. Zhou, D. Neelakantan, and H. L. Ford, "Clonal cooperativity in heterogenous cancers," *Seminars in Cell and Developmental Biology*, vol. 64, pp. 79–89, 2017.

[161] R. Sender, S. Fuchs, and R. Milo, "Revised estimates for the number of human and bacteria cells in the body," *PLoS Biology*, vol. 14, no. 8, 2016.

[162] L. You, J. S. Brown, F. Thuijsman, J. J. Cunningham, R. A. Gatenby, J. Zhang, and K. Staňková, "Spatial vs. non-spatial eco-evolutionary dynamics in a tumor growth model," *Journal of Theoretical Biology*, vol. 435, pp. 78–97, 2017.

[163] D. R. Welch, "Tumor heterogeneity - A 'contemporary concept' founded on historical insights and predictions," *Cancer Research*, vol. 76, no. 1, pp. 4–6, 2016.

[164] M. Archetti, "Stable heterogeneity for the production of diffusible factors in cell populations," *PLoS ONE*, vol. 9, no. 9, p. e108526, 2014.

[165] M. Uroz, S. Wistorf, X. Serra-Picamal, V. Conte, M. Sales-Pardo, P. Roca-Cusachs, R. Guimerà, and X. Trepat, "Regulation of cell cycle progression by cell-cell and cell-matrix forces," *Nature Cell Biology*, vol. 20, no. 6, pp. 646–654, 2018.

[166] A. Traulsen, N. Shoresh, and M. A. Nowak, "Analytical Results for Individual and Group Selection of Any Intensity," *Bulletin of Mathematical Biology 2008 70:5*, vol. 70, no. 5, pp. 1410–1424, 2008.